2009

Effect of Rib Turbulators on Heat Transfer Performance in Stationary Ribbed Channels

Aravind Rohan Sampath
Cleveland State University

EFFECT OF RIB TURBULATORS ON HEAT TRANSFER PERFORMANCE IN STATIONARY RIBBED CHANNELS

ARAVIND ROHAN SAMPATH

Bachelor of Production Engineering

Anna University

May, 2007

Submitted in partial fulfillment of requirements for the degree

MASTER OF SCIENCE IN MECHANICAL ENGINEERING

at the

CLEVELAND STATE UNIVERSITY

December, 2009

This thesis has been approved

for the Department of Mechanical Engineering

and the College of Graduate Studies by

_____ Date _____

Thesis chairperson, Dr. Mounir B. Ibrahim

Department of Mechanical Engineering

_____ Date _____

Dr. George P. Chatzimavroudis

Department of Chemical and Biomedical Engineering

_____ Date _____

Dr. Miron Kaufman

Department of Physics

DEDICATION

I dedicate this thesis to my dad, K.R. Sampath and my mom Usha Sampath for their inseparable support and prayers and who raised me with their caring and gentle love.

ACKNOWLEGEMENTS

This work was carried out at the Power and Energy Systems Laboratory, Department of Mechanical Engineering, Cleveland State University.

I would like to express my sincere thanks and deep sense of gratitude to my supervisor Dr. Mounir B. Ibrahim, for all his advice, guidance and support to this time. I hope this will continue.

I am grateful to Dr. Miron Kaufman, Department of Physics and Dr. George P. Chatzimavroudis, Department of Chemical and Biomedical Engineering, who amidst of all their activity, accepted to be the members of the thesis committee.

I would like to thank my friends Mukund Kumar and Olga Kartuzova for their constant support and inspiring talks.

I thank all my friends in this country and abroad for their constant love and care.

EFFECT OF RIB TURBULATORS ON HEAT TRANSFER PERFORMANCE IN STATIONARY RIBBED CHANNELS

ARAVIND ROHAN SAMPATH

ABSTRACT

The thermal performance was examined computationally for the stationary channels with rib turbulators oriented at 90 degrees. Ribs were placed on opposite walls and the heat transfer coefficients and frictional loss were calculated. Three stationary channels with aspect ratios (W/H) 1, 2 and 4 were considered for the analysis. The thermal performance was measured by calculating the Nusselt number and frictional losses. Square ribs (w/e = 1) were considered as the baseline configuration. The rib width and rib spacing varies while the rib height is maintained constant. Rib spacing (P/e) of 10 and 20 and rib width to rib height ratios (w/e) ranging from 1/8 to 14 were considered. The heat transfer performance for all the channels were calculated for Reynolds numbers 10,000, 30,000 and 60,000. The code was validated by comparing the results for channels with square ribs (w/e =1) with the experimental results. The results obtained for all the channels with different rib configuration proved that the increase in rib width reduced the thermal performance of the channels. By combined effect of rib width, rib spacing and flow parameters, the optimal cooling configuration was obtained.

TABLE OF CONTENTS

Page

ABSTRACT…… v

NOMENCLATURE…….. ix

LIST OF TABLES…….. xi

LIST OF FIGURES…… xv

CHAPTER

I. INTRODUCTION……..... 1

1.1 Literature Review ……... 3

1.2 Objective of the Work …… 6

1.3 Organization of the Thesis …… 7

II. FLOW PHENOMENA IN TURBINE BLADES 9

2.1 Rib Turbulators…….. 9

2.2 Rib Configuration…….. 10

2.3 Calculation Procedure and Formulae …… 12

2.3.1 Normalizing Nusselt number ……..... 13

2.3.2 Normalizing friction factor ……... 14

2.4 Conclusion …… 15

III. NUMERICAL METHOD…… 16

3.1 Governing equations…… 16

3.2 Geometry ……..…… 17

3.3 Boundary and Thermal Condition……. 19

3.4 Turbulence Model…….…… 21

3.5 Sequential vs. Coupled Approach……..……..... 22

3.6 Conclusion…….…. 24

IV. GRID INDEPENDENCE STUDY…….... .26

4.1 Introduction…… 27

4.2 Details of the Grid…….. 28

4.3 Results and Discussion……..... 32

4.4 Conclusion…….. 37

V. ANALYSIS OF HEAT TRANSFER IN STATIONARY SMOOTH CHANNEL…… 39

5.1 Computational Domain……... 40

5.2 Boundary Condition……..... 40

5.3 Correlations……. 42

5.4 Results and Discussion…….. 44

5.5 Conclusion……..... 46

VI. EFFECT OF RIB SPACING ON THE HEAT TRANSFER PERFORMANCE OF THE CHANNELS…….. 47

6.1 Effect of Rib Spacing in Square Channel……... 47

6.2 Effect of Rib Spacing in Rectangular Channel I…… 57

6.3 Effect of Rib Spacing in Rectangular Channel II……... 66

6.4 Conclusion……. 74

VII. EFFECT OF RIB WIDTH ON THE HEAT TRANSFER PERFORMANCE THECHANNELS……..... 77

7.1 Effect of Rib Width in Square Channel……..... 78

7.2 Effect of Rib Width in Rectangular Channel I…….....**..** 88

7.3 Effect of Rib Width in Rectangular Channel II……..….. 99

7.4 Conclusion……..……..… 108

VIII. HEAT TRANSFER PERFORMANCE OF THE CHANNELS…… 110

8.1 Effect of Reynolds Number …...…….. 110

8.2 Effect of Rib Spacing …….. 111

8.3 Effect of Rib Width ……. 112

8.4 Effect of Channel Aspect Ratio ……112

8.5 Overall Thermal Performance ……. 113

8.6 Future work…….…….….116

BIBLIOGRAPHY……..…….…..… 117

NOMENCLATURE

AR: Aspect ratio

d: Diameter of the channel, m

D: Characteristic length, m

D_h: Hydraulic diameter

DNS: Direct Numerical Study

E: Internal energy per unit mass, J/kg

e: Height of the rib, m

f: Friction factor

f_{FD}: Friction factor for fully developed flow in smooth channel

$f_{norm.}$: Normalized friction factor

G: Mass flux, kg/m

g_c: Conversion factor

h: Convective heat transfer coefficient, $W/m^2 K$

H: Height of the channel, m

k: Thermal conductivity, W/m K

L: Length of the channel, m

LES: Large Eddy Simulations

m: Mass flow rate, kg/s

n: Constant for heating

Nu: Nusselt number

Nu_{FD}: Nusselt number for Fully Developed flow in smooth channel

$Nu_{norm.}$: Normalized Nusselt number

P/e: Rib spacing ratio

P: Pitch of the rib, m

PBC: Periodic Boundary Condition

PBC: Periodic Boundary Condition

Pr: Prandtl number

q/A: Heat transfer per unit area, W/m^2

Re: Reynolds number

Re_D: Reynolds number based on Hydraulic diameter

RKE: Realizable k – ε turbulence model

SKW: Standard k – ω turbulence model

T_b: Local mean bulk temperature, K

T_w: Local wall temperature, K

V: Velocity of the flow, m/s

w/e: Rib width to rib height ratio

W/H: Channel aspect ratio

w: Width of the rib, m

W: Width of the channel, m

ΔP: Pressure drop across the domain, Pa

Greek Letters:

α: Orientation of the rib, degrees

Δ: Laplacian operator

ρ: Density of the coolant, kg/m^3

υ: Kinematic viscosity, m^2/s

LIST OF TABLES

Table **Page**

Table 1: Parameters studied in the work…… 6

Table 2: Normalized Nusselt number values for different turbulence models……. 22

Table 3: Normalized Nusselt number values for different computational approach……. 24

Table 4: Rib and channel geometries and flow parameters for grid independence study…….. 27

Table 5: Size functions specifications……... 29

Table 6: Boundary layer specifications……. 30

Table 7: Normalized Nusselt number for various meshes at various Re. no…… 33

Table 8: Normalized frictions factor various meshes at various Re. no……... 36

Table 9: Range of wall Y plus for various meshes at different Re. no…… 37

Table 10: Range of parameters used in analysis of smooth channel…… 40

Table 11: Mass flow rate and velocity for various flow parameters in the study…… 41

Table 12: Nusselt number values calculated using correlations……... 44

Table 13: Comparison of Nusselt number values for smooth channel with and without PBC and correlation…… 45

Table 14: Rib geometries for square channel with w/e = 1……..... 48

Table 15: Normalized Nusselt number for square channel with w/e = 1……. 52

Table 16: Average Nusselt number values for square channel at P/e = 10 & 20 …… 55

Table 17: Normalized friction factor for square channel with w/e = 1…… 56

Table 18: Rib geometries for rectangular channel I with w/e = 1…… 58

Table 19: Normalized Nusselt number for rectangular channel I with w/e = 1…… 61

Table 20: Average Nusselt number values for rectangular channel I at P/e = 10 & 20 ……..……...… 64

Table 21: Normalized friction factor for rectangular channel I with w/e = 1……65

Table 22: Rib geometries for rectangular channel II with w/e = 1…….. 67

Table 23: Normalized Nusselt number for rectangular channel II with w/e = 1…….. 70

Table 24: Normalized friction factor for rectangular channel II with w/e = 1……..… 72

Table 25: Average Nusselt number values for rectangular channel I at P/e = 10 & 20 ……..……...… 74

Table 26: Parameters used in the analysis of square channel with various rib widths.… 78

Table 27: Normalized Nusselt number for square channel with various rib width for rib spacing P/e = 10 ..…. 79

Table 28: Normalized Nusselt number for square channel with various rib width for rib spacing P/e = 20…….….79

Table 29: Normalized friction factor for square channel with various rib width for rib spacing, P/e = 10…….…87

Table 30: Normalized friction factor for square channel with various rib width for rib spacing, P/e = 20…… 87

Table 31: Parameters used in the analysis of rectangular channel I with various rib widths……. 89

Table 32: Normalized Nusselt number for rectangular channel I with various rib width for rib spacing P/e = 10……... .89

Table 33: Normalized Nusselt number for rectangular channel I with various rib width for rib spacing P/e = 20……..…….. 90

Table 34: Normalized friction factor for rectangular channel I with various rib width for rib spacing P/e = 10…….……... 97

Table 35: Normalized friction factor for rectangular channel I with various rib width for rib spacing P/e = 20…….……... 98

Table 36: Parameters used in the analysis of rectangular channel II with various rib widths……100

Table 37: Normalized Nusselt number for rectangular channel II with various

rib width for rib spacing P/e = 10…….. 100

Table 38: Normalized Nusselt number for rectangular channel II with various rib width for rib spacing P/e = 20…….. 101

Table 39: Normalized friction factor for rectangular channel II with various rib width for rib spacing P/e = 10…… 107

Table 40: Normalized friction factor for rectangular channel II with various rib width for rib spacing P/e = 20…… 107

LIST OF FIGURES

Figure **Page**

Figure 1: Different cooling techniques employed in turbine blades……..…… 2

Figure 2: Rib turbulators placed on opposite walls of the cooling passage showing separation and reattachment flow…….….10

Figure 3: Rib configuration for various rib width and rib spacing ……..… 11

Figure 4: Three dimensional view computational domain with rib turbulators…… 18

Figure 5: Two dimensional flow region of the ribbed channel……. 19

Figure 6: Periodic domain and the boundary conditions…….. 20

Figure 7: Local Nusselt number variation for different turbulence models…….……. 21

Figure 8: Local Nusselt number for different approach…….….. 23

Figure 9: Computational view of grid I – coarse mesh…… 28

Figure 10: Computational view of grid II – fine mesh with size functions……..… 30

Figure 11: Computational view of grid III – fine mesh with boundary layer and size functions……..…….…..…. 31

Figure 12: Computational view of Grid IV – Finer mesh with boundary layer and size

functions …… 32

Figure 13: Normalized Nusselt number for various meshes at different

Reynolds number…… 33

Figure 14: Velocity contours for various meshes at Reynolds number 60,000……..…. 35

Figure 15: Normalized friction factor for various meshes at different

Reynolds number…… 36

Figure 16: Computational domain for case a. without PBC and case b. with PBC…….. 41

Figure 17: Velocity profile for smooth channel without PBC at Re. no 10,000……45

Figure 18: Local Nusselt number variation for square channel with w/e = 1 and rib

spacing, P/e = 10 at different Reynolds number…… 48

Figure 19: Local Nusselt number variation for square channel with w/e = 1 and rib

spacing, P/e = 20 at different Reynolds number…… 50

Figure 20: Normalized Nusselt number for square channel with w/e = 1 and rib

spacing P/e = 10 and P/e = 20…… 51

Figure 21: Velocity contours for square channel with w/e = 1, P/e = 10 and P/e = 20… 53

Figure 22: Rate of increase in average Nusselt number for square channel …… 54

Figure 23: Normalized friction factor for square channel with w/e = 1 and rib

spacing P/e = 10 and P/e = 20……. 56

Figure 24: Local Nusselt number variation for rectangular channel I with w/e = 1 and rib spacing, P/e = 10 at different Reynolds number…….. 58

Figure 25: Local Nusselt number variation for rectangular channel I with w/e = 1 and rib spacing, P/e = 20 at different Reynolds number……. 59

Figure 26: Normalized Nusselt number for rectangular channel I with w/e = 1 and rib spacing P/e = 10 and P/e = 20…….. 60

Figure 27: Velocity contours for rectangular channel I with w/e = 1, P/e = 10 and P/e = 20……... 62

Figure 28: Rate of increase in average Nusselt number for rectangular channel I ..…… 63

Figure 29: Normalized friction factor for rectangular channel I with w/e = 1 and rib spacing P/e = 10 and P/e = 20……. 65

Figure 30: Local Nusselt number variation for rectangular channel II with w/e = 1 and rib spacing, P/e = 10 at different Reynolds number……..…….. 68

Figure 31: Local Nusselt number variation for rectangular channel II with w/e = 1 and rib spacing, P/e = 20 at different Reynolds number……. 68

Figure 32: Normalized Nusselt number for rectangular channel II with w/e = 1

and rib spacing P/e = 10 and P/e = 20…… 69

Figure 33: Normalized friction factor for rectangular channel II with w/e = 1

and rib spacing P/e = 10 and P/e = 20…… 70

Figure 34: Velocity contours for rectangular channel II with w/e = 1, P/e = 10 and

P/e = 20…….. 71

Figure 35: Rate of increase in average Nusselt number for rectangular channel II ..… 73

Figure 36: Normalized Nusselt number of square channel with various rib widths

for different Reynolds number……..……. 80

Figure 37: Velocity contours for square channel with rib spacing P/e = 10 for

Reynolds number 10,000 with rib widths……...…… 81

Figure 38: Velocity contours for square channel with rib spacing P/e = 10 for

Reynolds number 30,000 with rib widths……...…… 82

Figure 39: Velocity contours for square channel with rib spacing P/e = 10 for

Reynolds number 60,000 with rib widths……...…… 83

Figure 40: Velocity contours for square channel with rib spacing P/e = 20 for

Reynolds number 10,000 with rib widths…….…….. 84

Figure 41: Velocity contours for square channel with rib spacing P/e = 20 for

Reynolds number 30,000 with rib widths…….. 85

Figure 42: Velocity contours for square channel with rib spacing P/e = 20 for Reynolds number 60,000 with rib widths…….. 86

Figure 43: Normalized friction factor of square channel with various rib widths for different Reynolds number……. 88

Figure 44: Normalized Nusselt number of rectangular channel I with various rib widths for different Reynolds number…….. 90

Figure 45: Velocity contours for rectangular channel I with rib spacing P/e = 10 for Reynolds number 10,000 with rib widths……..… 91

Figure 46: Velocity contours for rectangular channel I with rib spacing P/e = 10 for Reynolds number 30,000 with rib widths…… 92

Figure 47: Velocity contours for rectangular channel I with rib spacing P/e = 10 for Reynolds number 60,000 with rib widths……...…… 93

Figure 48: Velocity contours for rectangular channel I with rib spacing P/e = 20 for Reynolds number 10,000 with rib widths……..…… 94

Figure 49: Velocity contours for rectangular channel I with rib spacing P/e = 20 for Reynolds number 30,000 with rib widths……... 95

Figure 50: Velocity contours for rectangular channel I with rib spacing P/e = 20 for

Reynolds number 60,000 with rib widths…….…… 96

Figure 51: Normalized friction factor of rectangular channel I with various rib widths for different Reynolds number…… 99

Figure 52: Normalized Nusselt number of rectangular channel II with various ribs widths for different Reynolds number……... 101

Figure 53: Velocity contours for rectangular channel II with rib spacing P/e = 10 for Reynolds number 10,000 with rib widths…….102

Figure 54: Velocity contours for rectangular channel II with rib spacing P/e = 10 for Reynolds number 30,000 with rib widths……103

Figure 55: Velocity contours for rectangular channel II with rib spacing P/e = 10 for Reynolds number 60,000 with rib widths……104

Figure 56: Velocity contours for rectangular channel II with rib spacing P/e = 20 for Reynolds number 10,000 with rib widths……105

Figure 57: Velocity contours for rectangular channel II with rib spacing P/e = 20 for Reynolds number 30,000 with rib widths……105

Figure 58: Velocity contours for rectangular channel II with rib spacing P/e = 20 for Reynolds number 60,000 with rib widths……..…….106

Figure 59: Normalized friction factor of rectangular channel II with various ribs

widths for different Reynolds number…….. 108

Figure 60: Heat transfer performance of the channels……... 114

CHAPTER I

INTRODUCTION

Gas turbine is a rotary engine that extracts power from the flow of combustion gases. Energy is extracted in the form of shaft power and thrust. The gas turbines are described thermodynamically by the Brayton cycle, in which air is compressed isentrophically, combustion occurs at constant pressure and expansion over the turbine occurs isentrophically back to the starting pressure.

Gas turbines play a vital role in today's world and as the demand of power increases, the thermal efficiency and power output of the engine should be optimized. One method of increasing both the power output and thermal efficiency is to increase the inlet temperature of the hot gases through the internal passages.

In advanced gas turbines, the turbine inlet temperature of the gases is as high as 1700° C – 2000° C. These temperatures exceed the melting point of the turbine components. Therefore it is very important to cool the turbine components so that they can withstand these extreme temperatures. With current cooling techniques the temperature is decreased to almost 1000° C, so that they can withstand this extreme environment.

There are several techniques such as jet impingement, film cooling, rib turbulators, shaped internal cooling passages, dimple cooling, shown in Figure 1, to cool a modern gas turbine blade. The jet impingement is used to cool the leading edge, pin fin cooling at the trailing edge and rib turbulators are used cool the internal passages. The present study focuses on the internal cooling turbine blades using rib turbulators or turbulence promoters.

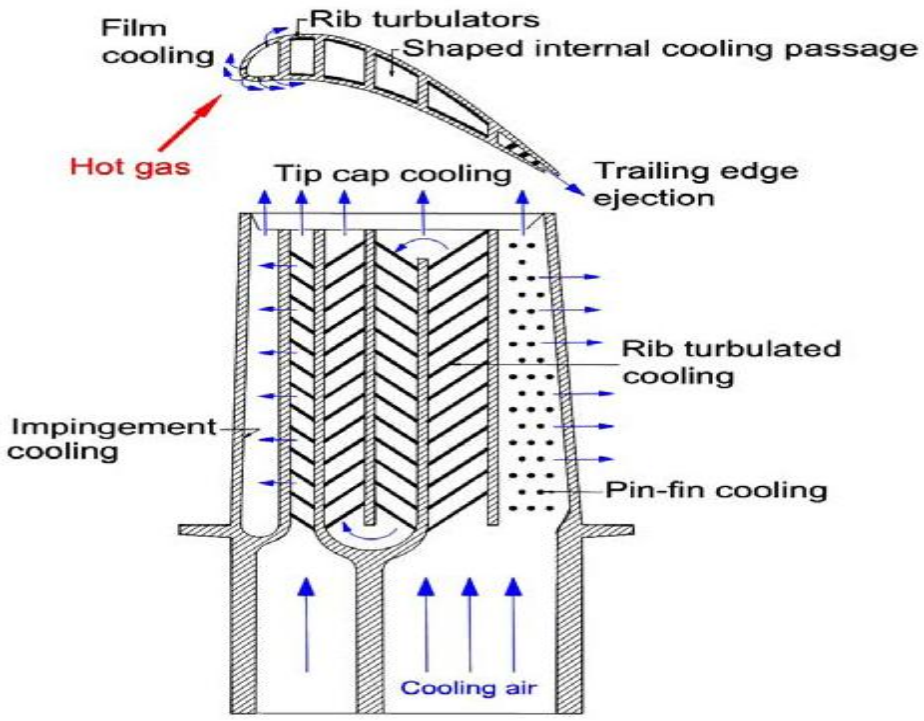

Figure 1: Different cooling techniques employed in turbine blades.

Rib turbulators are the most frequently used method to enhance the heat transfer in the cooling passages. The details of the internal cooling by rib turbulators are explained in chapter II.

1.1 Literature Review

A number of traditional cooling concepts are used in various combinations to adequately cool the turbine vanes and blades. Gas turbine heat transfer and cooling technology by Han, J. C., et al. (2001) provides a detailed description of turbine blade heat transfer and cooling technology. The author compiled a comprehensive review of gas turbine cooling technology including techniques to enhance the heat transfer in internal cooling passages. The book also includes a numerous studies that have been conducted over the years on a wide range of rib configurations in various cooling channels using many experimental techniques.

Early studies investigated cooling channels with orthogonal ribs. Han, J. C. (1988) has performed an experimental study on the ribbed channels with orthogonal square ribs. Three different ribbed channels with different aspect ratios were considered. Also the rib spacing and Reynolds number were taken into account. The work compiled a detailed study on the effect of rib spacing on the heat transfer performance of the ribbed channels. The author has also provided us with a heat transfer and friction correlation. This paper provides us with the experimental results which were compared with the numerical study obtained through the numerical analysis.

Han, J. C., et.al. (1992) performed experiments on various channels now with angled ribs. The ribs were oriented at angles 30, 45, 60 and 90. The effect of rib orientation on the thermal performance is the main objective of the study. It is concluded that the angled ribs have higher heat transfer performance than the orthogonal ribs. The friction and heat transfer correlations are derived from their study.

Iacovides, H. (1998) performed the computation work on the ribbed rectangular passages. In his study both stationary and rotating rectangular passages were considered. The computation work was based on the orthogonal square ribs. The work mainly concentrated on the effect of turbulence model on the channel performance. A differential stress model was developed and it proved to yield better results than the standard k-e model.

Bonhoff, B., et.al. (1999) performed an experimental and numerical study in coolant channels with 45 degree ribs. A stationary square channel is used in the study. Experimental results and the numerical results are obtained by using a Reynolds stress model. The results compared well. A cyclic boundary condition was used for the numerical study. Velocity and heat transfer distributions were recorded.

Iacovides, H. and Raisee, M. (2000) performed a computational study on a rib roughened passage using low Reynolds number turbulence model. A standard k-e and standard k-w turbulence models were used. The periodic boundary condition was employed and the parameters such as Nusselt number are obtained. The differential stress model was also developed. The DSM model provided an improved heat transfer predictions after flow reattachment and over the ribs. However the model failed to predict the effect of Reynolds number.

Lin, Y. L., et.al (2001) performed a numerical study of flow and heat transfer in a duct with 45 degree angled ribs. Both rotating and non rotating duct was considered. The analysis was performed on a three dimensional flow. With a 3D analysis, the secondary flow was predicted. These results also show how the nature of the fluid flow affects surface heat transfer. Also the secondary flow has pronounced effects on heat transfer.

Agarwal, P. (2001) performed a detailed study on the heat and flow transfer in serpentine cooling passages. The channel with aspect ratio 1:4 and 4:1 were constructed. The ribs at angle 90 and 45 degrees were used. Comparisons were made between the angle orientation and the effect of the channel aspect ratios. The angled ribs proved to have high heat transfer performance than the orthogonal ribs. Also the wider channels proved to be better than the narrow channel.

Bredberg, J. (2002) performed an extensive study on the turbulence modeling on the internal cooling of gas turbine blades. Stationary and rotating channels were taken into consideration. He concluded that the standard k-w model results in an accurate method for simulating complex geometries.

Wright, L. M. (2008) performed an experimental analysis on a 3:1 rectangular channel with angled ribs. The rib spacing of 10 and 20 are considered. Rib widths were altered and their effects on the performance were recorded. Also the effect of Reynolds number is taken into account. The study concludes that the angled ribbed channel has more heat transfer effect than the smooth channel. Heat transfer and friction correlations were obtained.

Many researchers like Qahtani, A. M. (2002), Han, J. C. (2005) and Wright, L. M. (2008) performed their works on the rotating channel with either orthogonal or angled ribs. These works were useful in studying the effect of rib spacing, rib width and the flow parameters on the heat transfer performance. The works gave an idea on how the heat transfer alters when the channel is roughened.

1.2 Objective of the Work

The objectives of the work are as follows:

i. To study the channel aspect ratio effect (W/H = 1, 2 and 4) on the heat transfer for the ribbed channels at different Reynolds number. The Reynolds number is in range of 10,000 – 60,000.

ii. To study the effect of the rib width to rib height aspect ratio (w/e = 1/8 – 20) on the Nusselt number and friction factor for different Reynolds number.

iii. To study the effect of the rib spacing, P/e = 10 and P/e = 20 on the heat transfer performance for different Reynolds number.

The parametric study of the analysis is shown in Table 1. The work consists of the combined effect of the parameters: Channel aspect ratio, rib spacing, rib width to height ratio and Reynolds number. Each case is combination of either of these parameters. The ultimate goal is to pick out the optimum cooling configuration.

Table 1: Parameters studied in the work

Parameters	**Symbol**	**Range of values**
Channel aspect ratio	W/H	1 2 4
Rib spacing	P/e	10 20
Rib width to rib height ratio	w/e	1/8 1 2 6 8 10 14 20
Reynolds number	Re	10,000 30,000 60,000

1.3 Organization of the Thesis

The thesis consists of eight chapters.

In chapter I, an introduction of the problem and objective of the work are given. The contributions of various researches on the study of internally cooling passages with rib turbulators are reviewed.

In chapter II, the data reduction procedure is described. The reduction method is based on the data provided in the literature. The procedure of normalizing the parameters is provided.

In chapter III, the detailed study of the numerical method is provided. The boundary condition and thermal condition used in the analysis are described. The method to find the best turbulence model and simplified approach is also given.

In chapter IV, the details of the grid independence study is discussed. Details of various grids and analysis are described and the results are provided.

In chapter III, the analysis of smooth channel is performed. The code is validated by performing the case analysis on a known result. The results from the analysis are compared with the correlation value. The Nusselt number is calculated for various types of flow.

In chapter VI, the effects of rib spacing in the stationary channels are provided. The comparison of numerical results with the experimental results is performed. Only the square ribs (w/e = 1) are used this chapter. The numerically data is acquired for three ribbed channels square channel, rectangular channel I and rectangular channel II. The local Nusselt number variation is obtained for various rib spacing. The normalized

Nusselt number and normalized friction factor are calculated for all the cases and are compared with the experiment results. The velocity contours are also provided to study the flow pattern. By this the CFD code is validated.

In chapter VII, the analysis is performed for different rib widths. The combined effect of rib spacing, rib width and Reynolds number on the heat transfer performance is analyzed. Again, the normalized Nusselt number and normalized friction factor values are calculated and presented.

In chapter VIII, the heat-transfer performance for the ribbed channels is analyzed. Finally we conclude with the best cooling configuration based on the combined effect of heat transfer, pressure loss and overall thermal performance.

CHAPTER II

FLOW PHENOMENA IN TURBINE BLADES

The combination of a complex geometry and the imposed forces develop a complex flow structures within the internal passages of the turbine blades. The physical understanding of the flow pattern is necessary. In this chapter we discuss the various rib configurations modeled and the flow pattern caused by the placement of the ribs. Also the calculation procedure to normalize the results is discussed.

2.1 Rib Turbulators

The purpose of introducing the ribs at regular intervals is to enhance the heat transfer rates. Ribs are manmade protrusions which are placed in a controlled way along the walls. The rib induces a separation in the flow and hence causes an increase in the frictional loss. The enhancement of the heat transfer has thus a drawback in the increased pressure drop, which sometimes can be several times larger than for a smooth channel.

The pressure drop and heat transfer are strongly connected to the height of the rib. Though the ribs can be placed at different orientation, our study focuses on the ribs placed orthogonally (at 90 degrees) to the mainstream flow. The size of the rib and the distance between the two successive ribs, the pitch has great importance.

The heat transfer performance of the ribbed channel depends on the channel aspect ratio, rib configuration and Reynolds number of the coolant. When the coolant passes over the ribs, the flow separates and reattaches as shown in Figure 2.

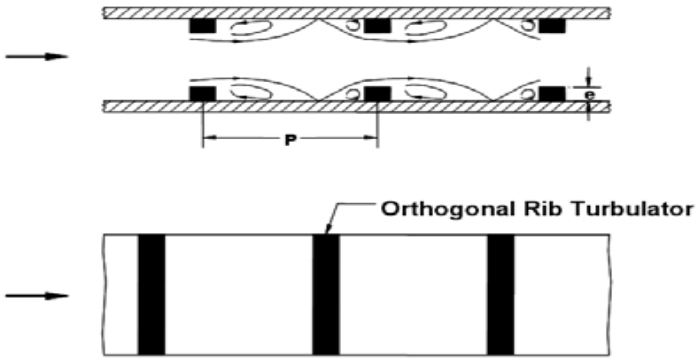

Figure 2: Rib turbulators placed on opposite walls of the cooling passage showing flow separation and reattachment

This separated and reattached boundary layer results in the increased heat transfer coefficient of the ribbed channel. The rib induces secondary flow which further enhances the heat transfer from the wall to the coolant. The rib also induces turbulent mixing in the channels which increases the velocity of the flow.

2.2 Rib Configuration

The channel and rib configuration used in the numerical analysis were obtained from the experimental investigation performed by Han, J. C. (1988). The ranges of all the

parameters were discussed in Chapter I and are provided in Table 1. The experimental results for normalized Nusselt number and normalized fiction factor for all the channels with square ribs were obtained from this literature. The average Nusselt number has an experimental uncertainty of 8% and average friction factor has an uncertainty of 9%. The numerical results are then normalized and compared with the experimental results.

w/e	P/e = 10	P/e = 20
1/8	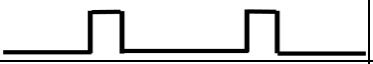	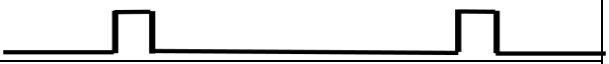
1	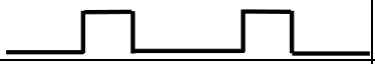	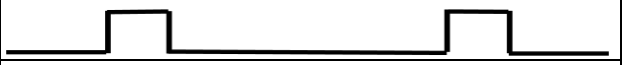
2	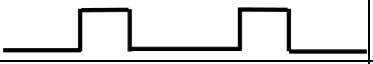	
4	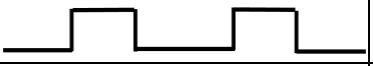	
6	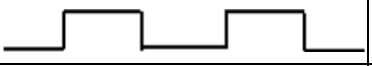	
8	-	
10	-	
14	-	

Figure 3: Rib configuration for various rib width and rib spacing

The analysis is performed for three basic channels, Square channel with AR 1:1, Rectangular channel with AR 2:1 and Rectangular channel II with AR 4:1. The values of the channel width and channel height will be discussed in further chapters. The ribs are placed at two different rib spacing P/e = 10 and 20. The experimental investigation is performed on these three channels and two rib spacing for only square ribs, w/e = 1. In this study the combined effect of rib width is also considered. The idea is to choose a

value for rib width to rib height ratio between 0 to 10 for P/e = 10 and 0 to 20 for P/e = 20. The rib width ratios w/e = 0, 10 and 20 represents a straight smooth channel. The value of w/e =1/8 is selected as anything below this value is similar to a smooth channel. Similarly when the values reach beyond w/e =6 for P/e = 10 and w/e = 14 for P/e = 20, the channel becomes similar to straight channel. So the idea is to pick five to six values between these ranges. Figure 3 shows the rib configuration pattern for various cases. For the rib spacing, P/e = 10 five values are selected and for P/e = 20 eight values are selected. The ratio w/e = 1 is a square rib which was used in experimental investigation. Since P/e = 20 has a wider rib spacing, a wide range of w/e ratio was needed. The optimum rib width size lies between these ranges as the two extreme values represents smooth channels. The heat transfer coefficients and frictional loss are calculated. From the combined effect an optimum rib width size is selected.

2.3 Calculation Procedure and Formulae

The experimental investigation performed by Han, J. C. (1988) provides us with experimental results for Nusselt number and friction factor for channels with orthogonal square ribs. As explained above, these results are normalized by using a normalizing factor to compare with our computational results. The procedure of normalizing the parameters is discussed in the following sections.

2.3.1 Normalizing Nusselt number

Nusselt number is a dimensionless number which is used to estimate the heat transfer component. It is the ratio of convective to conductive heat transfer coefficients across the boundary. The Nusselt number, Nu no. is given by equation (1).

$$Nu = {}^{hD}/_{k} \qquad (1)$$

where,

h= heat transfer coefficient, W/m^2K

D = characteristic length, m

k = thermal conductivity of the fluid, W/ m K

The value of characteristic length depends on the type of the channel. The value of thermal conductivity of fluid, air in our case is 0.025 W/m K.

The local heat transfer coefficient is calculated from the local net heat transfer rate per unit surface area from wall to cooling air; local wall temperature and local bulk mean temperature.

$$h = \frac{({}^{q}/_{A})}{(T_w - T_b)} \qquad (2)$$

where,

q/A = heat transfer per unit area, W/m^2

T_w = local wall temperature, K

T_b = local bulk mean air temperature, K

The bulk mean temperature entering and leaving the section is obtained. The local bulk mean temperature, T_b is calculated by assuming a linear rise along the stream-wise

flow. The local wall temperature, T_w is also obtained. From these results, the heat transfer coefficient is calculated by applying it in equation (2).

The Nusselt number is calculated by applying the heat transfer coefficient values in equation (1). The obtained Nusselt number is now averaged. The normalizing factor is provided by the correlation by Dittus – Boelter equation for Nusselt number for fully developed turbulent flow for smooth tubes provided in equation (3).

$$Nu_{FD} = 0.023\, Re^{0.8} Pr^{n} \qquad (3)$$

where,

Nu_{FD} = Nusselt number for fully developed turbulent flow

Re = Reynolds number

Pr = Prandtl number

n = constant. The value for n = 0.4 for smooth tubes.

The Dittus – Boelter equation is an explicit function to calculate the Nusselt number. It is easy to solve and is completely tailored for the smooth channels.

The normalized Nusselt number is obtained by dividing the Nusselt number and the normalizing factor.

$$Nu_{norm.} = Nu / Nu_{FD} \qquad (4)$$

2.3.2 Normalizing friction factor

The friction factor estimates the pressure loss across the channel. To calculate the friction factor the pressure drop across the section is calculated and applied in the equation (5).

$$f = {\Delta P} \Big/ \left\{ 4\left({\Delta L}/{D}\right)\left[{G^2}/{(2\rho g_c)} \right] \right\} \qquad (5)$$

where,

ΔP = pressure drop across the section, Pa

G = mass flux, kg/m

ρ = density, kg/m^3

g_c = conversion factor, 1 for the analysis.

The normalized factor for the friction factor for fully developed flow for smooth tubes was proposed by Blasius and is given in equation (6).

$$f_{FD} = [0.046\, Re^{-0.2}] \qquad (6)$$

The friction factor is then normalized by dividing the friction factor obtained by computation and friction factor obtained by correlation.

$$f_{norm.} = {f}/{f_{FD}} \qquad (7)$$

2.4 Conclusion

The normalized Nusselt number and friction factor are then compared with the normalized experimental results. Thus normalizing of results simplifies the calculation. The effects of ribs and Reynolds number on the pressure loss and heat transfer are easily correlated.

CHAPTER III

NUMERICAL METHOD

The CFD commercial code Fluent is used in this thesis. The computational simplification and geometrical configurations are addressed.

3.1 Governing equations

The equations that govern the fluid motion and heat transfer are continuity, momentum and energy equations. The equations are called Navier Stokes equations. The fluid is assumed to be incompressible as the temperature rise of the fluid across the domain is minimal and the density of the fluid remains constant.

The continuity equation states the conservation of mass. For an incompressible fluid the continuity equation is

$$\frac{\delta \rho}{\delta t} + \frac{\delta \rho U_i}{\delta x_j} = 0 \qquad (8)$$

The momentum equation is give by Newton's second law which states that the mass times the acceleration is equal to the imposed force. Assuming a Newtonian

incompressible fluid, the momentum equation is described as

$$\frac{\delta U_i}{\delta t} + U_j \frac{\delta U_i}{\delta x_j} + \frac{1}{\rho}\frac{\delta \rho}{\delta x_i} = \vartheta \Delta U_i \qquad (9)$$

The first law of thermodynamics states that the exchange of energy for the system is the result of applied work and heat transfer through that region. The energy equation is given by

$$\frac{\delta E}{\delta t} + U_j \frac{\delta E}{\delta x_j} = \Phi + \frac{1}{\rho}\frac{\delta}{\delta x_j}\left(k \frac{\delta T}{\delta x_j}\right) \qquad (10)$$

where,

Δ – Laplacian operator

E – Internal energy per unit mass, J/kg

Φ - rate of dissipation of mechanical energy per unit mass, J/ kg s

υ – kinematic viscosity, m^2/s

3.2 Geometry

For a constant property fluid flowing with constant cross section area the velocity profile becomes independent on the stream-wise flow at some distance from the inlet. The flow will, after an entry length repeats itself in a periodic manner within each rib interval. In a section for which the ribs are located at specific intervals, the velocity components exhibit a periodic behavior in the stream-wise direction.

$$U(x, y) = U(x + \Delta L, y)$$

$$V(x, y) = V(x + \Delta L, y)$$

The pressure is also decomposed in a similar manner. If the pressure distribution is plotted for two different rib intervals, the plot will have identical shapes with little

change in their level. The change in level is because of the friction loss due to the presence of the ribs. The thermal equation may also be treated in the similar manner.

The three dimensional geometry of the domain is shown in Figure 4. The aspect ratio of the channel is described as width to height, W/H. The channel height has a direct influence in the analysis. The domain is halved and a symmetry boundary condition is employed to simplify of the analysis. Since the analysis is two dimensional, the channel width has no direct influence in the analysis. But the mass flow rate is calculated only on the basis of hydraulic diameter and hence the channel width is taken into consideration. The mass flow rate increases as the channel width increases. This mass flow rate affects the velocity of the flow. Since there is a change in the velocity, the heat transfer coefficient may increase or decrease finally affecting the heat transfer performance.

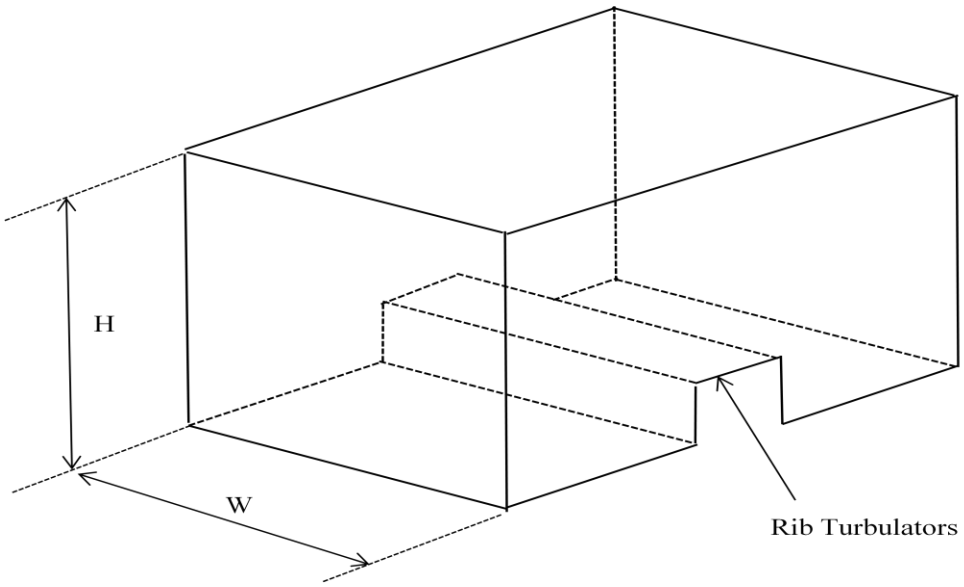

Figure 4: Three dimensional view of the computational domain with rib turbulators.

The two dimensional flow region of the ribbed channel is shown in Figure 5. The channel is roughened with ribs with height, e and width, w. The pitch, P determines the rib spacing. The variation in distance between the ribs and rib width may alter the heat transfer performance.

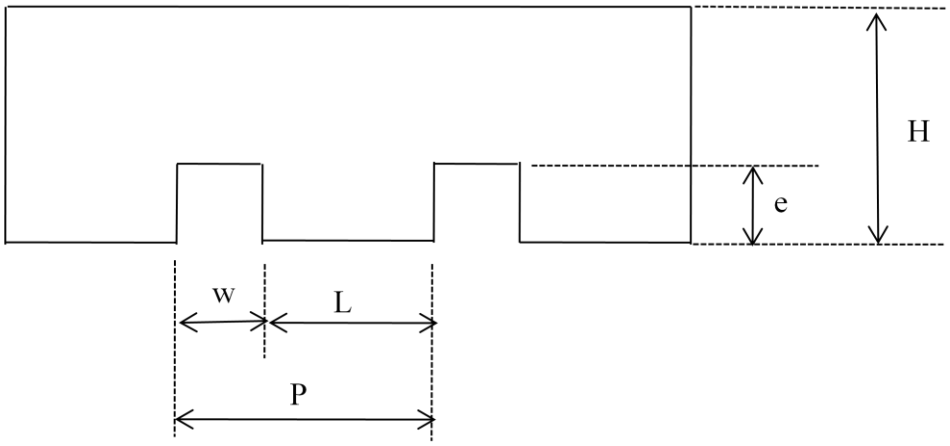

Figure 5: Two dimensional flow region of the ribbed channel.

3.3 Boundary and Thermal Condition

The boundary condition distinguishes how a fluid flow varies from one case to another. It is of paramount importance in numerical simulation. Improper boundary condition treatment may cause significant discrepancies in the predicted results.

In this numerical simulation there exists wall, periodic and a symmetry boundary condition. The general geometry and boundary conditions are given in the Figure 6.

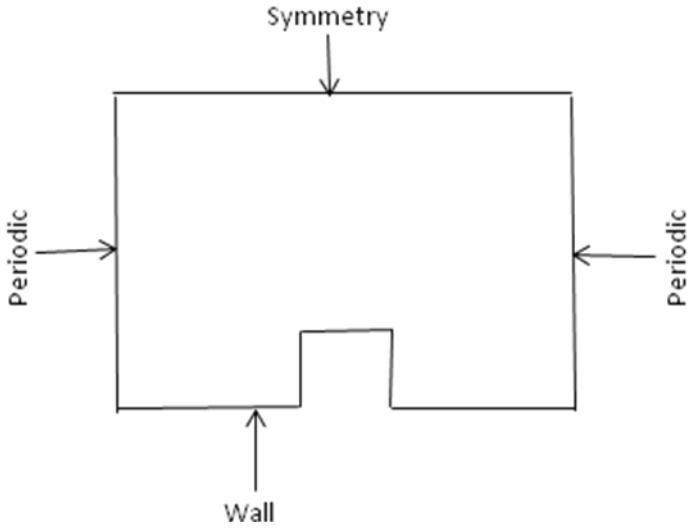

Figure 6: Periodic domain and the boundary conditions.

For certain flow with periodic repeated geometries, the specification of inlet and outlet are given by the periodic boundary condition. The mass flow rate is applied at the inlet of the periodic flow. Also a mean bulk temperature of 298K is applied at the inlet.

For the stationary wall the near wall behavior is governed by a no-slip condition. The thermal boundary condition is case dependent for all the analysis within this thesis. A constant heat flux is applied along the wall. The value of heat flux varies with different flow conditions.

Since the ribs are placed on two opposite walls, a symmetry boundary condition is applied. This eventually minimizes the grid generation difficulties along the wall. The ribs are placed orthogonal to the flow.

3.4 Turbulence Model

The selection of suitable turbulence model is very important in any computational analysis to predict the accurate results. The analysis consists of flow with low Reynolds number. The two turbulence models: standard k-w and realizable k-e model are generally used for low Reynolds number analysis.

An analysis is performed on a 1:1 square channel with rib spacing, P/e 10 at Reynolds number 10,000 using both SKW and RKE turbulence models. All the input parameters such as wall heat flux (2500 W/m^2), inlet bulk temperature (298K) is maintained constant for both the analysis. The local Nusselt number distribution along the channel is obtained and plotted in Figure 7.

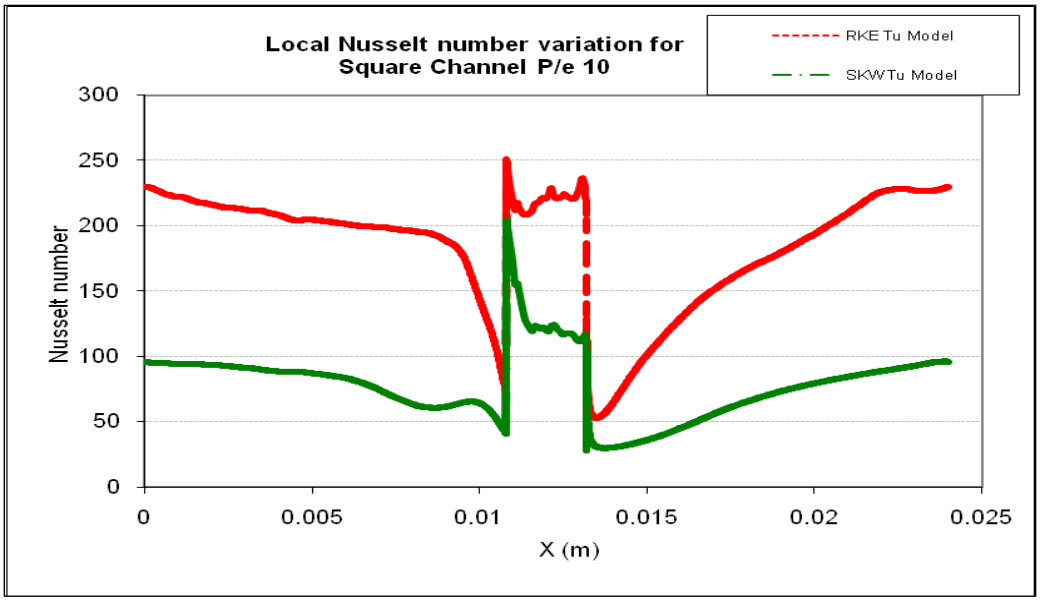

Figure 7: Local Nusselt number variation for different turbulence models.

The normalized Nusselt number and normalized friction factor is also calculated and compared with the experimental data. The values are shown in Table 2.

Table 2: Normalized Nusselt number values for different turbulence models

	RKE	**SKW**	**Experimental**
Normalized Nusselt number	5.428	2.372	2.395
Normalized friction factor	3.618	3.847	3.954

It is clearly evident from the results that the SKW turbulence model is better than the RKE model. The reason for the difference in results is because the RKE model fails to predict the secondary flow across the channel. The presence of ribs causes a recirculation flow at inlet and also downstream the channel and hence the temperature of the wall is high. This increase in wall temperature decreases the Nusselt number.

The percentage error is very high for RKE model. It is 12% for normalized Nusselt number and 8% for friction factor calculation. The percentage error is 0.8% and 3% for Nusselt number and friction factor respectively for SKW turbulence model. The high percentage error hence eliminates the choice of RKE turbulence model for further analysis. The SKW model is always preferred for low Reynolds number flow analysis. The reason as mentioned earlier is the prediction of the separation flow.

3.5 Sequential vs. Coupled Approach

The analysis was first performed using a coupled method. In this approach all the governing equations, continuity, turbulence and energy equations are solved together. By this approach both the flow and temperature were made periodic which resulted in

erroneous results. To overcome the problem and to make only the flow periodic, a sequential method was approached.

A sequential or segregated approach was used to perform the periodic heat transfer flow. The segregated approach solves the governing equations separately. The flow is made periodic by solving the continuity and turbulence equations and then the energy equation is solved for heat transfer. By this approach the flow is made periodic without affecting the temperature field. This is also an efficient method as it saves more time and memory size.

The difference in the two approaches is illustrated with the local Nusselt number distribution along the flow channel. The case shown in Figure 8 is a square channel with an aspect ratio P/e 10 at Reynolds number 10,000.

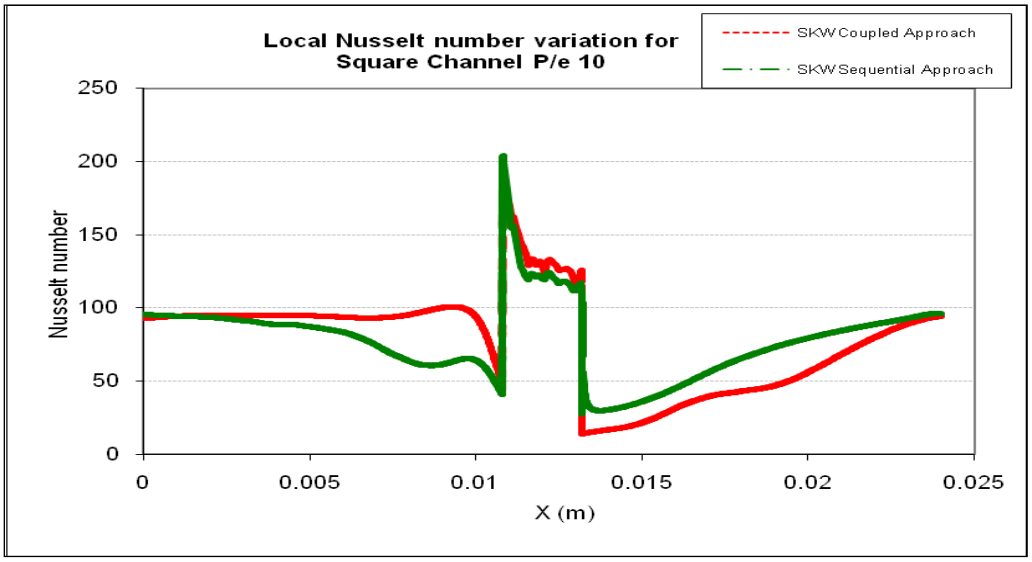

Figure 8: Local Nusselt number variation for different approach

Table 3: Normalized Nusselt number values for different computational approach

	Coupled method	**Sequential method**	**Experimental**
Normalized Nusselt number	2.362	2.372	2.395
Normalized friction factor	3.626	3.847	3.954

The values of normalized Nusselt number and normalized friction factor are compared for both the methods and shown in Table 3. The results obtained from the sequential approach are much closer to the experimental than the coupled method. The percentage error is 2% for normalized Nusselt number and 8% for friction factor in case of coupled method. The percentage error is 0.8% and 3% for Nusselt number and friction factor respectively in case of sequential method. The sequential approach has proved to be more efficient than the coupled approach.

3.6 Conclusion

In this chapter we discussed the boundary and thermal conditions. The values of initial conditions are given. The turbulence models are tested and the result for the standard k-ω model provides better results when compared with the experiment results. Next the approach for the analysis is studied. The sequential approach proved to be better in acquiring the results. Also the computation time is minimized as the governing equations are solved separately. By this approach only the velocity is maintained periodic

and the temperature is independent of the boundary condition. Now, the mesh has to be tested. A grid independence study is performed and is provided in the next chapter.

CHAPTER IV

GRID INDEPENDENCE STUDY

The grid generation plays a vital role in any analysis. A proper mesh provides us with approximate solutions to the partial differential equations. The mesh can be coarse or fine depending on the operating conditions specifically the Reynolds number. Since the present study consists of flow with separation and reattachment, a fine mesh is required along the wall to predict the recirculation zone. Moreover a fine mesh through the entire domain will increase the computation time. An extensive study is required so as to create an optimum mesh which will decrease the computation time with no loss in the accuracy of the results. The exclusive study of the grid independence is discussed in this chapter. Various grids are generated and the effects on the flow parameters are described. The results are obtained and compared with the experimental results. The grid that provides the valid results is used for further investigation.

4.1 Introduction

The grid independence study is performed for the flow through a square channel (AR 1:1) with orthogonal ribs and rib spacing, P/e = 10. The details of the rib and channel geometries and flow parameters are provided in the Table 4.

Table 4: Rib and channel geometries and flow parameters for the grid independence study

W	**H**	**W/H**	**w**	**e**	**w/e**	**P/e**	**α**	**Re**
0.051	0.051	1	0.0024	0.0024	1	10	90°	10,000 30,000 60,000

The square rib w/e = 1 is used as the baseline configuration. The height of the rib is 0.0024m. The Reynolds number of 10,000, 30,000 and 60,000 are considered for the analysis. A standard k-ω turbulence model is used. The normalized Nusselt number and normalized friction factor are calculated and compared with the experimental data. The wall y plus is also calculated for all the cases. Turbulent flows are significantly affected by the presence of the walls. The turbulence models require verification to make sure it is valid when used near walls. The near wall model is sensitive to the grid resolution which is assessed by the wall y plus. Hence it is required to consider the wall y plus when generated grid for flow involving turbulence or separation.

4.2 Details of the Grid

The independence study was performed for several grids but in this study we discuss the four types of grids. The details of each grid and mesh parameters are described below.

Grid-I is a basic coarse mesh. The computational view of the grid is shown in Figure 9. The edges are meshed first. The edges have an interval count of 40. Then the domain is meshed with a uniform mesh with an interval size of 0.4579 using mapping method. The near wall meshes are not refined. The main objective to generate a coarse mesh is to show how the near wall refinement affects the turbulent flow. Though we are aware that the standard k-ω turbulence model requires a fine mesh for a turbulent flow, the coarse mesh is included in this study to show how there is a significant variation in the results when compared with the experimental data.

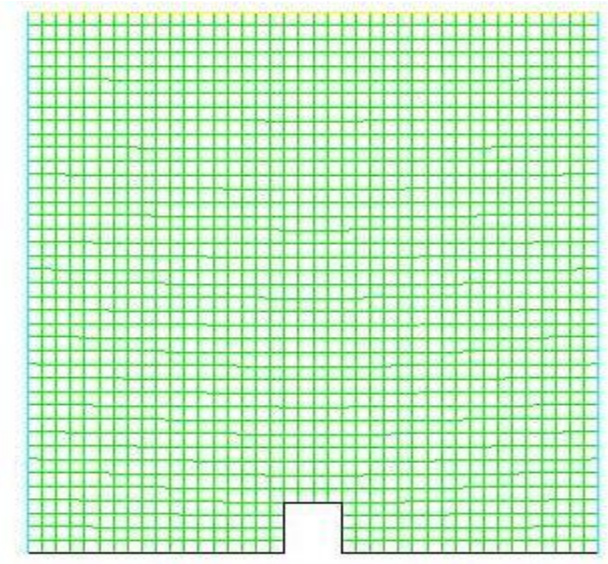

Figure 9: Computational View of Grid I – Coarse mesh

In Grid II, the domain is meshed with the use of size functions. The size functions controls the size of the mesh element edges. Though similar to boundary layer, they differ

with respect to the manner by which they are specified and they control the mesh. The size functions control the maximum edge element length. The details of the values used in size functions are described in Table 5.

A fixed type size function is used. The edges (*source*) are attached to the face (*attachment*). The source entity is the region where size function is applied and the attachment entity is the region that is affected by the size function. The *start size* is the mesh-element edge length in the region immediately adjacent to the source entity. The *growth rate* represents the increase in mesh-element edge length with each succeeding layer of elements. The *size-limit* specification represents the maximum allowable mesh-element edge length for the attachment entity.

Table 5: Size functions specifications

Factor	**Value**
Start Size	1 e-05
Growth rate	1.15
Max. size	0.001

The computational view of the grid is shown in Figure 10. The near wall meshes are finely refined. The region is meshed by the pave method. The separation of the flow can be captured by the use of this fine mesh.

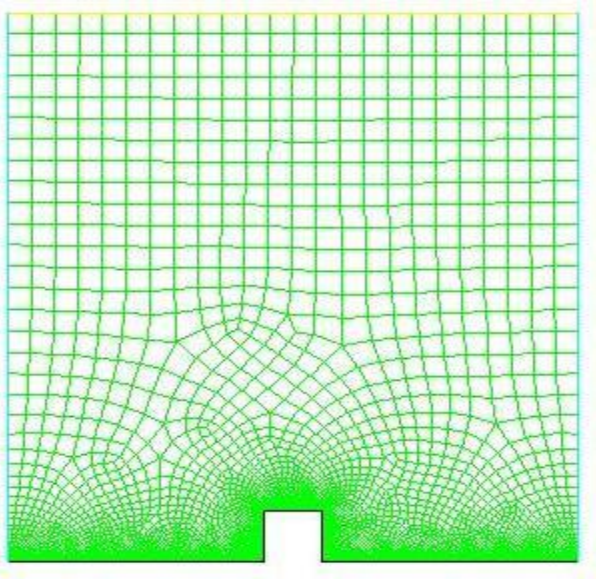

Figure 10: Computational View of Grid II – Fine mesh with size functions

Grid III was generated with the use of both size functions and boundary layer. Though the near wall meshes are refined, the region around the ribs develops a high wall Y plus values. This is because of the sudden change in shape along the flow. Enhanced wall treatment enables us to predict friction drag, separation etc. Though size functions and boundary layer control the meshes in a similar manner, the boundary layers prescribe specific mesh patterns. The boundary layer specifications are given in Table 6. The specifications of the size functions are same as described in Table 5.

Table 6: Boundary layer specifications

Factor	**Value**
First row	1 e-07
Growth factor	1.15
Number of rows	16

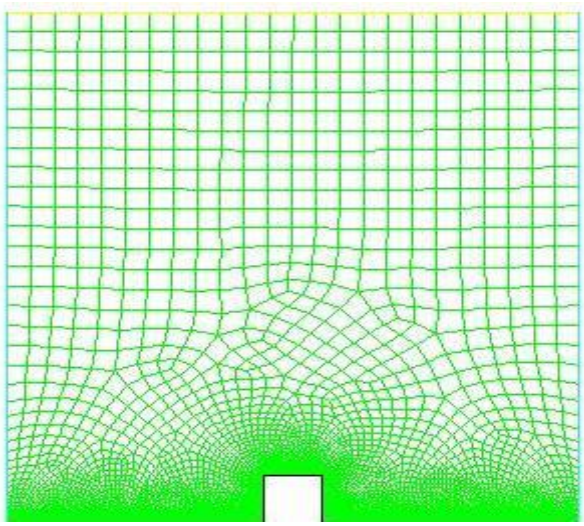

Figure 11: Computational view of Grid III – Fine mesh with boundary layer and size function

The computational view of the mesh is shown in Figure 11. The domain is meshed using the pave method. The number of elements is 49122. The region around the rib is finely meshed now. The internal continuity and wedge shape factor is enabled using the boundary layer option. By this, the sharp edges are removed and there is no sudden change in shape.

Grid IV again was created with size functions and boundary layer. In this case the same value of boundary layer as discussed in Table 6 is maintained but the values of size functions are varied. The start size for the size function in this case is 1 e-06. The computational view of the grid is provided in Figure 12. The elements near the rib are more clustered. The total number of elements is 57074.

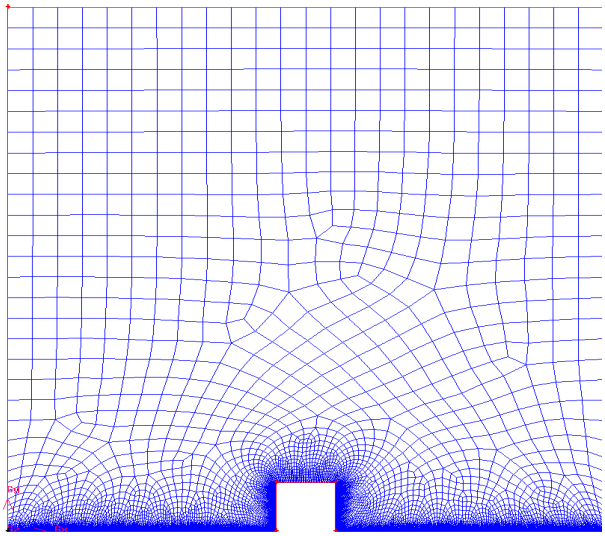

Figure 12: Computational view of Grid IV – Finer mesh with boundary layer and size function

4.3 Results and Discussion

The results for the normalized Nusselt number and normalized friction factor are provided only for the three grids. The Reynolds number of 10,000, 30,000 and 60,000 are used. The normalized Nusselt number and normalized friction factor are calculated. The calculated results are also compared with the experimental data. The Figure 13 shows a plot for normalized Nusselt number for various cases. The values are also tabulated and shown in Table 7.

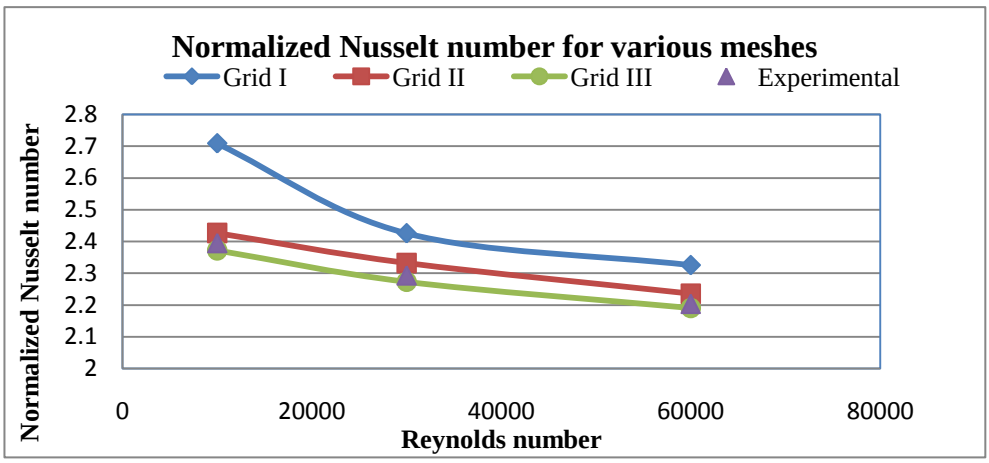

Figure 13: Normalized Nusselt number for various meshes at different Re.

The plot clearly shows the effect of mesh refinement. The grid I values are very high when compared with the experimental results. As described above, the near wall meshes are coarse and hence it failed to predict the separation and reattachment of the flow.

Table 7: Normalized Nusselt number for various meshes at various Re.

Reynolds number	Experimental data	Grid I (1684)	Grid II (23371)	Grid III (49122)	Grid IV (57074)
10,000	2.395	2.709	2.427	2.372	2.372
30,000	2.294	2.426	2.332	2.273	2.272
60,000	2.204	2.325	2.236	2.191	2.190

The error is as high as 13% for low Reynolds number and 6% for higher Reynolds number. Grid II provides results that are reasonable when compared with the

experimental data. The percentage error is less than 2% for all the Reynolds number. Grid III also provides us with good results. The values compare well with the experimental results. The percentage error is less than 1% for all the Reynolds number. The selection of the mesh cannot be identified by comparing only the Nusselt number. The values obtained from the analysis using Grid IV did not have a significant effect. The values were same as produced by Grid III. There was no significant change in the result and hence the option of using Grid IV was eliminated.

The velocity contours for all the meshes at Reynolds number is shown in the Figure 14.

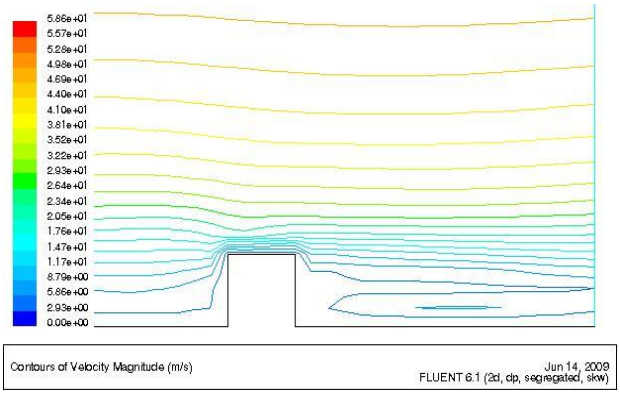

a

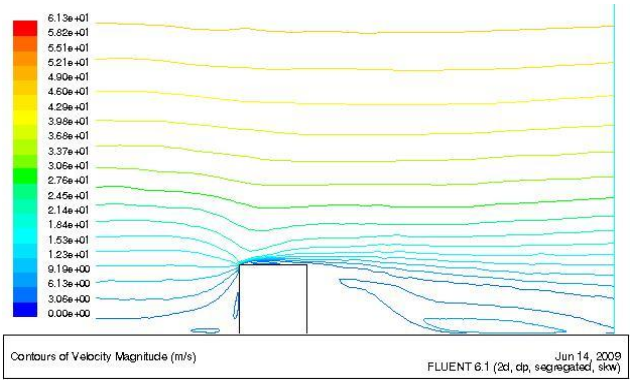

b

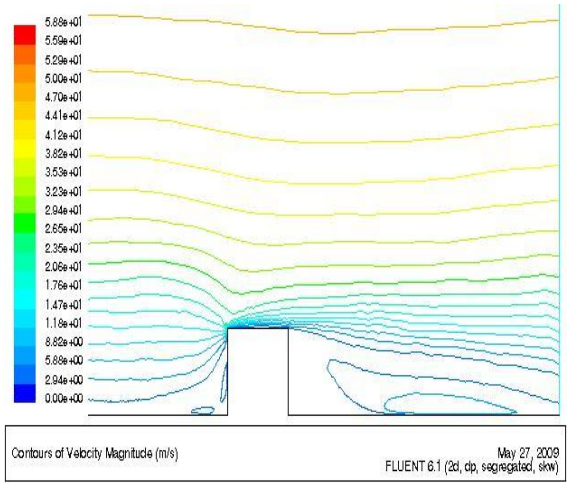

c

Figure 14: Velocity Contours for various meshes at Reynolds number 60,000,

a. Grid I, b. Grid II and c. Grid III

The velocity profile for grid I clearly indicates that the coarse mesh failed to predict the separation and reattachment in the flow. The profile is not smooth around and behind the rib region. The grid II and III have a smooth profile providing details of a separation flow. But the profile at the region near the nose of the rib varies. A sharp edge in grid II predicts more random flow than the smooth meshes in grid III. The profile is more clustered and hence there is some change in the velocity of the flow. It will be clearly evident when we compare the normalized friction factor. The normalized friction factor is calculated for all the meshes at different Reynolds numbers of 10,000, 30,000 and 60,000. The plot and values are provided in Figure 15 and Table 8 respectively.

Table 8: Normalized friction factor for various meshes at various Re.

Reynolds number	Experimental data	Grid I (1684)	Grid II (23371)	Grid III (49122)	Grid IV (57074)
10,000	3.954	1.657	3.274	3.847	3.847
30,000	4.229	1.848	3.749	4.077	4.079
60,000	5.005	1.985	4.287	4.853	4.855

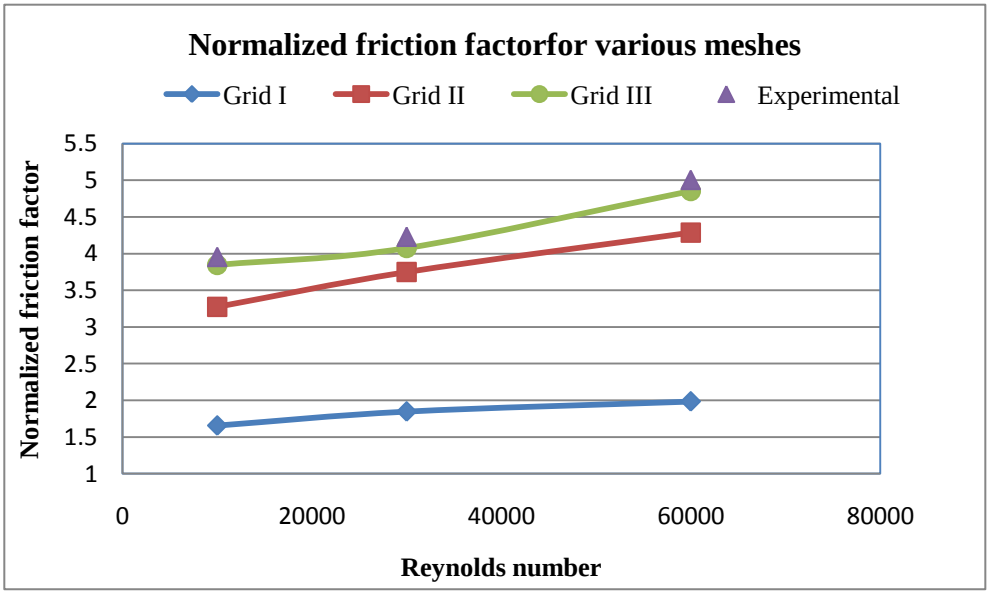

Figure 15: Normalized friction factor for various meshes at different Reynolds number

As described above, the value of pressure loss is very low in case of coarse mesh. The transition from laminar to turbulent is not recorded accurately and hence the low value in the friction factor. The comparison of friction factor for grid II and grid III with experimental results shows us a different pattern. The percentage error for grid II is as

high as 17% and the error for grid III is as low as 3%. Grid IV again had no significant effect on the results. The results clearly prove that enabling a smooth, integral continuity meshes predicts the recirculation better.

Also the wall Y plus is calculated for all the meshes. The ranges of values are provided in Table 9.

Table 9: Range of wall Y plus for various meshes at different Re.

Reynolds number	**Grid I**	**Grid II**	**Grid III**
10,000	>10	<2	<1
30,000	>25	>2.5	<1
60,000	>50	>5	<1

The value of wall Y plus for grid II is less than 1 throughout the wall except at the nose region of the rib. This is minimized in case of grid III. The value of wall Y plus is maintained below 1 even for higher Reynolds number. More compact, refined meshes are used in grid III and the effect is reflected in the results.

4.4 Conclusion

Three different meshes were generated for the study. Three parameters, Nusselt number, friction factor and wall Y plus are considered to study the effect of the grids. Grid I with coarse mesh failed to provide us with efficient results. The normalized

Nusselt number and normalized friction did not compare well with the experiment data and the wall Y plus was as high as 50. With the help of size functions, a refined grid II is created. Though the normalized Nusselt number values compared well, the normalized friction factor had more deviation when compared with the experiment data. The wall Y plus was controlled to a value less than 5 for high Reynolds number. The Grid III was generated with the help of both size functions and boundary layer. A well refined mesh was produced. The values of Nusselt number and friction factor agreed well with the experimental data. Grid IV again was generated with help of size functions and boundary layers. The results obtained with the help of Grid IV had no significant effect. The difference between the results from Grid III and Grid IV was almost zero. Also the computation time and cost increases due to the refinement of the meshes. Hence the option of Grid IV was ruled out. The wall Y plus values are maintained below 1 for all the Reynolds number. The refinement of mesh was concentrated only at the near wall region so as to decrease the computation time. The velocity contours are obtained and the pattern of the flow is observed. The grid III provides us with good results with a minimum error and hence is used for further investigation.

CHAPTER V

ANALYSIS OF HEAT TRANSFER IN STATIONARY SMOOTH CHANNEL

The main objective of the analysis is to validate the code to be used for further analysis. The heat transfer analysis for the smooth channel is performed with and without the periodic boundary condition for three types of flow: laminar, transition and turbulent. The Nusselt number is calculated for Reynolds numbers 600, 10,000, 30,000 and 60,000. The results are compared with the correlations used for flow through smooth tubes. The study also shows how the use of periodic boundary condition simplifies the computational work for analysis involving complex geometries.

The analysis consists of two parts. A smooth, long channel, with length ten times greater than the diameter ($L > 10d$) is used to predict the heat transfer in a fully developed region. A small portion of the channel at the fully developed region is picked to perform the analysis using periodic boundary condition. The average Nusselt number at the fully developed region is constant for any flow parameters at the fully developed region. The Nusselt number is calculated and the values are compared for both the cases. If the values are close enough, the use of periodic boundary condition is validated.

5.1 Computational Domain

As discussed before the analysis consists of two parts, Case a. Without periodic boundary condition and case b. With periodic boundary condition (PBC). The values of length and diameter for both the cases are provided in the Table 10.

Table 10: Range of parameters used in the analysis of smooth channel.

Case	Diameter, d (meters)	Length, L (meters)
Without PBC	0.2	8
With PBC	0.2	0.51

The computational domains for both the cases are shown in Figure 16. The boundary layer and size functions are used to refine the near wall region. The domain is meshed using pave method. The use of boundary layer and size functions are explained in detail in chapter IV.

5.2. Boundary Condition

The boundary condition of the present analysis is described in this section. For the analysis of smooth channel with no periodic condition (case a), the velocity inlet is applied at the entrance region and pressure outlet boundary condition is applied at downstream. For the analysis using periodic condition (case b), the mass flow rate is applied as the inlet condition at the periodic sides. For both the cases, a constant heat flux is applied at the wall region at no slip condition. The symmetry boundary condition ensures a simplified computational domain. The value of velocity and mass flow rate

varies with the Reynolds number and are provided in the Table 11. The boundary conditions used are pictorially showed along with the computational domain in Figure 16.

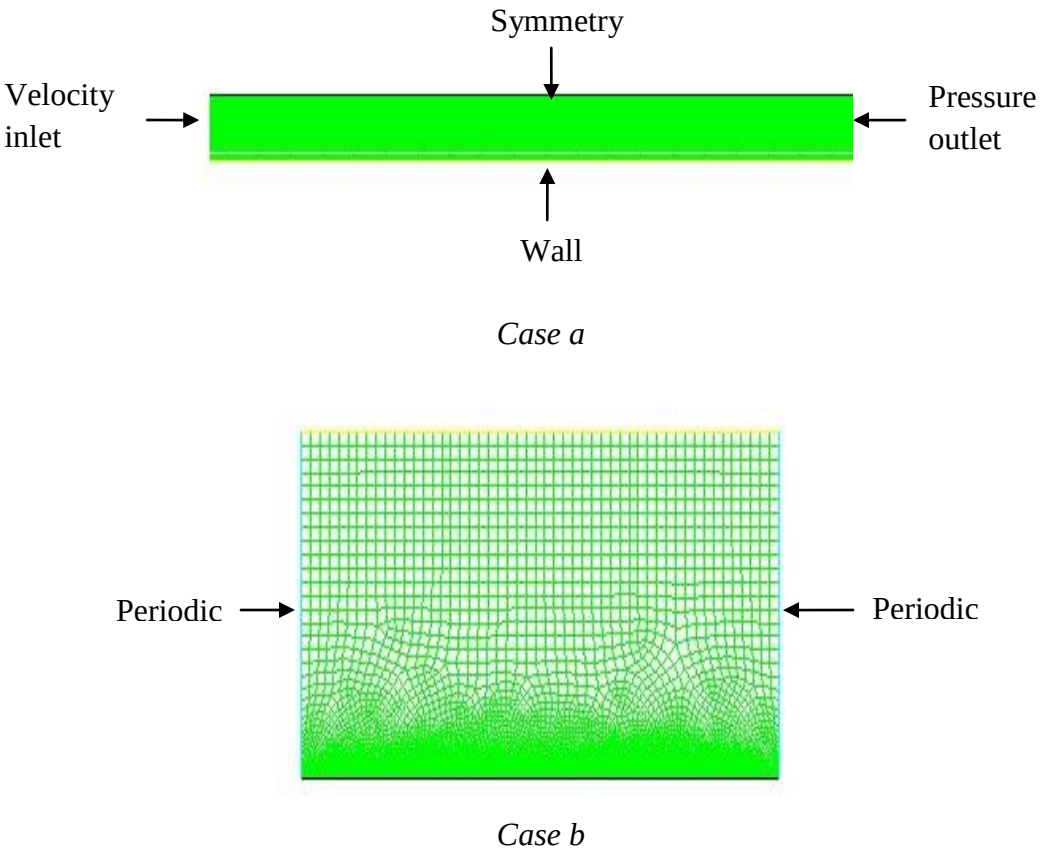

Figure 16: Computational domain for case a. without PBC and case b. with PBC

Table 11: Mass flow rate and velocity for various flow parameters in the study

Reynolds number	Velocity, V (m/s)	Mass flow rate, m (kg/s)
600	0.088	0.0013
10,000	1.461	0.021
30,000	4.382	0.062
60,000	8.764	0.125

5.3 Correlations

The empirical correlations provide us with an easy approach in calculation. The Nusselt number and friction factor calculated using computation is compared with the correlations. The correlations for fully developed laminar and turbulent flow in a smooth channel are provided in equations 1, 8 & 9. Though there are many correlations available in literature, the Dittus – Boelter equation and Gnielinski correlation are used in this study.

For fully developed flow in a circular tube subjected to a constant heat flux, the Nusselt number is a constant. There is no dependence in the Reynolds numbers. The value of Nusselt number is 4.36.

For fully developed turbulent flow in smooth tubes, a simple correlation called the Dittus – Boelter equation is used. Due to its simple nature, the equation is used by researchers to compare their experimental results.

The Nusselt number obtained from the previous correlation may give errors as high as 25 percent. The error can be reduced to as low as 5 percent by the use of Gnielinski correlation. Many literatures recommend us to use Gnielinski correlation as it is insensitive to the thermal condition applied at the surfaces. They can also be used to predict the friction loss and heat transfer coefficients for transition region with reasonable accuracy.

$$Nu = \frac{\left(f/8\right)(Re_D - 1000)\,Pr}{1.07 + 12.7\left(f/8\right)^{0.5}\left(Pr^{2/3} - 1\right)} \qquad (11)$$

The friction factor, f is calculated using the Petukhov correlation given by equation 9.

$$f = (0.79\ln(Re_D) - 1.64)^{-2} \qquad (12)$$

where,

f = friction factor

Re_D = Hydraulic diameter Reynolds number.

The values of Nusselt number for the fully developed turbulent flow is calculated using equations 1 and 8 and are provided in Table 12. As discussed, the Gnielinski correlation provides us with better results than the Dittus – Boelter equation. Since the values of Nusselt number is difficult to predict theoretically, the values calculated from both the correlations are compared with the computational results and the best correlation is picked based on the minimum percentage error.

Table 12: Nusselt number values calculated using correlations

Reynolds number	Nusselt number	
	Dittus – Boelter equation	**Gnielinski correlation**
10,000	31.786	30.028
30,000	76.547	70.822
60,000	133.276	121.035

5.4. Results and Discussion

The heat transfer performance for flow through smooth channel is analyzed and the results are provided in this section. Many research works shows us that the laminar flow is easily predictable, but the analysis involving transition and turbulent flow are difficult to predict. The flow nature varies drastically once it shifts from laminar to turbulent.

The results for analysis of channel without the periodic boundary condition (PBC) are discussed first. Figure 17 shows the velocity profile for flow through the smooth channel is provided at Reynolds number 10,000.

The Figure 17 shows that the flow becomes periodic after the length of 4 meters, in the downstream region of the tube. This is the fully developed region and the flow parameters are constant in this region. The heat transfer calculations are performed in the fully developed region. The Nusselt number is calculated for various Reynolds number and is provided in Table 13.

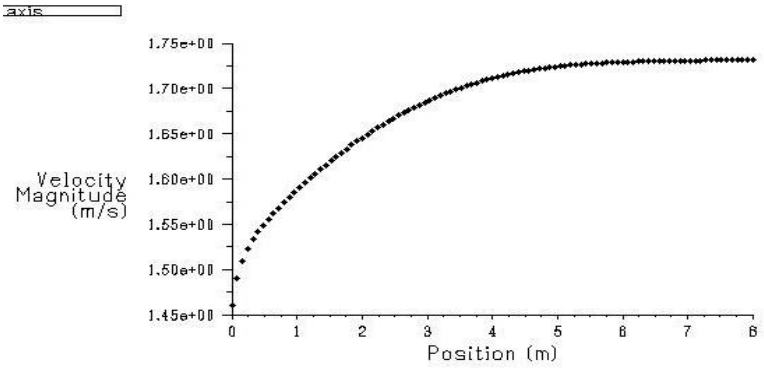

Figure 17: Velocity profile for smooth channel without PBC at Re. no. 10,000

Now, the analysis of the smooth channel with periodic boundary condition is discussed. A small portion in the fully developed region *i.e.* after the flow becomes periodic is picked and analysis is performed to calculate the Nusselt number. The results are provided in Table 13.

Table 13: Comparison of Nusselt number values for analysis of smooth channel with and without PBC and correlation.

Reynolds number	**Nusselt number**		
	Case a Without periodic condition	**Case b. With periodic condition**	**Correlation**
600	4.36	4.362	4.36
10,000	30.903	31.090	30.028
30,000	72.831	73.131	70.822
60,000	123.756	125.562	121.035

The computational results are compared with the Gnielinski correlation as it provides a much better result than the Dittus – Boelter equation. The Reynolds number 600 compares well with the correlation for both the cases. As discussed before, the laminar flow has no flow discrepancies and hence a closer result is obtained. The percentage error is less than 0.5 for both the cases.

The flow is in the transition region for Reynolds number 10,000 and 30,000. The results though difficult to predict, compares well with the correlation for both the cases. The error is less than 3 percent for all the cases. The Reynolds number 60,000 has an error of 2.2 and 3.7 percent for case a. and case b. respectively. Since the transition and turbulent flow are difficult to predict, the error of 2 to 4 is acceptable.

5.5. Conclusion

The analysis was performed with and without periodic condition. The analysis of smooth channel without periodic condition (case a) gave us a better result than the analysis with the periodic condition (case b). The percentage error when the case a. and case b. are compared is 0.6, 0.4 and 1.2 for Reynolds number 10,000, 30,000 and 60,000 respectively. Though the case with periodic condition provides us with results with slight deviation, it is acceptable when the computation time and size of the domain are taken into consideration. Thus it is concluded that the use of periodic condition did not affect the results by a large margin and will have an error of ± 2 percent.

CHAPTER VI

EFFECT OF RIB SPACING ON THE HEAT TRANSFER PERFORMANCE OF THE CHANNELS

With the turbulence model determined, the suitable approach for the analysis identified and the optimum grid picked out, the fluent code is validated now. The code is validated by comparing the acquired data with the experimental results. In this chapter, the numerically results are obtained for channels with square ribs and are compared with the experimental results. The velocity contours are obtained for various cases to study the details of the flow pattern. Normalized Nusselt number is obtained to the study the heat transfer performance and the normalized friction factor is obtained to study the pressure and friction loss.

6.1 Effect of Rib Spacing in Square Channel

The computation analysis is performed in a 1:1 square channel with ribs. The ribs have a configuration of $e/D_h = 0.048$. The value of $e/H = 0.048$ and $e/W = 0.048$. The analysis was conducted for Reynolds number of 10,000, 30,000 and 60,000.

The rib geometries for the analysis for a square channel are shown in the Table 14. A constant heat flux of 2500 W/m^2 is applied at the wall for the Reynolds number 10,000, 30,000 and 60,000 respectively. The inlet bulk temperature is 298K.

Table 14: Rib geometries for the square channel with w/e = 1

W	H	W/H	e	w	P/e	Re	α
0.051	0.051	1	0.0024	0.0024	10 20	10,000 30,000 60,000	90°

The local Nusselt number is obtained for the all the Reynolds number at rib spacing, P/e = 10. The values are calculated and plotted in Figure 18.

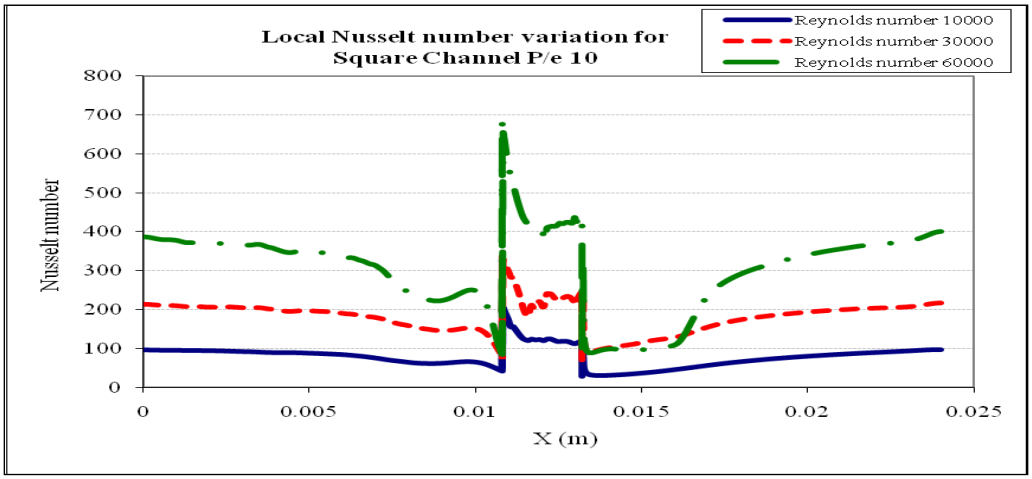

Figure 18: Local Nusselt number variation for square channel with w/e = 1 and rib spacing, P/e = 10 at different Reynolds numbers.

The local Nusselt number increases as the flow separates decreases as the flow reattaches and again increases as it approaches the next rib. There is a drastic increase in Nusselt number due to the presence of the rib. The rib induces a turbulence flow which causes more heat transfer in the region. The Nusselt number almost doubles once it reaches the rib region. But as the flow reattaches, behind the rib is a void zone which causes a decrease in heat transfer. This is the reason for a decrease in the Nusselt number. The pattern remains the same for all the Reynolds numbers.

Though the pattern remains the same, the values of the Nusselt number increases as the Reynolds number increases. The Nusselt number variation is different for the regions before and behind the ribs. The Nusselt number values are higher for high Reynolds number before the rib. But there is a slight variation in the values behind the rib. The values for Reynolds number 10,000 remains low. But the values for Reynolds number 60000 is slightly lower than the values for Reynolds number 30,000 just before the reattachment. The curve again increases after the reattachment. This is unique for the square channel with a rib spacing, P/e = 10. This reason is attributed to the combined effect of the narrow channel aspect ratio, Reynolds number and the placement of the rib.

The thick boundary layer behind the rib causes the velocity to decrease. This decreases the heat transfer coefficient and hence the Nusselt number ratio. But as the flow reattaches, the heat transfer coefficient increases and hence high Nusselt number values.

The rib spacing has an effect on the Nusselt number and heat transfer. The local Nusselt number plot for a square channel with rib spacing, P/e = 20 is shown in Figure 19. The values are plotted for Reynolds number 10,000, 30,000 and 60,000.

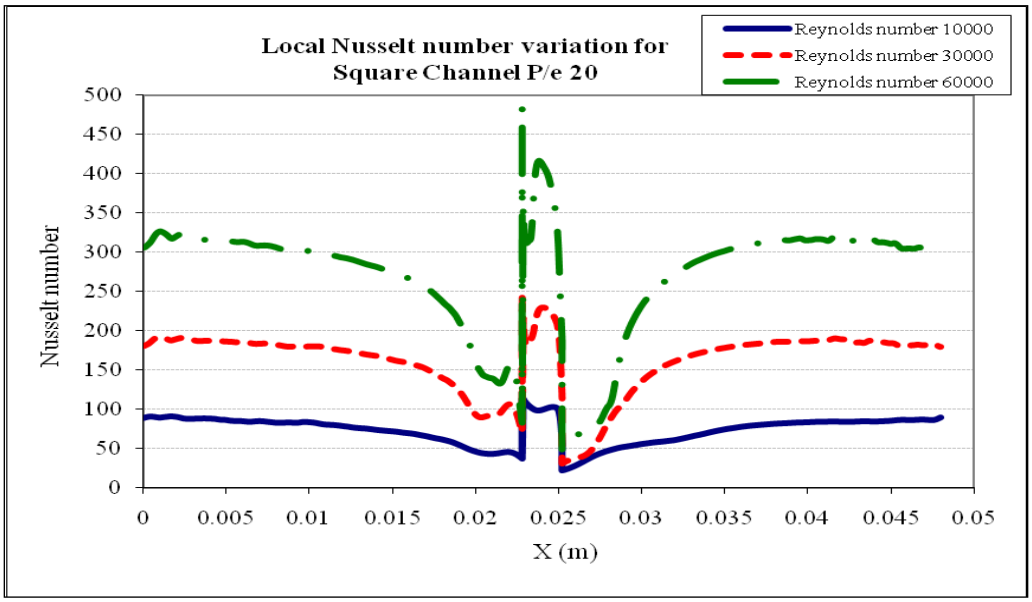

Figure 19: Local Nusselt number variation for square channel with w/e =1 and rib spacing, P/e = 20 at different Reynolds numbers.

The Nusselt number pattern for rib spacing 20 is similar to that of P/e = 10, except that the values of the Nusselt number remains high for higher Reynolds number throughout the region. The reason is because of the wider rib spacing. Also the values of Nusselt number is lower than the values for rib spacing, P/e = 10. It creates a thicker boundary layer after the flow reattaches between the ribs. The flow reattaches faster for P/e = 20 than P/e = 10.

The wider rib spacing decreases the heat transfer performance of the ribbed channel. The analysis is performed using a periodic boundary condition and it is difficult to compare the local Nusselt number with the experiment data. The results are thus

averaged and compared with the experimental results. The normalized Nusselt number is calculated and compared with the experimental results to study the heat transfer performance. The values are plotted and are shown in Figure 20. The values are also tabulated and provided in Table 15.

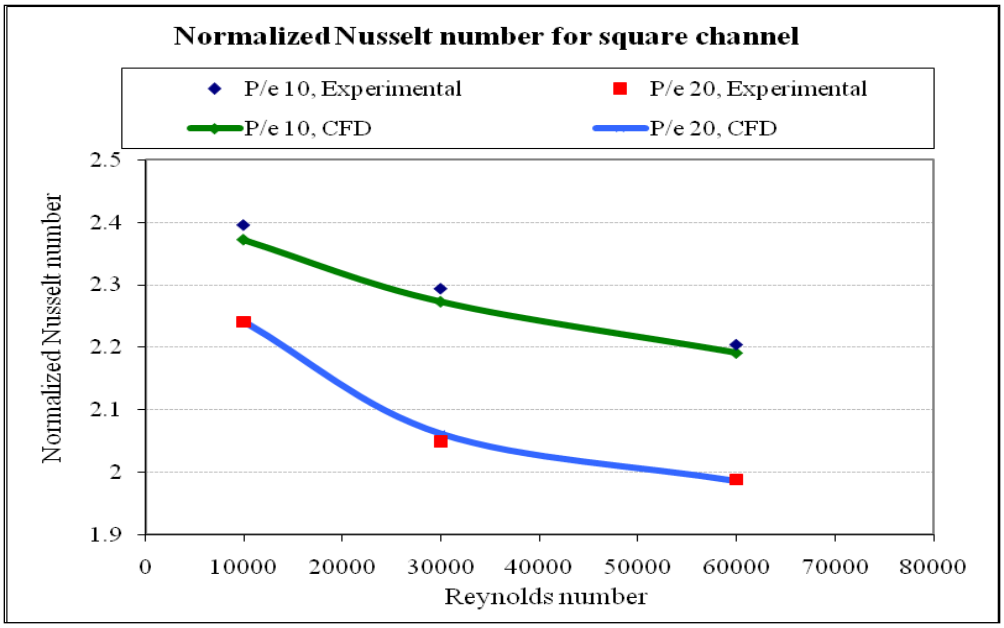

Figure 20: Normalized Nusselt number for square channel with w/e = 1 and rib spacing, P/e = 10 and P/e = 20

The values of normalized Nusselt number decreases as the Reynolds number increases. Also the values are lower for P/e = 20 than P/e = 10. As discussed above, the decrease in values is because of the wider rib spacing and the influence of the adjacent periodic ribs.

Table 15: Normalized Nusselt number for square channel with w/e = 1

Reynolds number	P/e = 10, Exp.	P/e = 10, CFD	P/e = 20, Exp.	P/e = 20, CFD
10,000	2.396	2.372	2.241	2.248
30,000	2.294	2.273	2.049	2.061
60,000	2.204	2.191	1.988	1.985

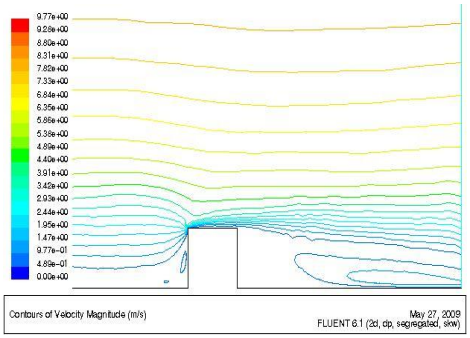

a

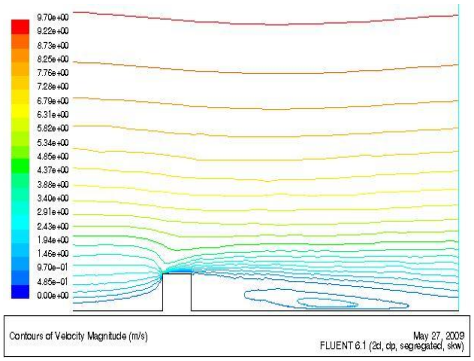

d

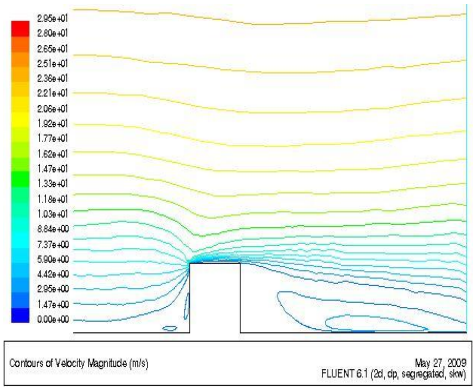

b

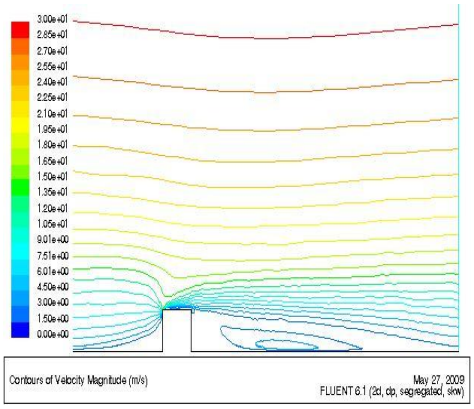

e

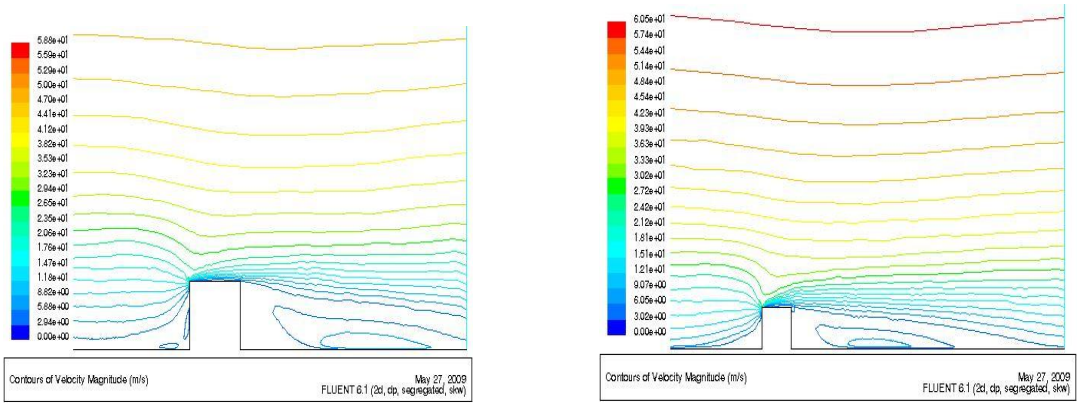

c **f**

Figure 21: Velocity contours showing separation and reattachment for square channel with w/e =1, P/e = 10 a) Reynolds number 10,000 b) Reynolds number 30,000 c) Reynolds number 60,000 and P/e = 20 d)Reynolds number 10,000 e) Reynolds number 30,000 f) Reynolds number 60,000

The computational results compare well with the experiment results. The percentage error is less than 2%. To explain the variation in the Nusselt number values the velocity contours are plotted and shown in Figure 21.

The Figure 21 a, b and c shows the velocity contours for rib spacing, P/e = 10 and Figure 21 d, e and f shows the velocity contours for rib spacing, P/e = 20. The flow pattern is evident from these figures. As the rib spacing widens the flow reattaches faster before reaching the next rib. The flow is along the wall and this eventually causes a decrease in the velocity. The normalized Nusselt number values are calculated based on the Nusselt number for a smooth tube. The values for the smooth tubes doubles as the Reynolds number increases. But with the presence of the rib, the flow pattern changes creating a separation bubble. A boundary layer is formed creating a recirculation zone. This zone has a lower heat transfer rates. The higher Reynolds number creates a thicker boundary layer causing a lower heat transfer zone. The flow also reattaches at a faster rate as the Reynolds number increases.

The values of average Nusselt number is provided for smooth channel and ribbed square channel. As mentioned before, the Nusselt number values increases as the Reynolds number increases. But the rate of increase in Nusselt number for the smooth channel is higher than the ribbed square channel. Nusselt number for the ribbed channel is then normalized using the values for smooth channel. Thus the values of normalized Nusselt number decrease as the Reynolds number increases. This is clearly shown in Figure 22.

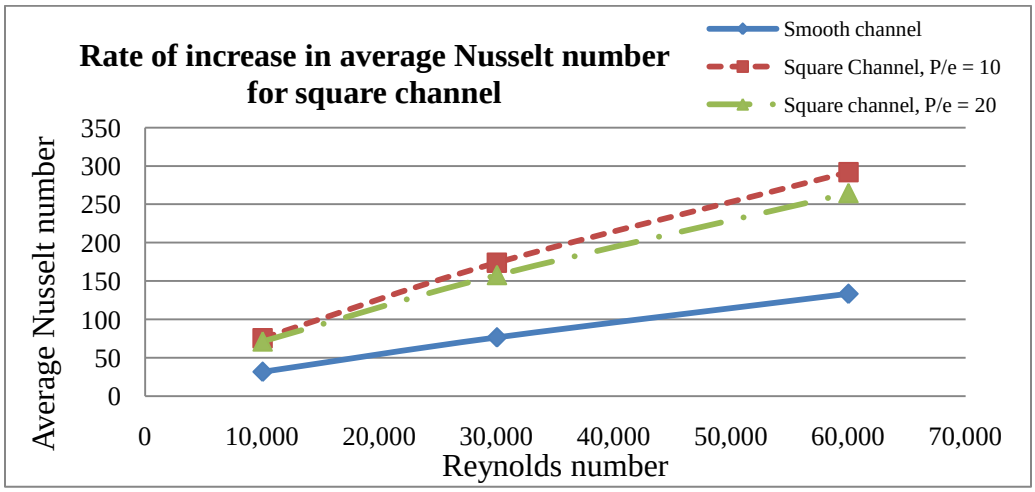

Figure 22: Rate of increase in average Nusselt number for Square channel.

As we can see from the plot that the ribbed channel produced a high heat transfer rate than the smooth channel. The average Nusselt number values are also tabulated in Table 16. The Nusselt number for the ribbed channel is two - three times higher than the smooth channel for respective Reynolds number.

Also the average Nusselt number value for P/e = 10 is higher than P/e = 20. As mentioned before, the wide rib spacing creates a thick boundary layer and a wider recirculation zone. The heat transfer rates decrease and hence the values of the Nusselt number decrease.

Table 16: Average Nusselt number values for Square channel at P/e = 10 & 20.

Reynolds number	**Smooth channel**	**Square Channel**	
		P/e = 10	**P/e = 20**
10,000	31.786	75.409	71.258
30,000	76.547	173.995	157.788
60,000	133.276	291.998	264.583

The rate of increase in Nusselt number is high for smooth channel than the ribbed channel. The rate of increase of Nusselt number form Reynolds number 10,000 to Reynolds number 30,000 is 1.41 for smooth channel, 1.30 for square channel with P/e = 10 and 1.21 for square channel with P/e = 20. Thus the rate of increase in value is low for ribbed channel. Also the rate of increase of Nusselt number form Reynolds number 30,000 to Reynolds number 60,000 is 0.75 for smooth channel, 0.69 for square channel with P/e = 10 and 0.67 for square channel with P/e = 20. Thus as the Reynolds number increases the rate of increase is low and this is the reason why the values of the normalized results for square channel decrease as the Reynolds number increases.

The performance of the channel cannot be judged only with their heat transfer characteristics. The friction drag and pressure loss should also be taken into account. The normalized friction factor is plotted in the Figure 23.

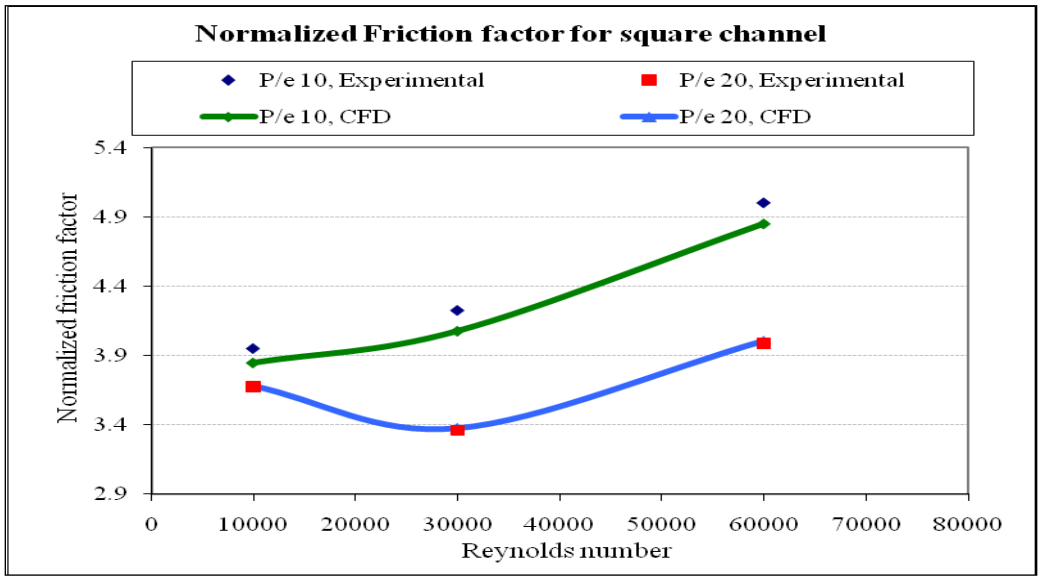

Figure 23: Normalized friction factor for square channel with w/e =1 and rib spacing, P/e = 10 and P/e = 20

The values for the normalized friction factor are also tabulated and are provided in Table 17.

Table 17: Normalized friction factor for square channel w/e = 1

Reynolds number	**P/e = 10, Exp.**	**P/e = 10, CFD**	**P/e = 20, Exp.**	**P/e = 20, CFD**
10,000	3.954	3.847	3.675	3.680
30,000	4.229	4.077	3.361	3.377
60,000	5.005	4.853	3.987	4.006

The normalized friction factor shows a different trend. Unlike the normalized Nusselt number, the normalized friction factor values increase with increasing Reynolds number. The pattern remains the same with increasing rib spacing. The friction factor decreases with increasing rib spacing. The decrease in friction factor ratio is because of the lower pressure loss across the section. The flow reattachment is faster and there is no secondary flow in the case of larger rib spacing. Though the friction factor decreases, the heat transfer performance also decreases for wider rib spacing.

There is one exception in the case of Reynolds number 30,000 for rib spacing P/e = 20. Unlike other profile, the normalized friction factor for square channel with rib spacing P/e = 20 at Reynolds number 30000 is lower than at Reynolds number 10,000 and 60,000. This is because the flow reattaches at a distance smaller than for other Reynolds numbers. This can be viewed in the Figure 21. e. This case in interesting as the heat transfer is high with a less compensation in the friction loss. Before we conclude at any remarks, the other ribbed channels should also be studied.

6.2. Effect of Rib Spacing in Rectangular Channel I

The computation analysis is performed in a 2:1 rectangular channel I with ribs. The ribs have a configuration of $e/D_h = 0.048$. The value of $e/H = 0.06275$ and $e/W = 0.032$. The analysis was conducted for Reynolds number of 10,000, 30,000 and 60,000 in order to examine the effect of aspect ratio. The height of the rib is maintained constant at 0.0032m.

The rib geometries for the analysis for a rectangular channel-I is shown in the Table 18. A constant heat flux of 2500 W/m^2 is applied at the wall for the Reynolds number 10,000, 30,000 and 60,000 respectively.

Table 18: Rib geometries for Rectangular Channel I with w/e = 1

W	H	W/H	e	w	P/e	Re	α
0.102	0.051	2	0.0032	0.0032	10 20	10,000 30,000 60,000	90°

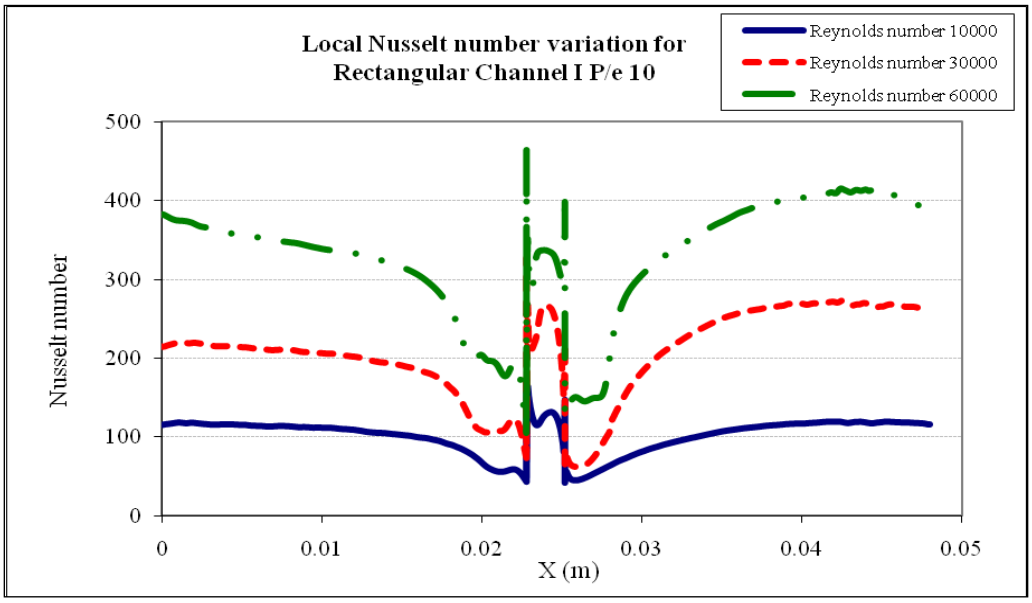

Figure 24: Local Nusselt number variation for rectangular channel I with w/e =1 rib spacing, P/e = 10 at different Reynolds numbers.

The local Nusselt number is obtained for the all the Reynolds number at rib spacing, P/e = 10. The values are calculated and plotted in Figure 24.

The local Nusselt number is plotted for Reynolds number 10,000, 30,000 and 60,000. The pattern is the same as that for the square channel with P/e = 10. The Nusselt number increases as the flow separates decreases and again increases as the flow reaches the next rib. The value of the Nusselt number again is doubled as the Reynolds number increases. In this case, the Nusselt number remains high for higher Reynolds number throughout the domain. This again is because of the wider channel aspect ratio than the square channel.

The rib spacing has an effect on the Nusselt number and heat transfer. The local Nusselt number plot for a square channel with rib spacing, P/e = 20 is shown in Figure 25. The values are plotted for Reynolds number 10,000, 30,000 and 60,000.

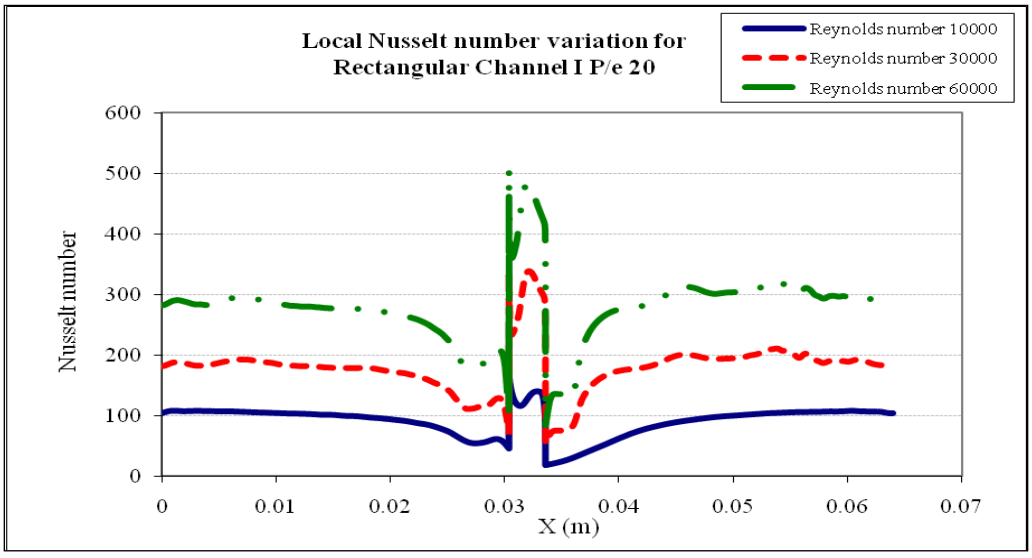

Figure 25: Local Nusselt number variation for rectangular channel I with w/e = 1, rib spacing, P/e = 20 at different Reynolds numbers.

The plot follows the same trend as the Nusselt number variation for a square channel with P/e = 20. The Nusselt number pattern for rib spacing 20 is similar to that of P/e = 10. The values of Nusselt number is lower than the values for rib spacing, P/e = 10. The reason is the same as the flow reattaches faster for P/e = 20 than P/e = 10.

The wider rib spacing decreases the heat transfer performance of the ribbed channel. The results are averaged and compared with the experimental results for the reason mentioned above. The normalized Nusselt number is calculated and compared with the experimental results to study the heat transfer performance. The values are plotted and are shown in Figure 26.

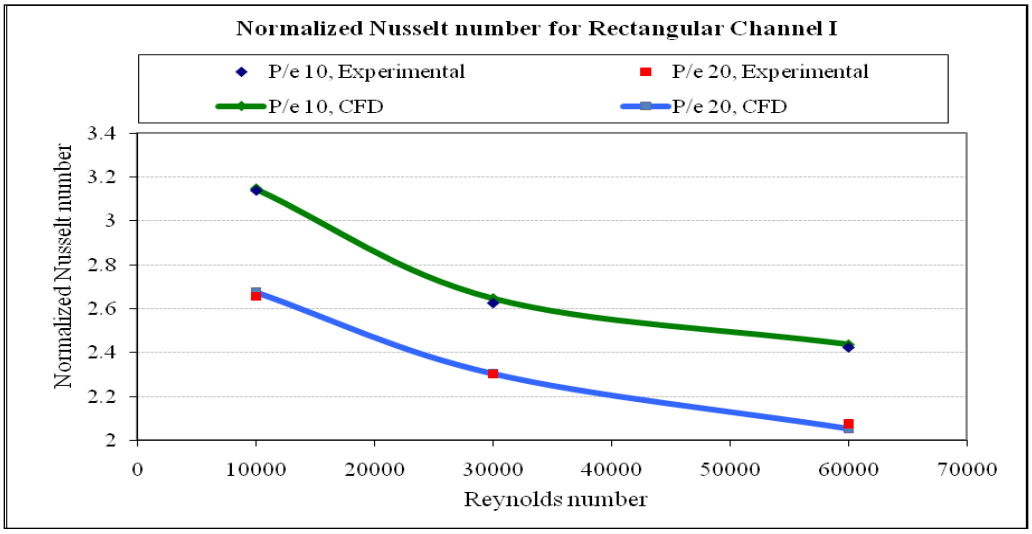

Figure 26: Normalized Nusselt number for rectangular channel I with w/e = 1, rib spacing, P/e = 10 and P/e = 20

The plot gives a clear picture of the effect of Reynolds number and rib spacing on the heat transfer performance. The value of normalized Nusselt number decreases with increasing Reynolds number. Also as the rib spacing increases, the value of the

normalized Nusselt number decreases. The reason as already mentioned is the distance by which the flow separates and reattaches and the size of the separation region.

The values are given in the Table 19. The numerical results compare well with the experimental data. The percentage error is just 1% with respect to the experiment values.

Table 19: Normalized Nusselt number for rectangular channel-I w/e = 1

Reynolds number	**P/e = 10, Exp.**	**P/e = 10, CFD**	**P/e = 20, Exp.**	**P/e = 20, CFD**
10,000	3.140	3.149	2.657	2.677
30,000	2.626	2.648	2.303	2.305
60,000	2.423	2.439	2.076	2.053

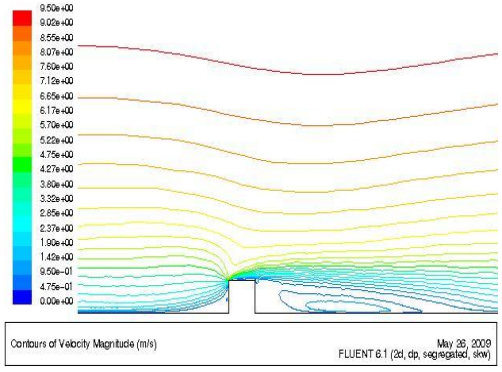

a

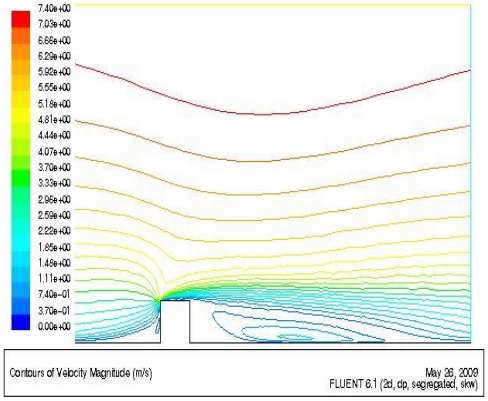

d

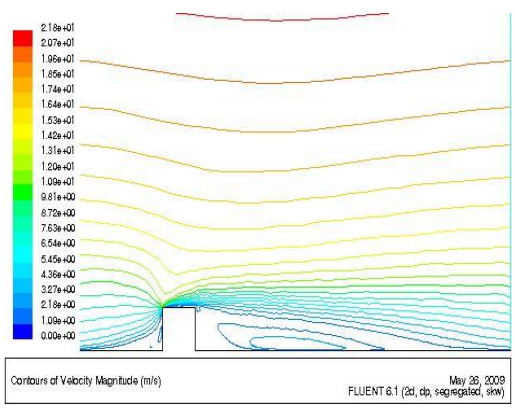

b

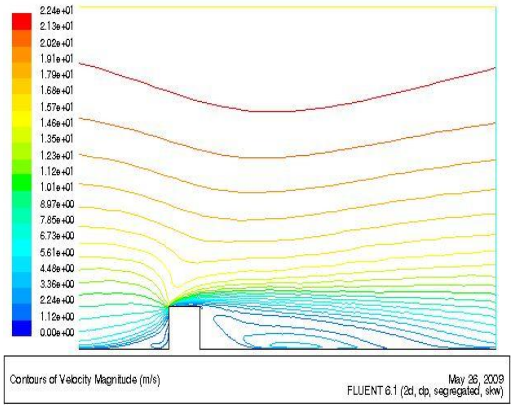

e

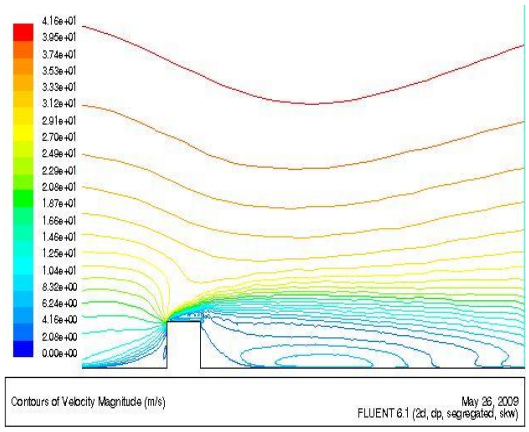

c

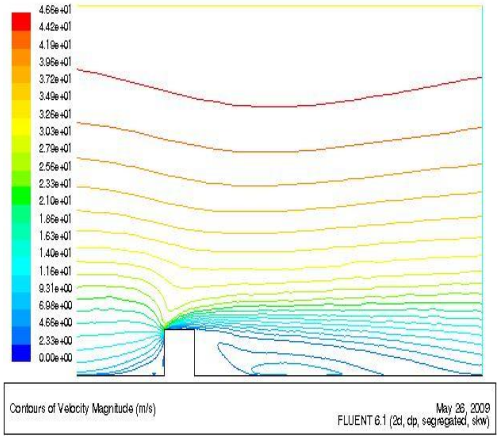

f

Figure 27: Velocity contours showing separation and reattachment for rectangular channel I with w/e = 1, P/e = 10 a) Reynolds number 10,000 b) Reynolds number 30,000 c) Reynolds number 60,000 and P/e = 20 d)Reynolds number 10,000 e) Reynolds number 30,000 f) Reynolds number 60,000

The velocity contours are shown to provide details of the flow pattern and the effect of Reynolds number and rib spacing. The Figure 27 a, b and c shows the velocity contours for rib spacing, P/e = 10 and Figure 27 d, e and f shows the velocity contours for rib spacing, P/e = 20. The flow pattern is similar to that of the square channel. The details and the causes are already explained and discussed in detail in the previous section. However the value of Nusselt number changes. The values are higher when compared to

that for the square channel. In fact the rectangular channel I provide us with a higher heat transfer performance for any Reynolds number.

The values of average Nusselt number is provided for smooth channel and ribbed rectangular channel I. The pattern is similar as explained for square channel. As mentioned before, the Nusselt number values increases as the Reynolds number increases. But the rate of increase in Nusselt number for the smooth channel is higher than the ribbed rectangular channel I. This is clearly shown in Figure 28.

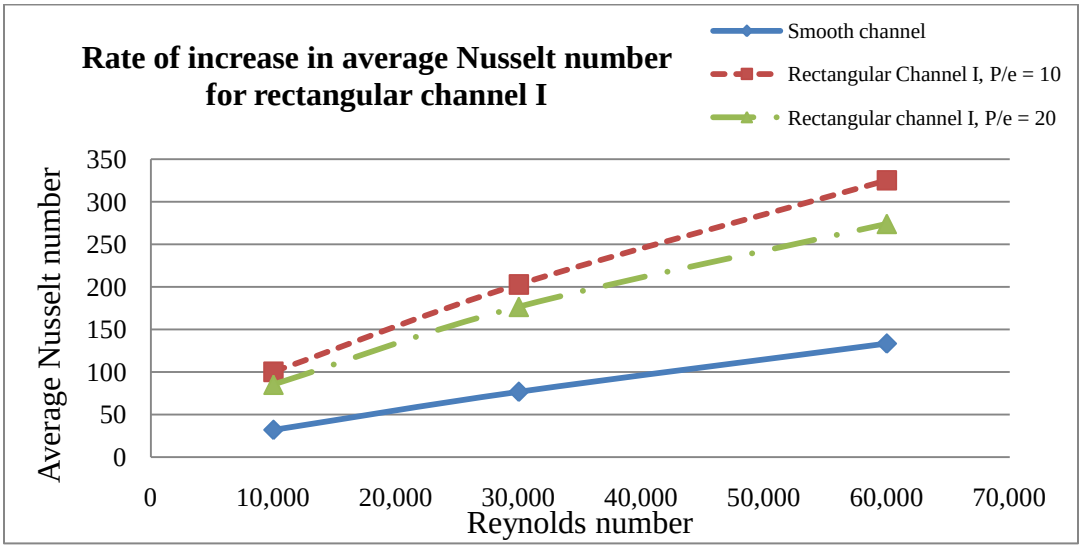

Figure 28: Rate of increase in average Nusselt number for Rectangular channel I

As we can see from the plot that the ribbed channel produced a high heat transfer rate than the smooth channel. The average Nusselt number values are also tabulated in Table 20. The Nusselt number for the ribbed channel is three times higher than the smooth channel for respective Reynolds number.

Also the average Nusselt number value for P/e = 10 is higher than P/e = 20. The pattern is same as in case of square channel. As mentioned before, the wide rib spacing creates a thick boundary layer and a wider recirculation zone. The heat transfer rates decrease and hence the values of the Nusselt number decrease.

Table 20: Average Nusselt number values for rectangular channel I at P/e = 10 & 20.

Reynolds number	**Smooth channel**	**Rectangular channel I**	
		P/e = 10	**P/e = 20**
10,000	31.786	100.092	85.093
30,000	76.547	202.748	176.437
60,000	133.276	325.031	273.753

The rate of increase in Nusselt number is high for smooth channel than the ribbed channel. The rate of increase of Nusselt number form Reynolds number 10,000 to Reynolds number 30,000 is 1.41 for smooth channel, 1.02 for rectangular channel I with P/e = 10 and 1.07 for rectangular channel I with P/e = 20. Thus the rate of increase in value is low for ribbed channel. Also the rate of increase of Nusselt number form Reynolds number 30,000 to Reynolds number 60,000 is 0.75 for smooth channel, 0.61 for rectangular channel I with P/e = 10 and 0.55 for rectangular channel I with P/e = 20. Thus as the Reynolds number increases the rate of increase in Nusselt number is low.

The friction and pressure loss is also studied. The values for the normalized friction factor are given in the Table 21.

Table 21: Normalized friction factor for rectangular channel I w/e = 1

Reynolds number	**P/e = 10, Exp.**	**P/e = 10, CFD**	**P/e = 20, Exp.**	**P/e = 20, CFD**
10,000	5.209	5.178	4.111	4.105
30,000	6.784	6.725	5.313	5.285
60,000	7.943	7.788	6.919	6.858

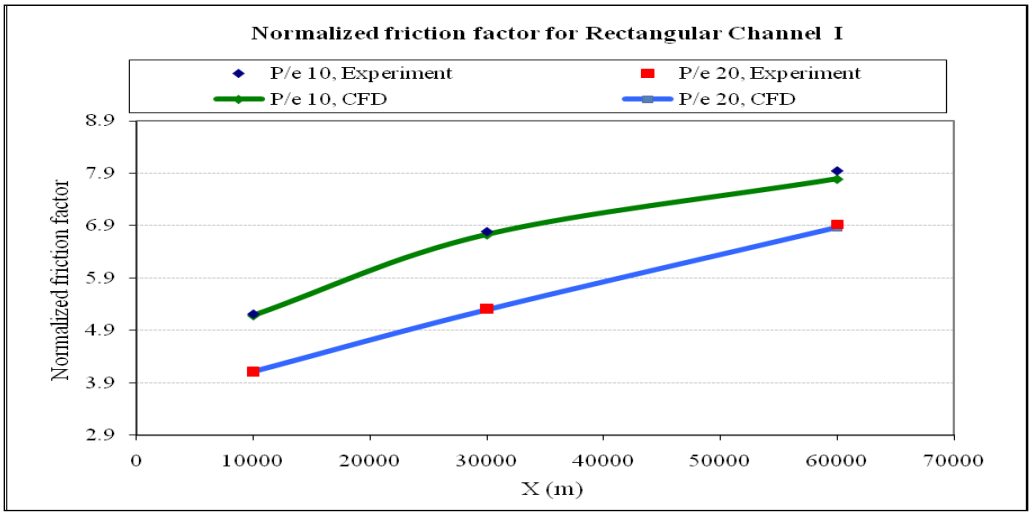

Figure 29: Normalized friction factor for rectangular channel I with w/e = 1, rib spacing, P/e = 10 and P/e = 20

The values are also plotted and are shown in Figure 29. The plot is similar to that of a square channel. The normalized friction factor increases as the Reynolds number

increases. The normalized friction factor also decreases as the rib spacing increases for the same Reynolds number.

For the case P/e = 20 and Reynolds number 30,000, the normalized friction factor do not decrease as in the case of the square channel. The reason is because of a wider rib channel. The rib induces a secondary flow which causes more pressure loss across the section than the square channel. So the normalized friction factor increases as the channel width increases. The channel width influences the mass flow rate which in turn affects the pressure loss.

The rectangular channel I not only provide high heat transfer performance but also have a high pressure loss ratio. Further investigation on channel aspect ratio is required so as to conclude with the final result. The rectangular channel II is studied in the next section.

6.3. Effect of Rib Spacing in Rectangular Channel II

The computation analysis is performed in a 4:1 rectangular channel II with ribs. The ribs have a configuration of e/D_h = 0.048. The value of e/H = 0.01255 and e/W = 0.048. The analysis was conducted for Reynolds number of 10,000, 30,000 and 60,000 in order to examine the effect of aspect ratio. The height of the rib is maintained constant at 0.0032m.

The rib geometries for the analysis for a rectangular channel-II are shown in the Table 22. A constant heat flux of 2500 W/m^2 is applied at the wall for the Reynolds number 10,000, 30,000 and 60,000 respectively.

Table 22: Rib geometries for Rectangular Channel II with w/e = 1

W	H	W/H	e	w	P/e	Re	α
0.102	0.0255	4	0.0032	0.0032	10 20	10,000 30,000 60,000	90°

The local Nusselt number is obtained for the all the Reynolds number at rib spacing, P/e = 10. The values are calculated and plotted in Figure 30. The local Nusselt number is plotted for Reynolds number 10,000, 30,000 and 60,000. The pattern is the same as that for the square channel and rectangular channel I with P/e = 10. The Nusselt number increases as the flow separates decreases and again increases as the flow reaches the next rib. The value of the Nusselt number again is doubled as the Reynolds number increases. The Nusselt number remained high like that of the rectangular channel I for higher Reynolds number throughout the domain. This again is because of the wider channel aspect ratio than the square channel.

The rib spacing has an effect on the Nusselt number and heat transfer. The local Nusselt number plot for a square channel with rib spacing, P/e = 20 is shown in Figure 31. The values are plotted for Reynolds number 10,000, 30,000 and 60,000.

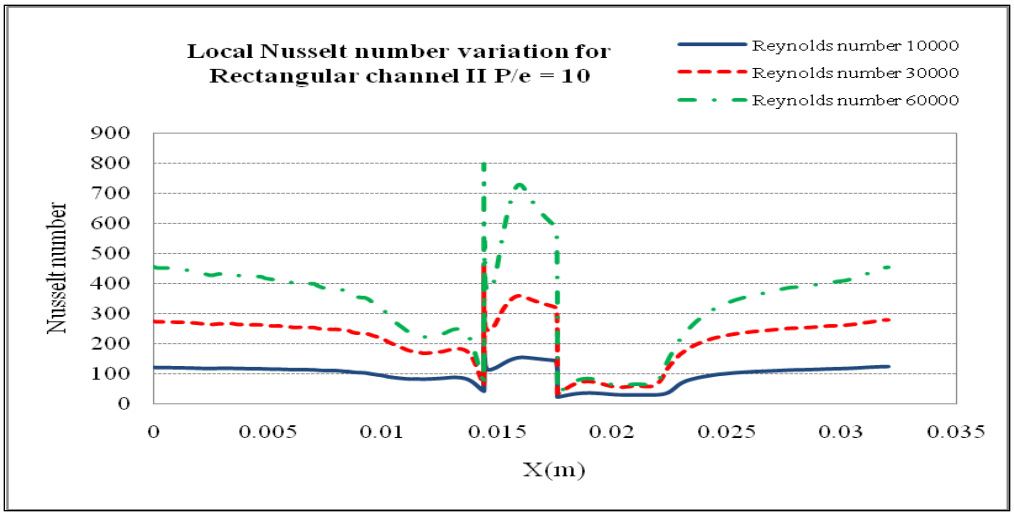

Figure 30: Local Nusselt number variation for rectangular channel II with w/e = 1, rib spacing, P/e = 10 at different Reynolds numbers**.**

The plot follows the same trend as the Nusselt number variation for a rectangular channel-I with P/e = 20. The values of Nusselt number is lower than the values for rib spacing, P/e = 10 for the same reason explained in the previous section. The wider rib spacing decreases the heat transfer performance of the ribbed channel.

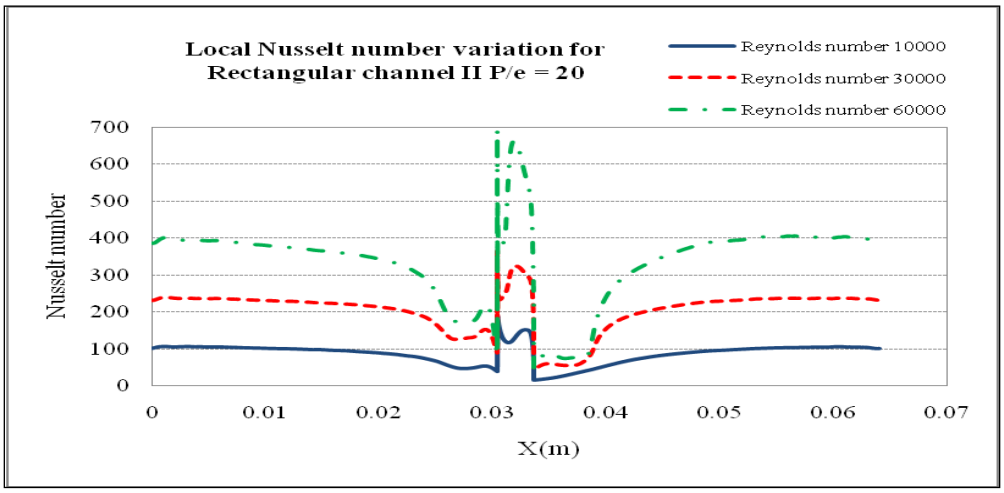

Figure 31: Local Nusselt number variation for rectangular channel II with w/e = 1, rib spacing, P/e = 20 at different Reynolds numbers.

The results are averaged and compared with the experimental results for the reason mentioned above. The normalized Nusselt number is calculated and compared with the experimental results to study the heat transfer performance. The values are plotted and are shown in Figure 32.

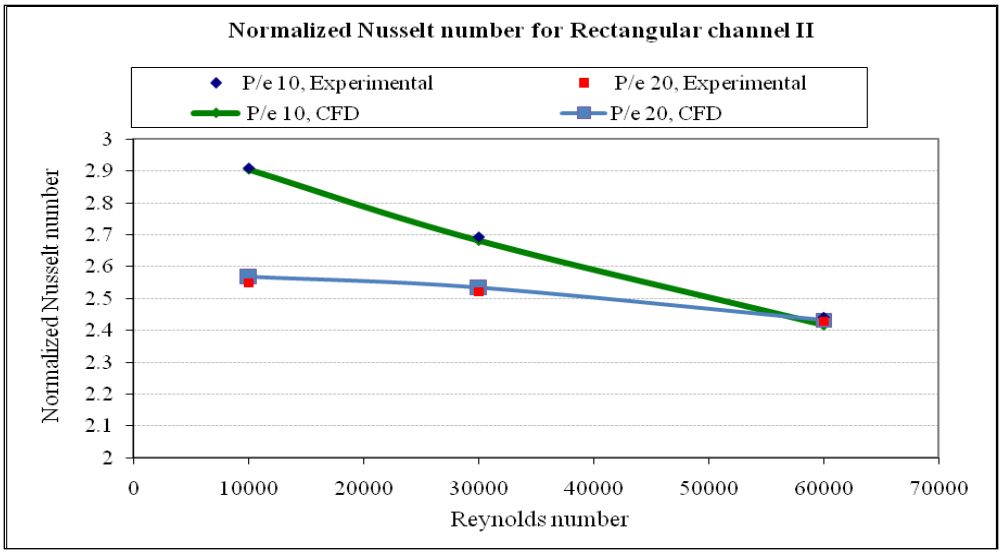

Figure 32: Normalized Nusselt number for rectangular channel II with w/e =1, rib spacing, P/e = 10 and P/e = 20

Figure 32 provides us with details of the effect of Reynolds number and rib spacing on the heat transfer performance. The value of normalized Nusselt number decreases with increasing Reynolds number. Also as the rib spacing increases, the value of the normalized Nusselt number decreases.

The values are given in the Table 23. The numerical results compare well with the experimental data. The percentage error is just 1% with respect to the experiment values.

Table 23: Normalized Nusselt number for rectangular channel-II w/e = 1

Reynolds number	P/e = 10, Exp.	P/e = 10, CFD	P/e = 20, Exp.	P/e = 20, CFD
10,000	2.908	2.906	2.549	2.569
30,000	2.693	2.684	2.521	2.534
60,000	2.441	2.439	2.429	2.439

The values for the rectangular channel II are lower than the rectangular channel I, but are higher than the square channel. This gives us an idea that the narrow channels have a less heat transfer performance than the wider ribbed channels. The normalized friction factor is also plotted and shown in Figure 33.

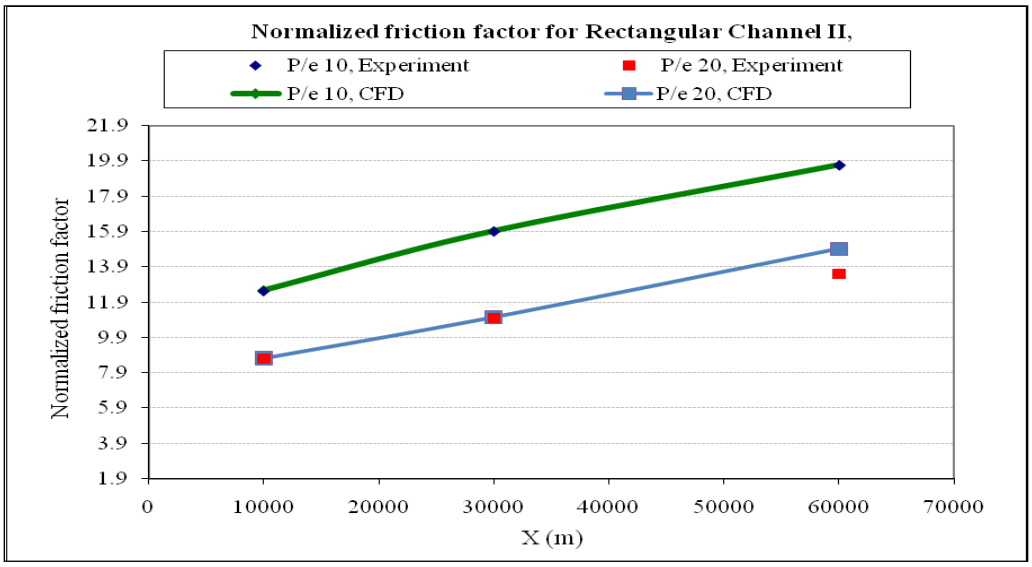

Figure 33: Normalized friction factor for rectangular channel II with w/e = 1, rib spacing, P/e = 10 and P/e = 20

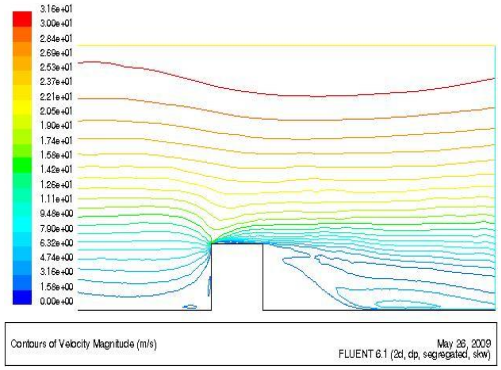

a

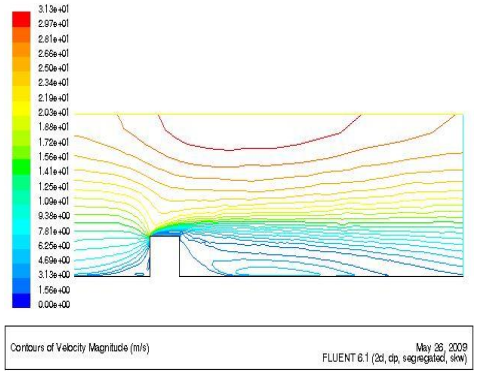

d

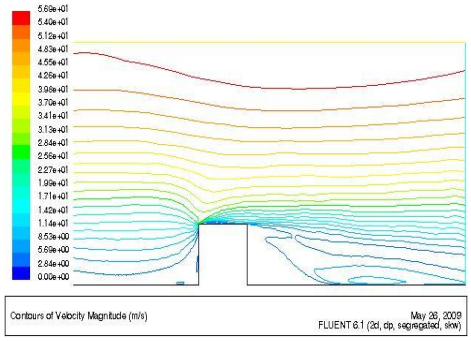

b

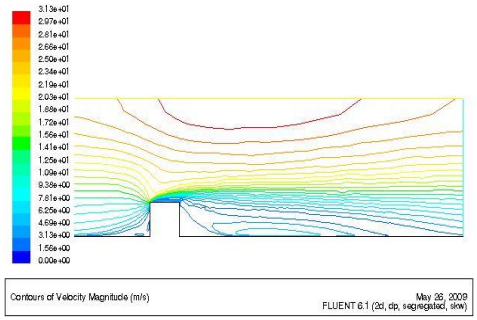

e

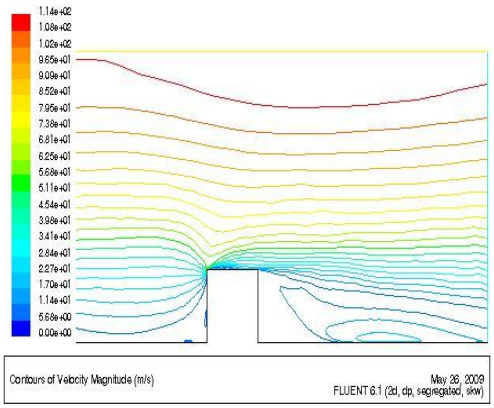

c

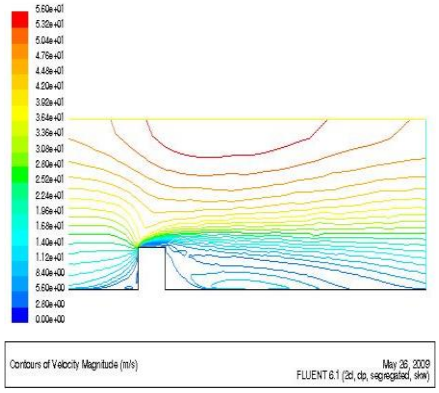

f

Figure 34: Velocity contours showing separation and reattachment for rectangular channel II with w/e = 1, P/e = 10 a) Reynolds number 10,000 b) Reynolds number 30,000 c) Reynolds number 60,000 and P/e = 20 d)Reynolds number 10,000 e) Reynolds number 30,000 f) Reynolds number 60,000

The values of normalized friction factor are also tabulated and given in Table 24.

Table 24: Normalized friction factor for rectangular channel II with w/e = 1

Reynolds number	**P/e = 10, Exp.**	**P/e = 10, CFD**	**P/e = 20, Exp.**	**P/e = 20, CFD**
10,000	12.496	12.581	8.686	8.703
30,000	15.879	15.933	10.977	10.997
60,000	19.636	19.666	13.508	13.697

The values of normalized friction factor increases with Reynolds number. The normalized friction factor decreases with increasing rib spacing for the same Reynolds number. But the values of normalized friction factor are very high when compared to other ribbed channels. The pressure loss across the section is very high. Also there is no much increase in heat transfer for such a huge loss in friction. The rectangular channel II has the least heat transfer performance of all the channels.

Figure 34 a, b and c shows the velocity contours for P/e = 10 and Figure 34 d, e and f shows the velocity contours for P/e = 20. The flow pattern is same as for that of the square channel and rectangular channel I. The rib spacing P/e = 10 has a less recirculation zone than the rib spacing P/e = 20.

The values of average Nusselt number is provided for smooth channel and ribbed rectangular channel II. The pattern is similar as explained for previous channels. The Nusselt number values increases as the Reynolds number increases. But the rate of increase in Nusselt number for the smooth channel is higher than the ribbed rectangular channel II. This is clearly shown in Figure 35.

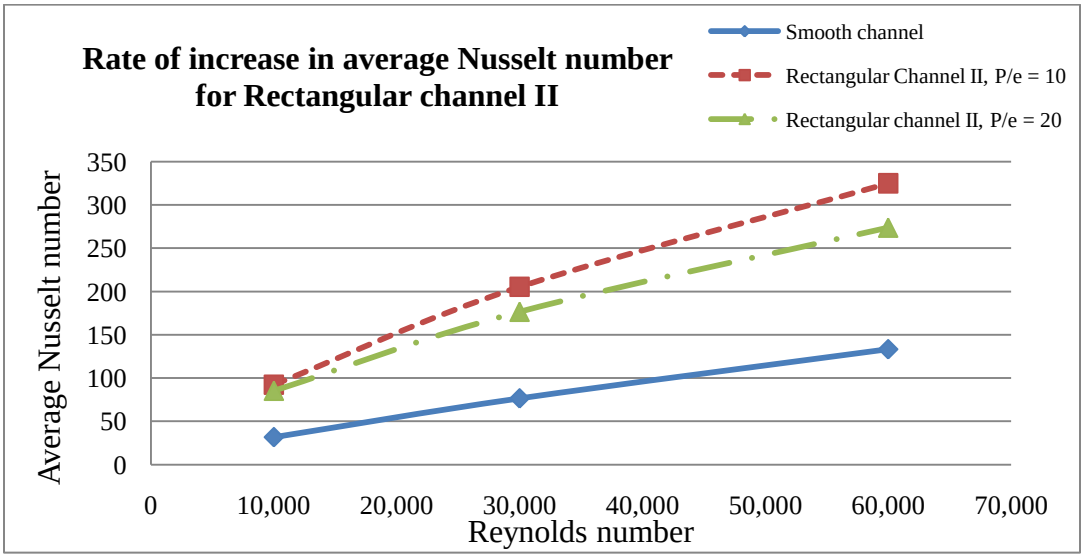

Figure 35: Rate of increase in average Nusselt number for Rectangular channel II

As we can see from the plot that the ribbed channel produced a high heat transfer rate than the smooth channel. The average Nusselt number values are also tabulated in Table 25. The Nusselt number for the ribbed channel is three times higher than the smooth channel for respective Reynolds number.

Also the average Nusselt number value for P/e = 10 is higher than P/e = 20. The pattern is same as in case of square channel. As mentioned before, the wide rib spacing creates a thick boundary layer and a wider recirculation zone. The heat transfer rates decrease and hence the values of the Nusselt number decrease.

Table 25: Average Nusselt number values for rectangular channel II at P/e = 10 & 20.

Reynolds number	**Smooth channel**	**Rectangular channel II**	
		P/e = 10	**P/e = 20**
10,000	31.786	100.092	85.093
30,000	76.547	202.748	176.437
60,000	133.276	325.031	273.753

The rate of increase in Nusselt number is high for smooth channel than the ribbed channel. The rate of increase of Nusselt number form Reynolds number 10,000 to Reynolds number 30,000 is 1.41 for smooth channel, 1.2 for rectangular channel II with P/e = 10 and 1.37 for rectangular channel II with P/e = 20. Thus the rate of increase in value is low for ribbed channel. Also the rate of increase of Nusselt number form Reynolds number 30,000 to Reynolds number 60,000 is 0.58 for smooth channel, 0.67 for rectangular channel II with P/e = 10 and 0.55 for rectangular channel II with P/e = 20. Thus as the Reynolds number increases the rate of increase in Nusselt number is low.

6.4. Conclusion

The normalized Nusselt number and normalized friction factor was calculated for various channels with square ribs. The local Nusselt number was also calculated for the channels.

The local Nusselt number for all the channels follows the same pattern. The value of Nusselt number increases as the Reynolds number increases. The presence of ribs increases the velocity and hence the higher heat transfer rate. The flow separates before the flow hit the rib and reattaches behind the rib. So a recirculation zone is created and hence a low Nusselt number in the recirculation zone. The heat transfer rate over the rib is high.

The normalized Nusselt number values were calculated and plotted for all the channels. The value of normalized Nusselt number decreases as the Reynolds number increases. The increase in rib spacing causes the normalized Nusselt number to decrease. The value of normalized friction factor decreases as the rib spacing increases for the same Reynolds number.

Due to the wider rib spacing, the flow reattaches at a longer distance and hence has a high void zone. The flow reattaches the wall at a long distance before it hits the next rib causing the velocity to decrease. This eventually decreases the heat transfer rate.

But wider rib spacing causes a less blockage of the flow. Hence the pressure loss due to the presence of the flow disturbance is less. This is the reason for the less normalized friction factor values for wider ribs.

Also the wider ribs have a high heat transfer rate and also high pressure drop. The value of normalized Nusselt number is high for rectangular channel I than the square channel. Also the normalized friction factor value are as high as 20 for rectangular channel II. Though we cannot conclude which channel aspect ratio produces a good heat transfer performance without analyzing the effect of rib width, from this study we

conclude that the idea of wider rib spacing do not help in increase in the heat transfer performance.

The effect of rib width on all the ribbed channels is analyzed in chapter VII.

CHAPTER VII

EFFECT OF RIB WIDTH ON THE HEAT TRANSFER PERFORMANCE OF THE CHANNELS

In Chapter VI, the effect of rib spacing on the heat transfer performance of channels with square ribs was discussed. In this chapter the combined effect of rib spacing and rib width on the heat transfer performance of channels is analyzed. The range of rib width to rib height ratio (w/e) varies from 1/8 to 14. The analysis again is performed for channels with three different aspect ratios and different flow parameters. There are no experimental results to compare the results obtained by the computational work, but the fact that the code was validated in previous analysis proves that the results obtained are reliable. By studying the effect of rib width, the optimal cooling configuration for the internal cooling of the channels can be obtained. The results obtained are substantiated by studying the velocity contours and flow pattern. The normalized Nusselt number and normalized friction factor are obtained to study the heat transfer performance and frictional loss.

7.1 Effect of Rib Width in Square Channel

The effect of rib width in a square channel with aspect ratio 1:1 is performed. The rib width, w is varied while the rib height, e is maintained constant. The analysis was performed for Reynolds number 10,000, 30,000 and 60,000. The channel and rib configuration used in the analysis of square channel is provided in Table 26. The initial condition includes a constant heat flux of 2500 W/m^2 applied at the wall and an inlet bulk temperature of 298 K.

Table 26: Parameters used in the analysis of square channel with various rib widths

W/H	1
e	0.0024
P/e	10 20
w/e	1/8 1 2 3 4 6 10 14
Re	10,000 30,000 60,000

The Nusselt number is calculated for the fully developed flow and the results are normalized using values obtained by the Dittus – Boelter equation. The rib spacing P/e = 10 and P/e = 20 are considered to study the combined effect on the heat transfer coefficient. The values of normalized Nusselt number at three Reynolds numbers for rib spacing P/e = 10 are provided in Table 27 and the values for rib spacing P/e = 20 are provided in Table 28.

Table 27: Normalized Nusselt number for square channel with various rib width for rib spacing P/e = 10

w/e vs. Re	0.125	1	2	4	6
10,000	1.976	2.372	2.288	2.125	1.985
30,000	1.845	2.273	2.178	2.050	1.834
60,000	1.724	2.191	2.125	1.984	1.795

Table 28: Normalized Nusselt number for square channel with various rib width for rib spacing P/e = 20

w/e vs. Re	0.125	1	4	6	8	14
10,000	1.302	2.248	2.103	1.625	1.462	1.403
30,000	1.129	2.060	1.966	1.500	1.268	1.236
60,000	1.118	1.985	1.674	1.389	1.161	1.148

The results for normalized Nusselt number are also plotted in Figure 36. From the plot we can see that as the rib width increases the normalized Nusselt number decreases. Also as the rib spacing increases, the normalized Nusselt number value decreases for the same Reynolds number. The pattern is same as seen in chapter VI for channels with square ribs.

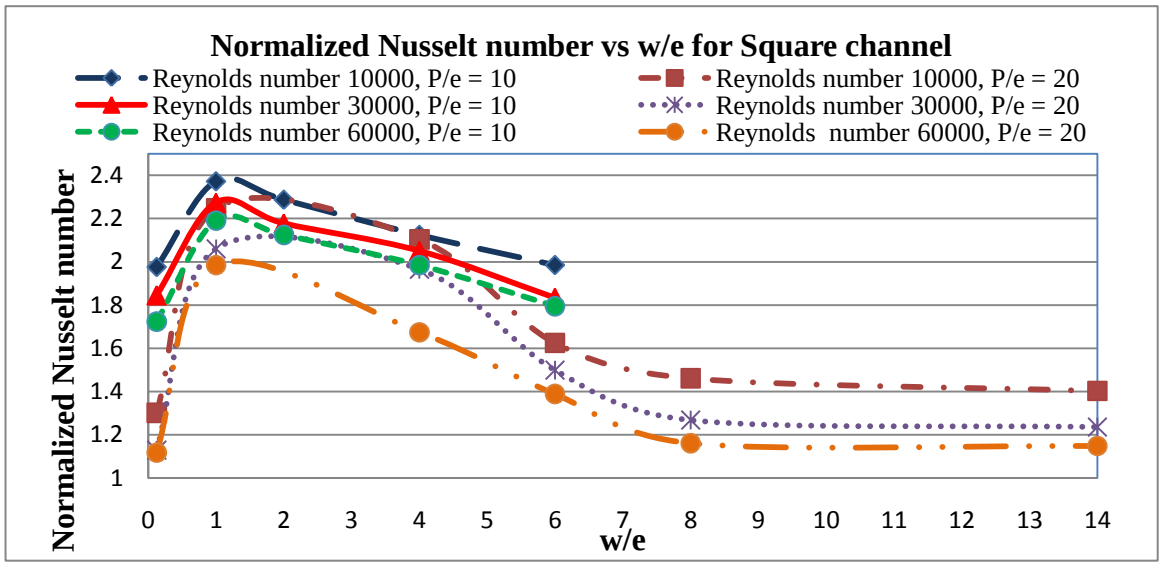

Figure 36: Normalized Nusselt number of square channel with various rib widths for different Reynolds number.

For each case, the value reaches its peak for square ribs with w/e = 1 and then gradually decreases. The plot also shows that at lower Reynolds number, the change in rib width produce a normalized Nusselt number in a close range for both the rib spacing. For instance the w/e ratio of 4 for P/e = 10 and P/e = 20 has the normalized Nusselt number values of approximately 2.12 and 2.10 respectively. The increase in rib width is ineffective in case of high Reynolds numbers. For example, the value of normalized Nusselt number at w/e = 6 has a difference of almost 20 percent. Also the plot shows that the value of normalized Nusselt number for the case w/e = 14 with P/e = 20 at Reynolds number 60,000 is much closer to that of a smooth channel.

The variation of the normalized Nusselt number values as the rib width changes can be explained with the help of flow pattern. The velocity contours for various cases are presented in Figure 37 – Figure 42.

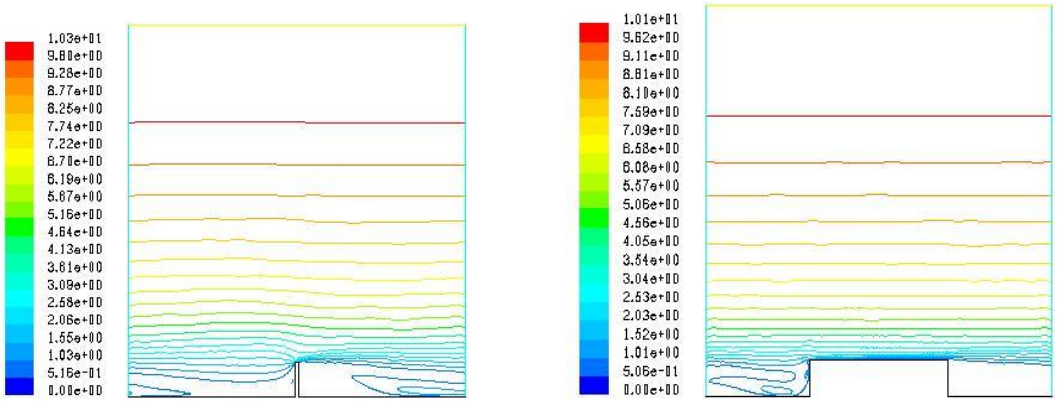

Case I Case II

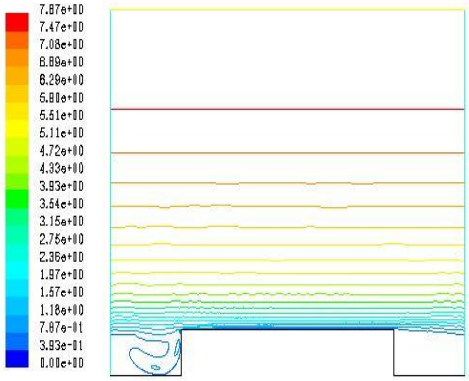

Case III

Figure 37: Velocity contours for square channel with rib spacing P/e = 10 for Reynolds number 10,000 with rib widths Case I: w/e = 1/8, Case II: w/e = 4 and Case III: w/e = 6

The flow pattern for various rib width cases at Reynolds number 10,000 is shown in Figure 37. The case I is a rib width to rib height ratio (w/e) of 1/8. The case is similar to that of a smooth channel as the rib width is much smaller than the rib height. In spite of a low w/e ratio, the normalized Nusselt number is high than expected. The reason is the high velocity values created by a small disturbance in the flow. The velocity value is 1.5 m/s in case of smooth channel. The case I create a velocity value of 3 m/s and hence a high heat transfer rate. The square rib, w/e = 1 was already explained in chapter VI. As

the w/e ratio increases, the flow is parallel to the rib. For high w/e ratios as in case II and case III, the flow reattaches several times on the rib. This creates thick boundary layer over the rib. The velocity is decreased and the heat transfer rate is low. Thus the normalized Nusselt number value decreases as the rib width increases.

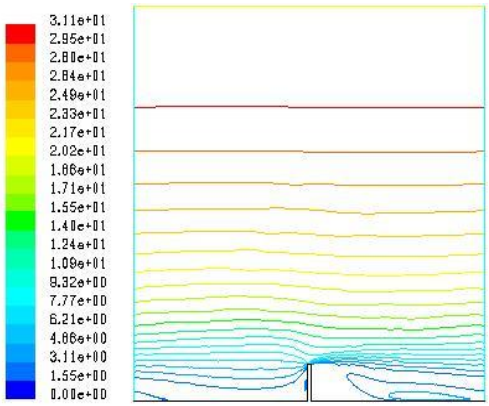

Case I

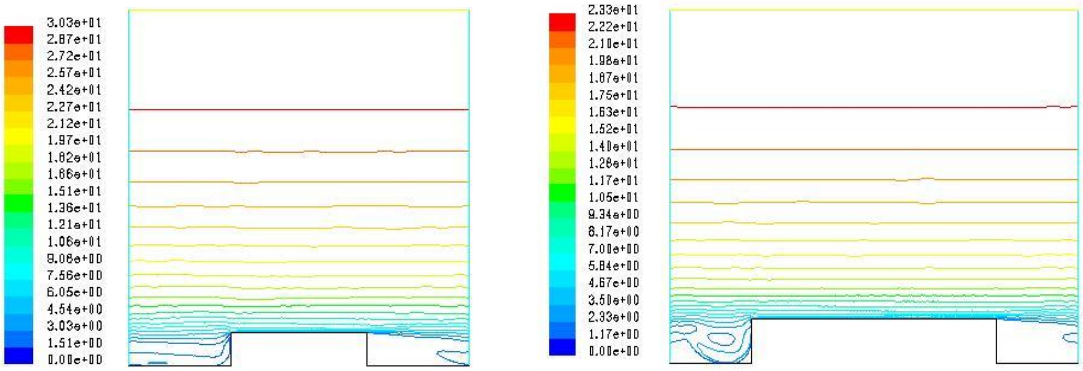

Case II Case III

Figure 38: Velocity contours for square channel with rib spacing P/e = 10 for Reynolds number 30,000 with rib widths Case I: w/e = 1/8, Case II: w/e = 4 and Case III: w/e = 6

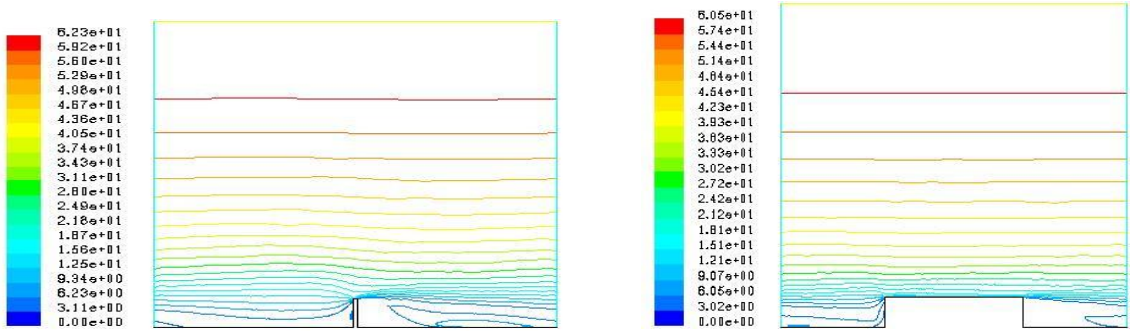

Case I Case II

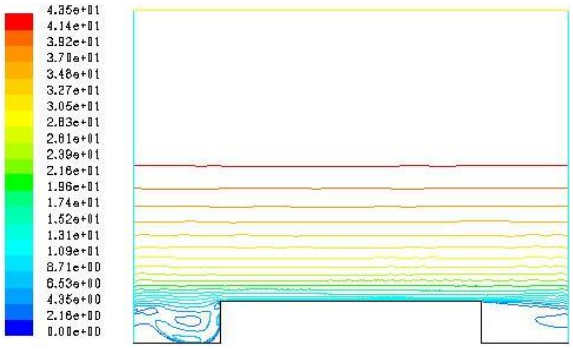

Case III

Figure 39: Velocity contours for square channel with rib spacing P/e = 10 for Reynolds number 60,000 with rib widths Case I: w/e = 1/8, Case II: w/e = 4 and Case III: w/e = 6

Figure 38 show the velocity contours for Reynolds number 30,000. The velocity increases as the Reynolds number increases. The Nusselt number value is higher than the Reynolds number 10,000, but as we normalize the results, the values are low. Since the high w/e ratio creates more recirculation zone the variation in Nusselt number decreases. Thus when we normalize the variation is not high. The case w/e = 4 has a Nusselt number value close to that for case II for Reynolds number 10,000. The rib width has no effect on the normalized Nusselt number in this case.

The velocity for Reynolds number 60,000 in Figure 39 also has the similar pattern. As the rib width increases, the normalized value of Nusselt number decreases.

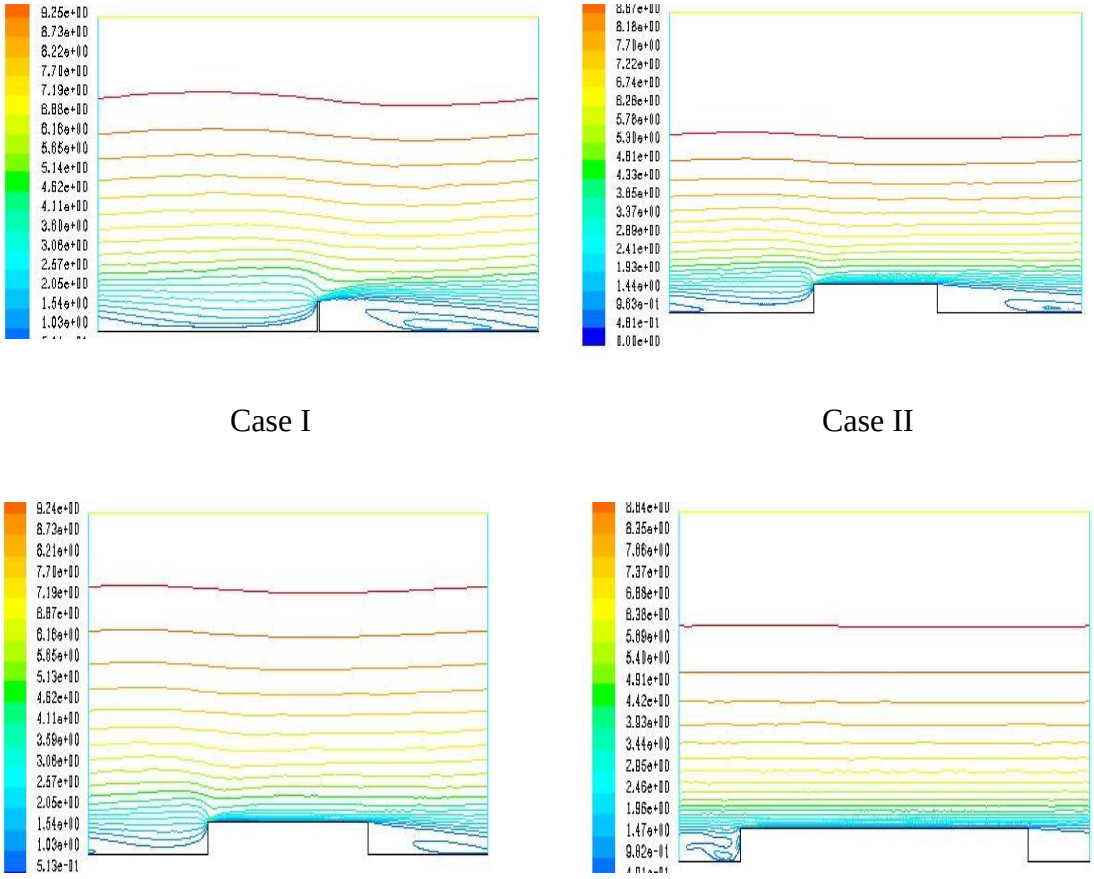

Case I Case II

Case III Case IV

Figure 40: Velocity contours for square channel with rib spacing P/e = 20 for Reynolds number 10,000 with rib widths Case I: w/e = 1/8, Case II: w/e = 4, Case III: w/e = 6 and Case IV: w/e = 14

The velocity contours for rib spacing P/e = 20 for Reynolds number 10,000 for various rib width is provided in Figure 40. The values of normalized Nusselt number for

case I and case IV are 1.3 and 1.4 respectively. The case I with w/e = 1/8 is almost a smooth channel. With wide rib spacing, the rib has no effect and the value is close to the smooth channel. The case IV with w/e = 14 is also similar to the smooth channel. The case II with w/e = 4 and case III with w/e = 6 also produces Nusselt number values less than rib spacing P/e = 10. Since the ribs are widely spaced, the recirculation zone is high. The velocity decreases as the flow reaches the next rib.

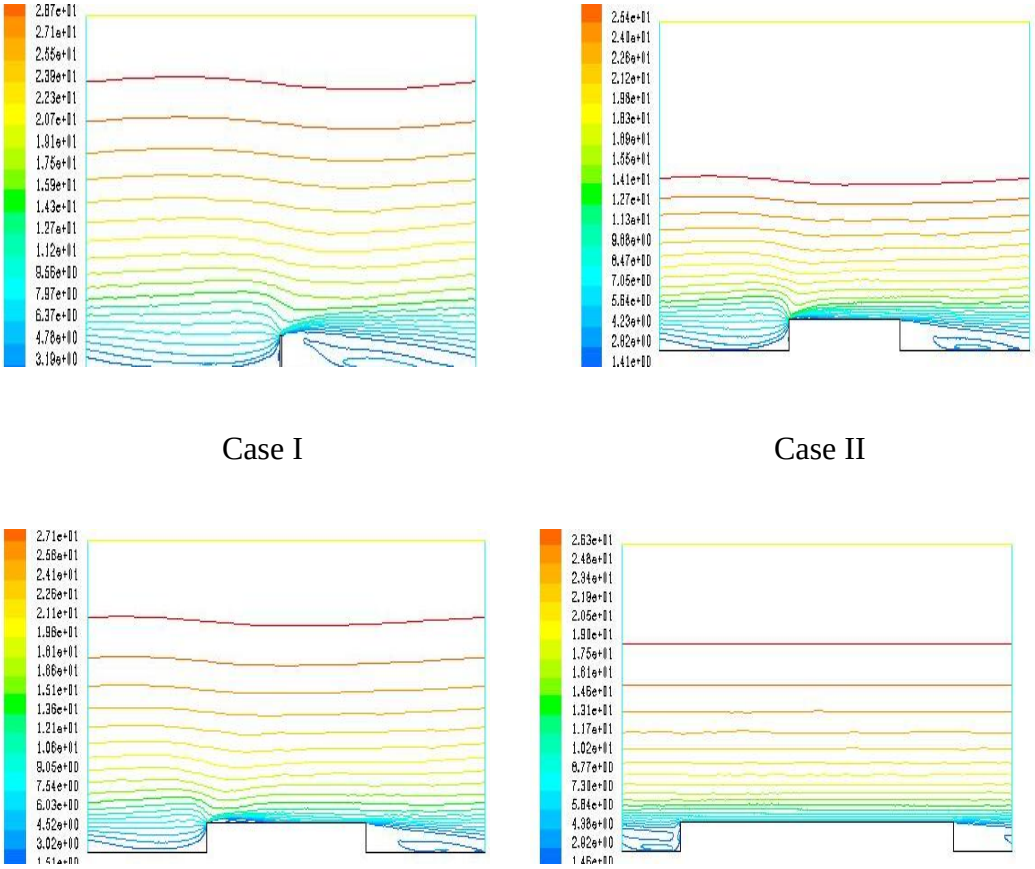

Case I Case II

Case III Case IV

Figure 41: Velocity contours for square channel with rib spacing P/e = 20 for Reynolds number 30,000 with rib widths Case I: w/e = 1/8, Case II: w/e = 4 and Case III: w/e = 6

Figure 41 and Figure 42 shows the velocity contours for rib spacing, P/e = 20 for Reynolds number 30,000 and 60,000. The normalized Nusselt number does not vary significantly as the rib width increases. The flow pattern remains the same as in previous cases. The value of normalized Nusselt number decreases as the rib width increases.

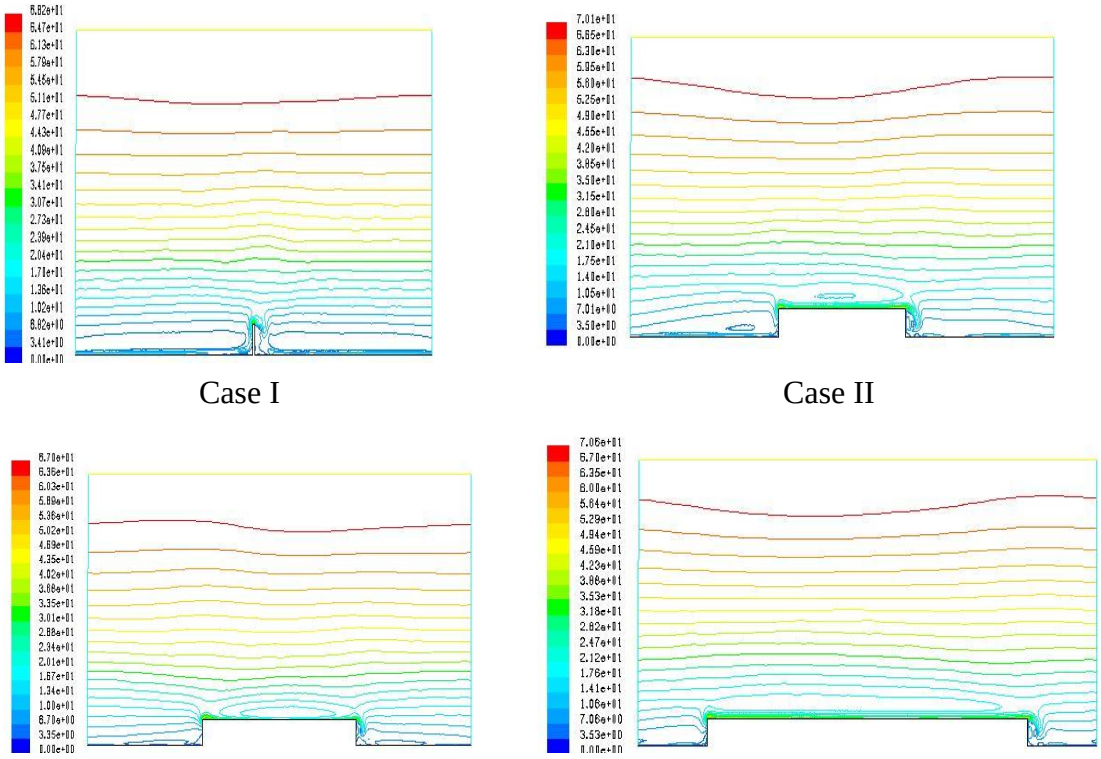

Case I Case II

Case III Case IV

Figure 42: Velocity contours for square channel with rib spacing P/e = 20 for Reynolds number 60,000 with rib widths Case I: w/e = 1/8, Case II: w/e = 4 and Case III: w/e = 6

The normalized friction factor is calculated and plotted in Figure 43. The value of friction factor increase and then decreases as the rib width increases. The value reaches its peak for w/e = 2 for P/e = 10 and w/e = 4 for P/e = 20.

Table 29: Normalized friction factor for square channel with various rib width for rib spacing, P/e = 10

w/e vs. Re	0.125	1	2	4	6
10,000	1.851	3.847	4.387	3.152	2.515
30,000	2.182	4.077	4.792	3.285	2.789
60,000	2.570	4.853	5.504	3.565	3.269

Table 30: Normalized friction factor for square channel with various rib width for rib spacing, P/e = 20

w/e vs. Re	0.125	1	4	6	8	14
10,000	2.383	3.680	4.328	4.192	3.490	2.532
30,000	2.194	3.377	3.998	3.863	3.127	2.229
60,000	2.581	4.006	4.784	4.688	3.565	2.740

The plot in Figure 43 shows that as the rib spacing increases, the normalized friction factor values decreases. The high rib spacing causes a less flow blockage and hence the pressure loss is low. The frictional loss is high when the ribs are placed closer. The normalized friction factor is high for wider ribs. The value is high for rib width ratios w/e = 2 for P/e = 10 and w/e = 4 for case P/e = 10. The wide ribs create more frictional loss than other rib widths.

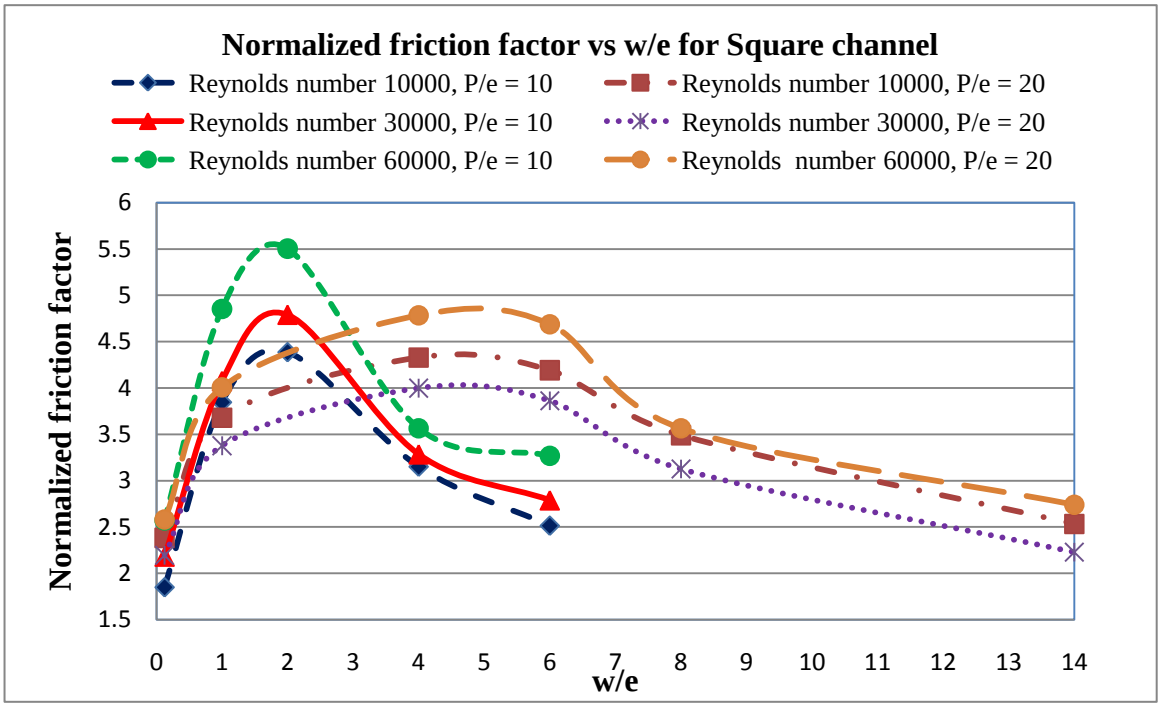

Figure 43: Normalized friction factor of square channel with various rib widths for different Reynolds number.

7.2 Effect of Rib Width in Rectangular Channel I

The effect of rib width in a rectangular channel I with aspect ratio 2:1 is performed. The rib width, w is varied while the rib height, e is maintained constant. The analysis was performed for Reynolds number 10,000, 30,000 and 60,000. The channel and rib configuration used in the analysis of rectangular channel I is provided in Table 31. The initial condition includes a constant heat flux of 2500 W/m^2 applied at the wall and an inlet bulk temperature of 298 K.

Table 31: Parameters used in the analysis of rectangular channel I with various rib widths

W/H	2
e	0.0032
P/e	10 20
w/e	1/8 1 2 4 6 10 14
Re	10,000 30,000 60,000

The heat transfer coefficients are calculated and the values of normalized Nusselt number are provided for case P/e = 10 and P/e = 20 in Table 32 and Table 33 respectively. The values of normalized Nusselt number for P/e = 10 is high than P/e = 20. Also as the rib width increases, the normalized Nusselt number value decreases.

Table 32: Normalized Nusselt number for rectangular channel I with various rib width for rib spacing P/e = 10

w/e vs. Re	**0.125**	**1**	**2**	**4**	**6**
10,000	2.117	3.149	2.570	2.323	2.208
30,000	2.056	2.648	2.349	2.224	2.128
60,000	1.987	2.439	2.221	2.023	1.900

Table 33: Normalized Nusselt number for rectangular channel I with various rib width for rib spacing P/e = 20

w/e vs. Re	0.125	1	2	4	6	10	14
10,000	2.107	2.677	2.463	2.429	2.380	2.299	2.128
30,000	1.882	2.305	2.192	2.158	2.114	2.054	1.894
60,000	1.695	2.053	1.988	1.936	1.826	1.775	1.693

The values of normalized Nusselt number are plotted and are shown in Figure 44. The plot shows that the value is high for case P/e =10 at Reynolds number 10000. The values are close to 1.7 for case p/e = 20 at Reynolds number 60,000 showing that the wider rib spacing at high Reynolds number approaches the values of the smooth channel.

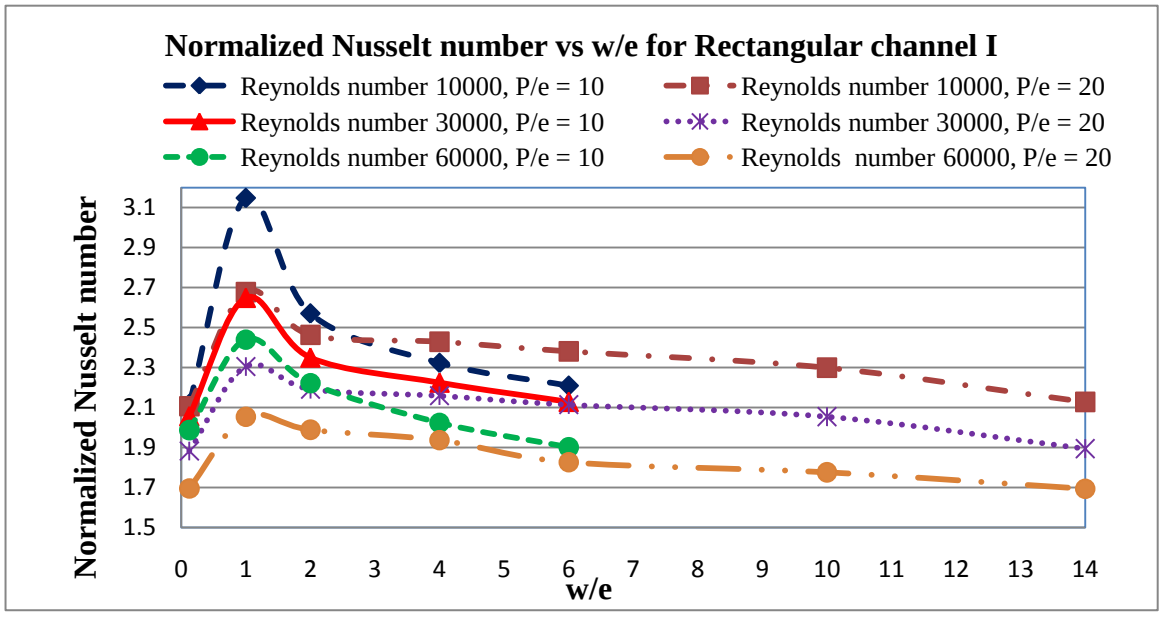

Figure 44: Normalized Nusselt number of rectangular channel I with various rib widths for different Reynolds number.

The values are higher than the square channel for respective Reynolds number. The velocity contours for all the cases are provided in Figure 45 through Figure 50.

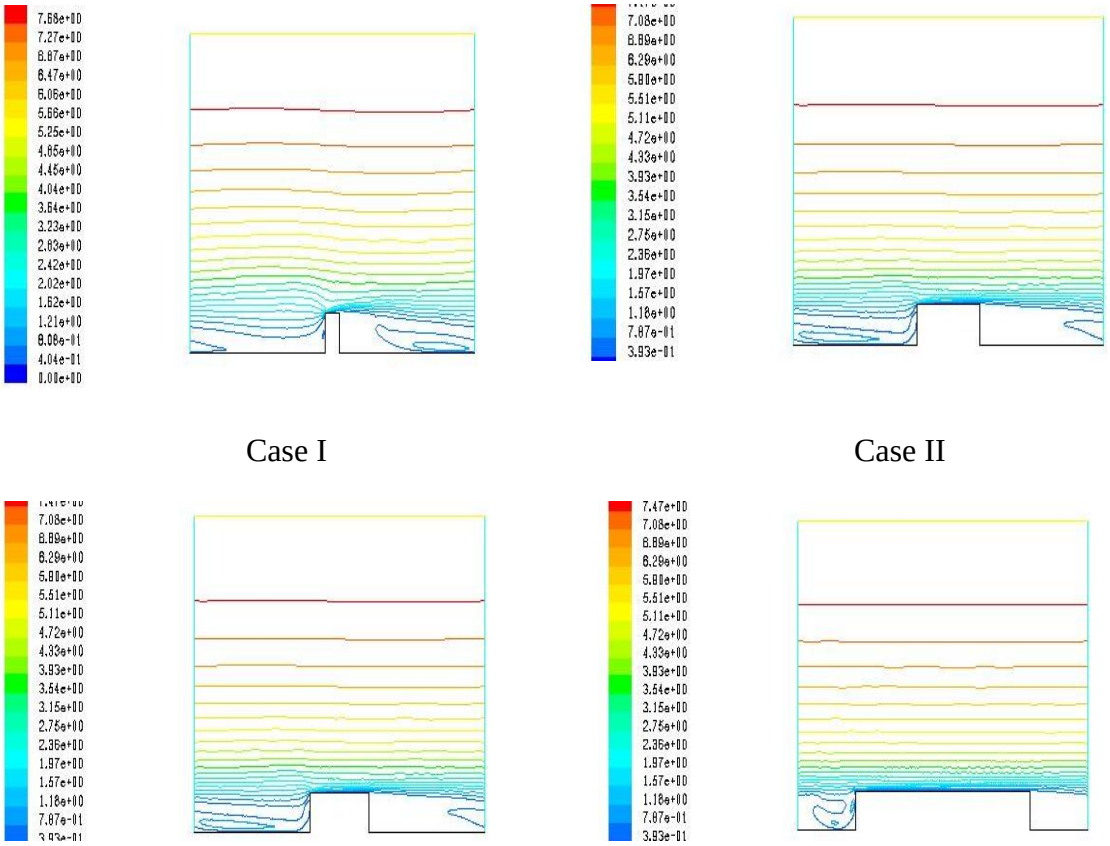

Case I Case II

Case III Case IV

Figure 45: Velocity contours for rectangular channel I with rib spacing P/e = 10 for Reynolds number 10,000 with rib widths Case I: w/e = 1/8, Case II: w/e = 2, Case III: w/e = 4 and Case IV: w/e = 6

The velocity pattern for case P/e = 10 for rectangular channel I at Reynolds number 10,000 is provided in Figure 45. The flow pattern is similar to that of the square channel. The rib width ratio w/e = 1/8 and w/e = 6 are similar to smooth channel. The flow separates before the rib and reattaches after the rib. The rib width w/e = 1/8 though low amplifies the velocity and hence produces a high Nusselt number than smooth

channel. The values of normalized Nusselt number decreases as the rib width ratio increases. This is because of wider recirculation zone in case w/e = 2. In case of w/e = 4 and w/e = 6, the flow reattaches several times over the rib creating a thicker boundary layer. The velocity is decreased and hence the normalized Nusselt number decreases.

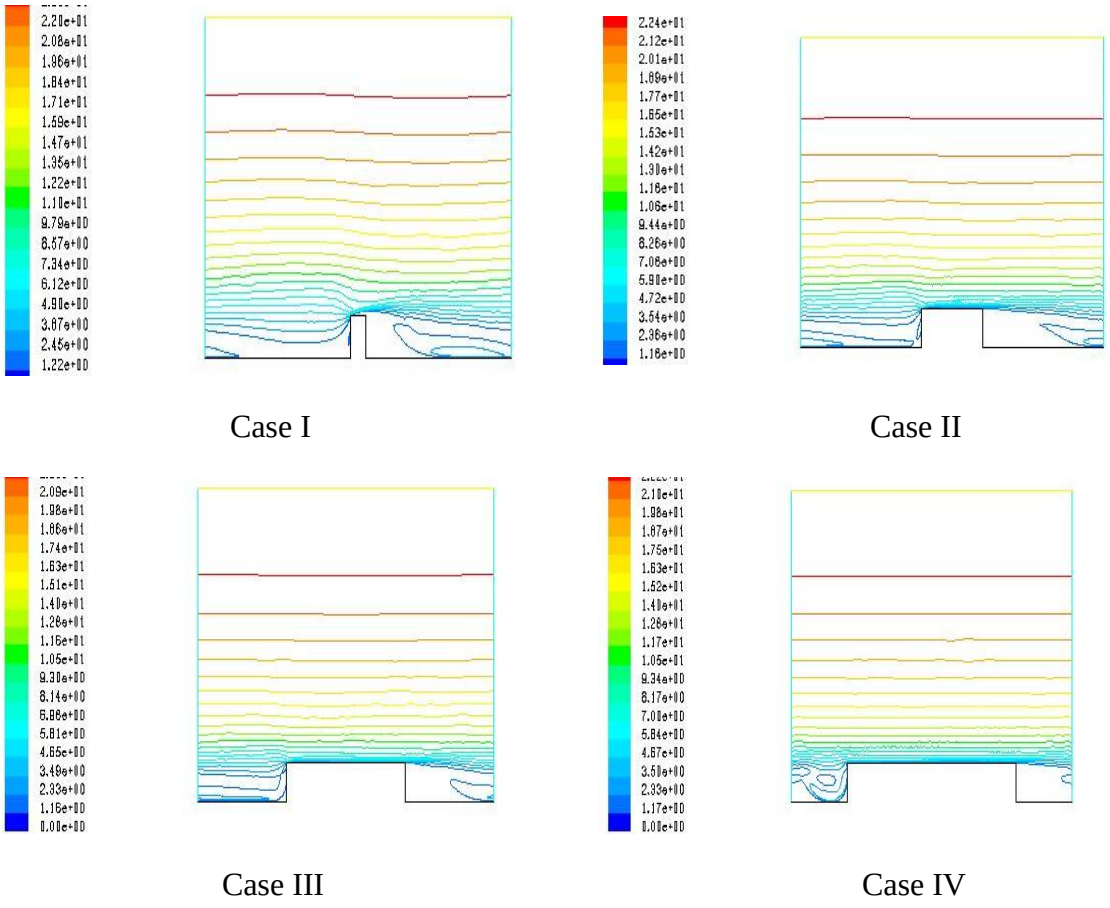

Figure 46: Velocity contours for rectangular channel I with rib spacing P/e = 10 for Reynolds number 30,000 with rib widths Case I: w/e = 1/8, Case II: w/e = 2, Case III: w/e = 4 and Case IV: w/e = 6

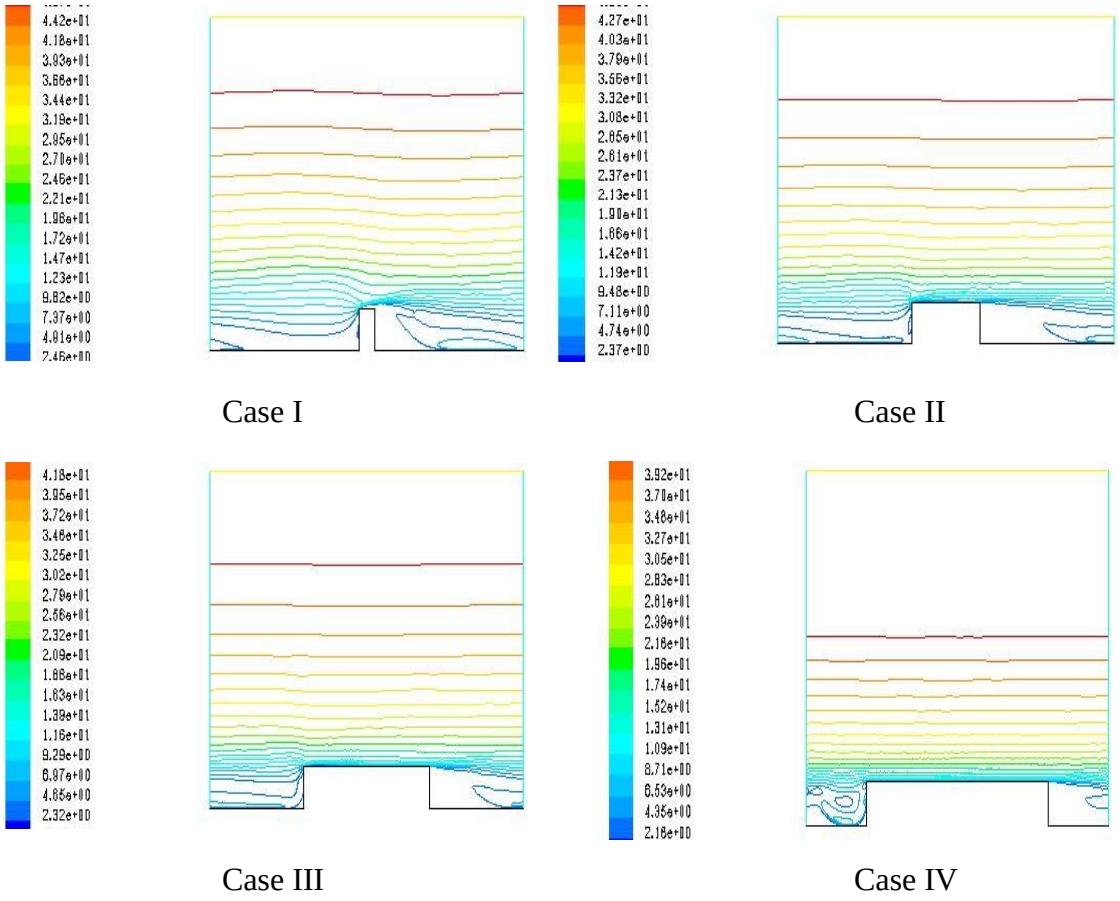

Figure 47: Velocity contours for rectangular channel I with rib spacing P/e = 10 for Reynolds number 60000 with rib widths Case I: w/e = 1/8, Case II: w/e = 2, Case III: w/e = 4 and Case IV: w/e = 6

Figures 46 and Figure 47 provide the velocity pattern for Reynolds number 30,000 and 60,000 respectively. The velocity of the flow increases as the Reynolds number increase. The flow pattern remains the same as in the case of Reynolds number 10,000. The flow is similar to smooth channel in case w/e = 1/8 and the flow reattaches over the rib for high rib width ratios.

The velocity pattern for case P/e = 20 for various Reynolds number are provided in Figure 48 – Figure 50.

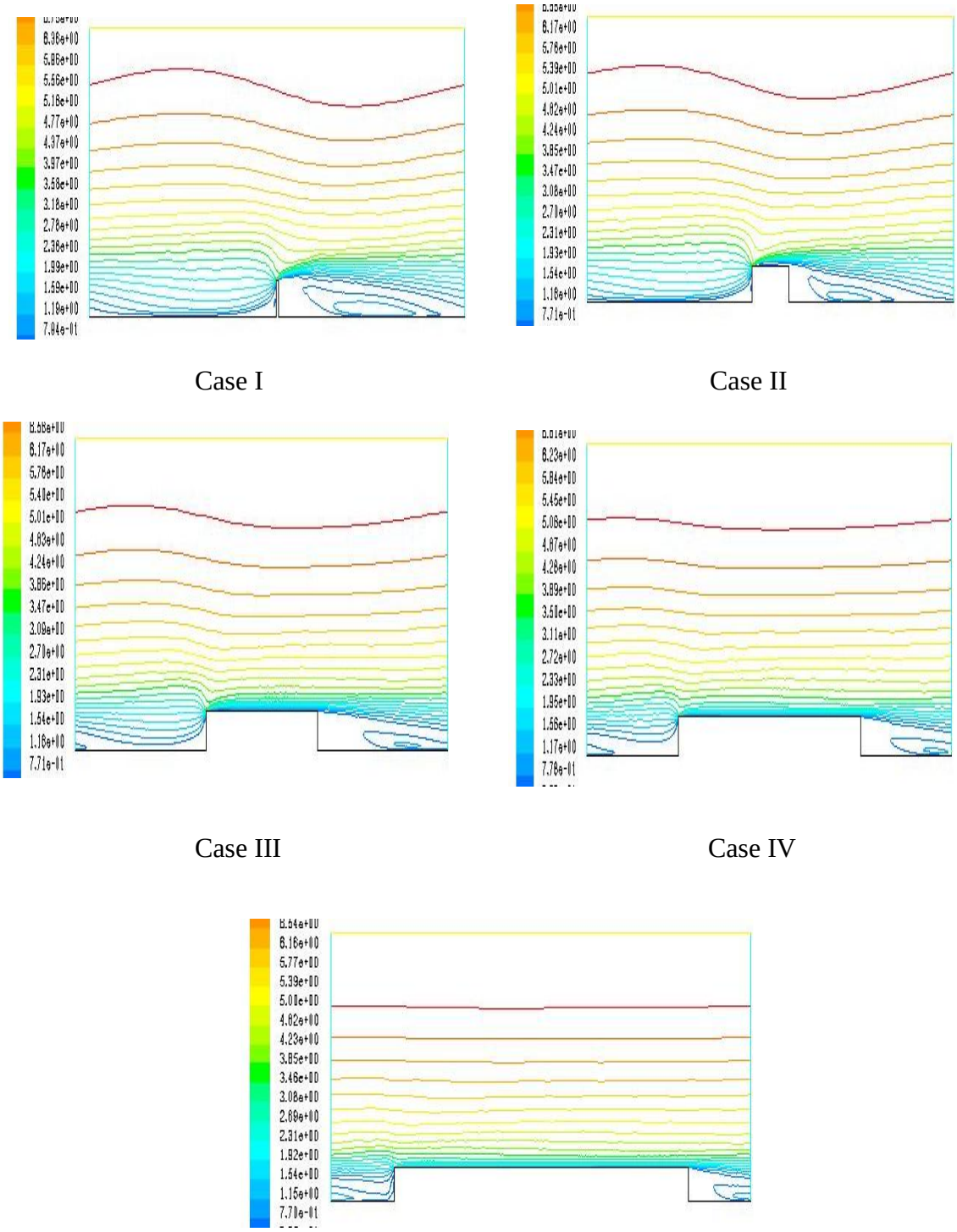

Figure 48: Velocity contours for rectangular channel I with rib spacing P/e = 20 for Reynolds number 10,000 with rib widths Case I: w/e = 1/8, Case II: w/e = 2, Case III: w/e = 6, Case IV: w/e = 10 and Case V: w/e = 14

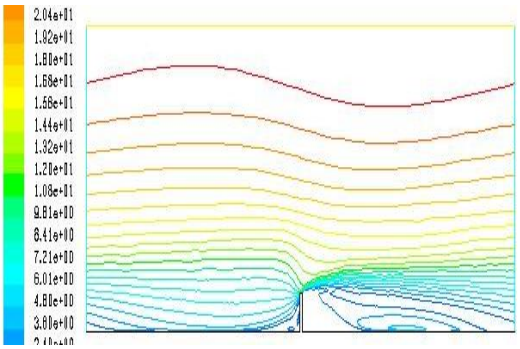

Case I

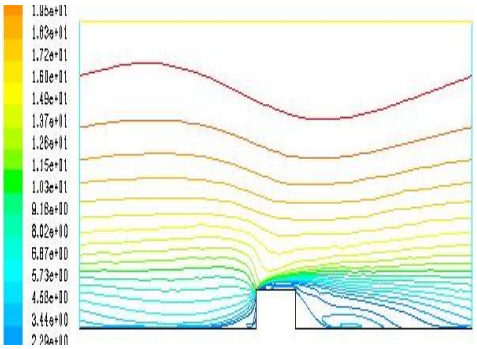

Case II

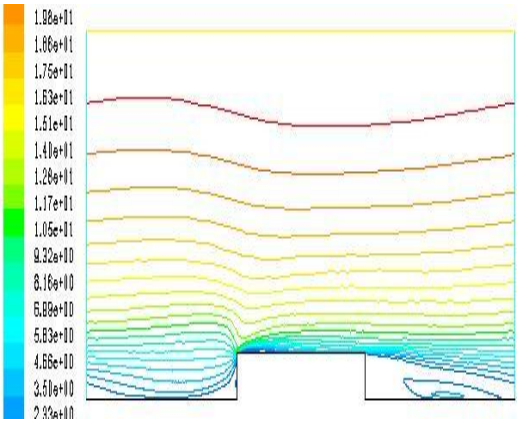

Case III

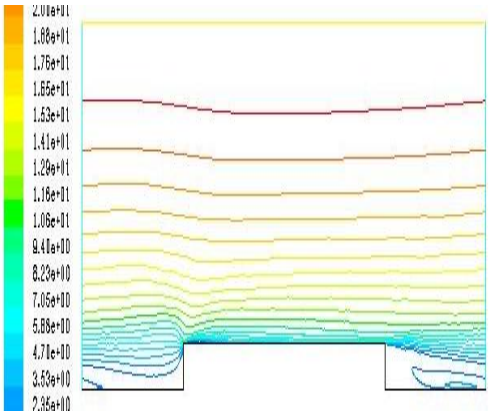

Case IV

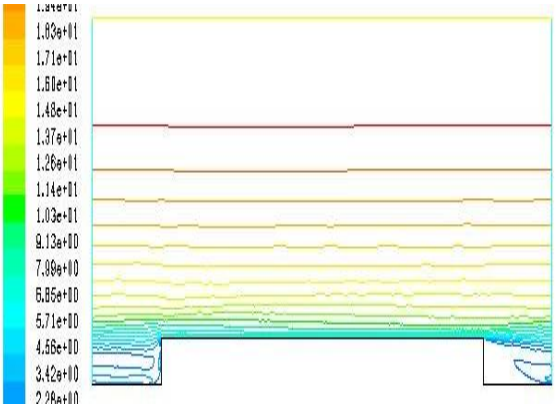

Case V

Figure 49: Velocity contours for rectangular channel I with rib spacing P/e = 20 for Reynolds number 30,000 with rib widths Case I: w/e = 1/8, Case II: w/e = 2, Case III: w/e = 6, Case IV: w/e = 10 and Case V: w/e = 14

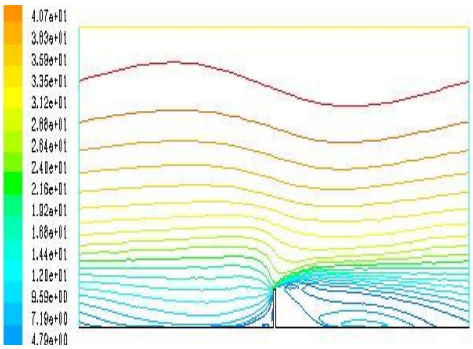

Case I

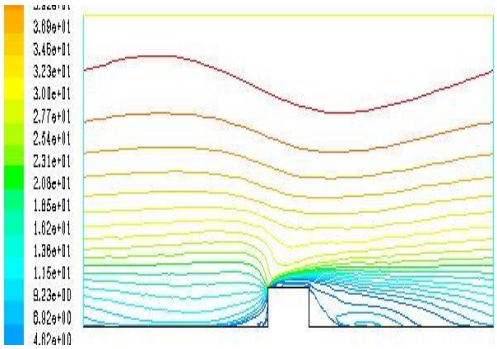

Case II

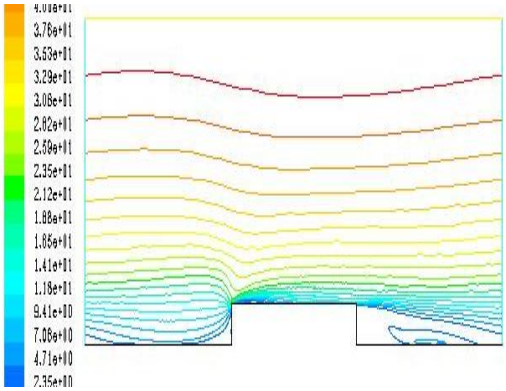

Case III

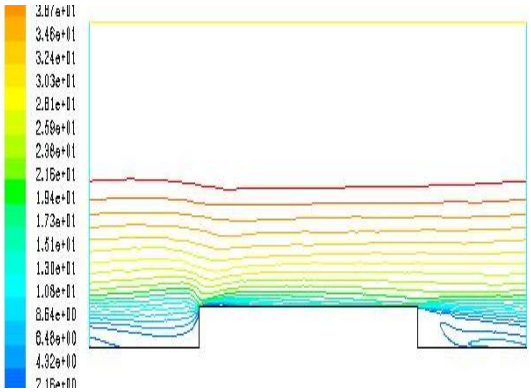

Case IV

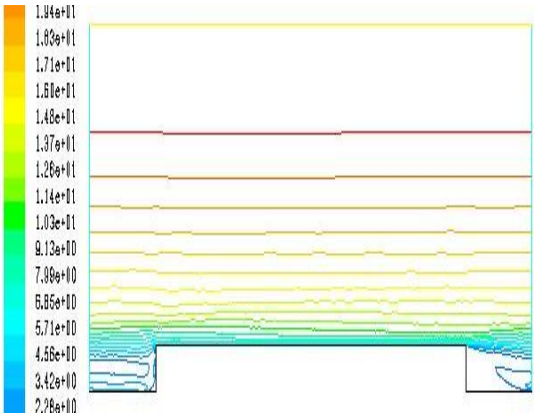

Case V

Figure 50: Velocity contours for rectangular channel I with rib spacing P/e = 20 for Reynolds number 60,000 with rib widths Case I: w/e = 1/8, Case II: w/e = 2, Case III: w/e = 6, Case IV: w/e = 10 and Case V: w/e = 14

The velocity pattern for case P/e = 20 for all the cases shows that as the rib spacing widens the flow re attaches at a distance longer than the using case P/e = 10 causing a wide void zone which decreases the heat transfer rate. The velocity increases as the Reynolds number increases.

The flow pattern remains the same for all the cases. The velocity is compared for case P/e = 10 and P/e = 20 for respective Reynolds number and the values decreases. This is attributed to the rib spacing. The wider rib spacing produces a less normalized Nusselt number value and this proves the remarks on effect of wider rib spacing provided in chapter 6.

The rib width has adverse effect on the Nusselt number. The values of the normalized Nusselt number decreases as the rib width increases.

The effect of rib width on the normalized friction factor is analyzed and the values for case P/e = 10 and P/e = 20 are provided in Table 34 and Table 35 respectively.

Table 34: Normalized friction factor for rectangular channel I with various rib width for rib spacing P/e = 10

w/e vs. Re	**0.125**	**1**	**2**	**4**	**6**
10,000	3.133	5.178	5.449	4.605	4.331
30,000	3.349	6.725	7.402	5.144	4.430
60,000	3.647	7.788	8.229	6.184	4.979

Table 35: Normalized friction factor for rectangular channel I with various rib width for rib spacing P/e = 20

w/e vs. Re	0.125	1	2	4	6	10	14
10,000	2.706	4.105	5.973	5.239	4.638	3.519	2.162
30,000	3.952	5.285	6.156	6.033	5.835	4.773	2.797
60,000	4.586	6.858	7.931	7.527	7.150	5.870	3.324

The friction factor for case P/e = 10 and P/e = 20 shows a different pattern. The value of normalized friction factor decreases as the rib spacing increases. This is because of the spacing of the ribs in the channel. But the values are higher than the square channel for all the cases.

But the rib width has the similar effect on the friction factor. The value increases as the rib width ratio reaches 2 and starts to decrease as the rib width increase. Since the rib width ratio w/e = 1/8 and w/e = 14 represents a smooth channel, the normalized friction factor is less. But the rib width ratio w/e = 2 in each case has a higher value. The rib width creates a void zone and hence the pressure loss across the section is high. The values of square ribs has a less friction factor than the case w/e = 2.

The values of normalized friction factor for various rib spacing and rib width are clearly plotted in Figure 51.

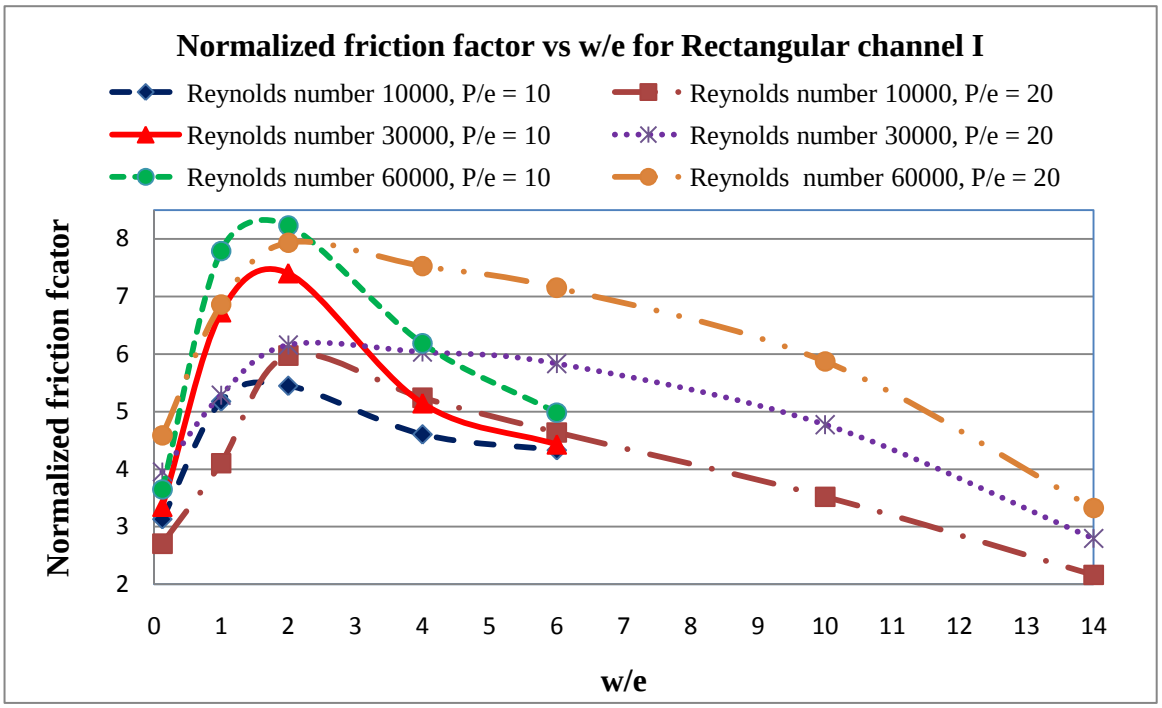

Figure 51: Normalized friction factor of rectangular channel I with various rib widths for different Reynolds number.

7.3 Effect of Rib Width in Rectangular Channel II

The effect of rib width in a rectangular channel II with aspect ratio 4:1 is performed. The rib width, w is varied while the rib height, e is maintained constant. The analysis was performed for Reynolds number 10,000, 30,000 and 60,000. The channel and rib configuration used in the analysis of rectangular channel II is provided in Table 36. The initial condition includes a constant heat flux of 2500 W/m^2 applied at the wall and an inlet bulk temperature of 298 K.

Table 36: Parameters used in the analysis of rectangular channel II with various rib widths

W/H	4
e	0.0032
P/e	10 20
w/e	1/8 1 2 3 4 6 14
Re	10,000 30,000 60,000

The heat transfer coefficients are calculated and the values of normalized Nusselt number are provided for case P/e = 10 and P/e = 20 in Table 37 and Table 38 respectively. The values of normalized Nusselt number for P/e = 10 is high than P/e = 20. Also as the rib width increases, the normalized Nusselt number value decreases.

Table 37: Normalized Nusselt number for rectangular channel II with various rib width for rib spacing P/e = 10

w/e vs. Re	**0.125**	**1**	**2**	**3**	**4**	**6**
10,000	2.218	2.906	2.522	2.424	2.352	2.208
30,000	2.056	2.684	2.449	2.368	2.292	2.128
60,000	1.987	2.439	2.207	2.167	2.123	1.900

Table 38: Normalized Nusselt number for rectangular channel II with various rib width for rib spacing P/e = 20

w/e vs. Re	0.125	1	2	4	6	14
10,000	1.949	2.569	2.385	2.287	2.244	2.126
30,000	1.782	2.534	2.414	2.349	2.239	2.031
60,000	1.643	2.439	2.355	2.259	2.187	1.800

The values of normalized Nusselt number are plotted and are shown in Figure 52. The plot shows that the value is high for case P/e =10 at Reynolds number 10,000. The values are close to 1.8 for case P/e = 20 at Reynolds number 60,000 showing that the wider rib spacing at high Reynolds number approaches the values of the smooth channel.

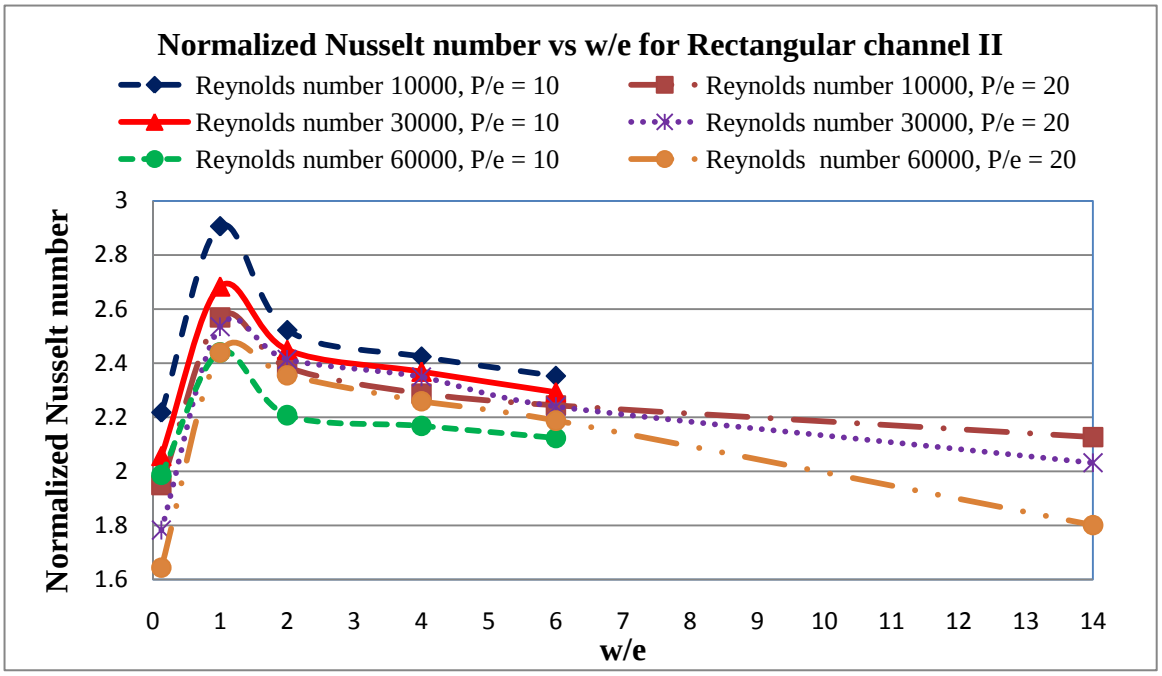

Figure 52: Normalized Nusselt number of rectangular channel II with various rib widths for different Reynolds number.

The velocity contours for case P/e = 10 at Reynolds number 10,000 is provided in Figure 53. The flow pattern is similar as in other case. The flow becomes turbulent due to the presence of the rib. The rib causes a separation flow and hence creates a recirculation zone. The flow remains parallel to the wall in case w/e = 1/8 causing a low heat transfer rate. The case with w/e = 6 is similar to that of a smooth channel due to wider ribs.

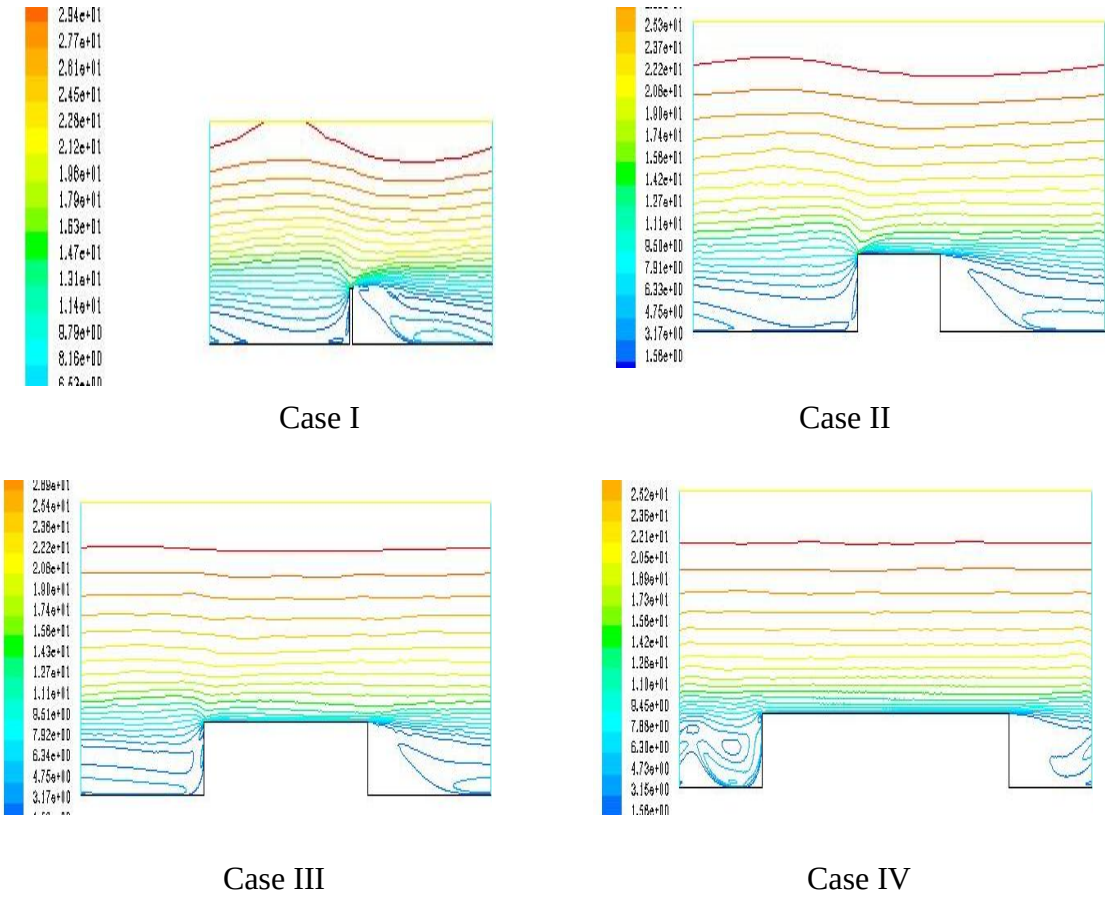

Figure 53: Velocity contours for rectangular channel II with rib spacing P/e = 10 for Reynolds number 10,000 with rib widths Case I: w/e = 1/8, Case II: w/e = 2, Case III: w/e = 4 and Case IV: w/e = 6

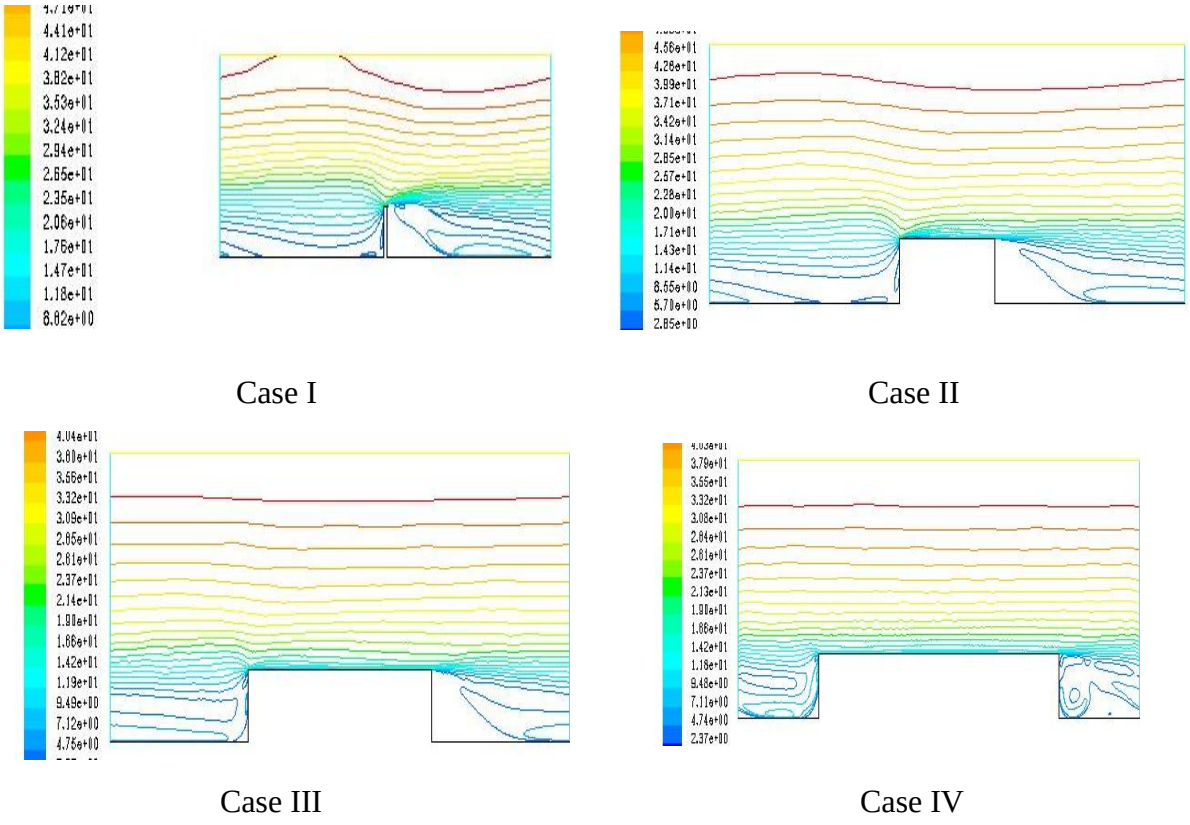

Figure 54: Velocity contours for rectangular channel II with rib spacing P/e = 10 for Reynolds number 30,000 with rib widths Case I: w/e = 1/8, Case II: w/e = 2, Case III: w/e = 4 and Case IV: w/e = 6

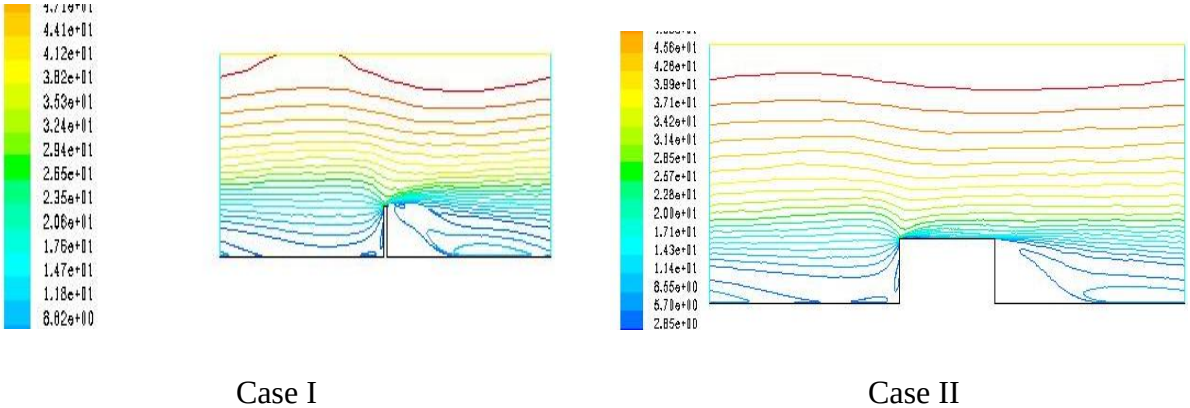

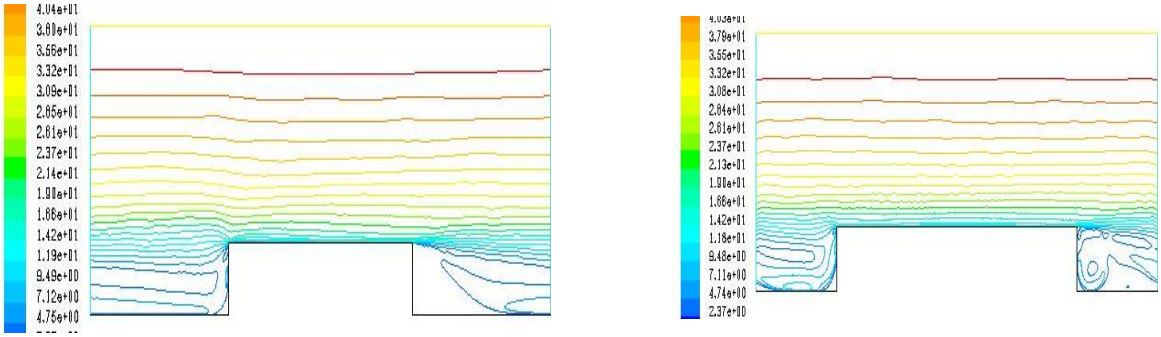

Case III Case IV

Figure 55: Velocity contours for rectangular channel II with rib spacing P/e = 10 for Reynolds number 60,000 with rib widths Case I: w/e = 1/8, Case II: w/e = 2, Case III: w/e = 4 and Case IV: w/e = 6

Figure 54 and Figure 55 show the velocity contours for Reynolds number 30,000 and 60,000 respectively. There is no variation in the flow pattern. Also the rib width ratio w/e = 1/8 and w/e = 6 shows the same pattern with an exception of high velocity values. The reason for variation in normalized Nusselt number is same as explained in case of rectangular channel I. The other reason for change in normalized Nusselt number is due to the channel aspect ratio.

The velocity contours for rib spacing, P/e = 20 for various Reynolds number is shown in Figure 56, Figure 57 and Figure 58.

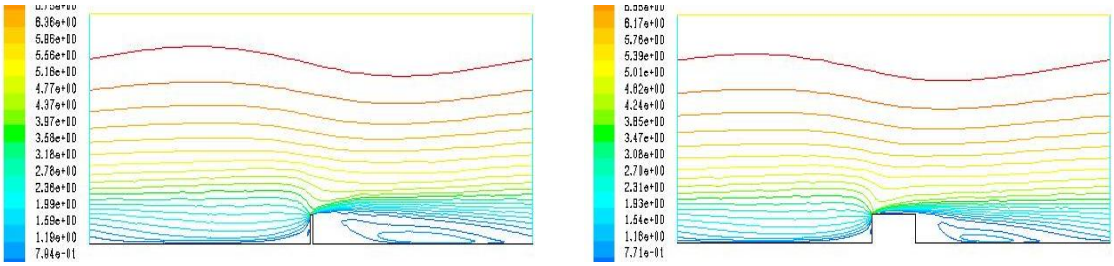

Case I Case II

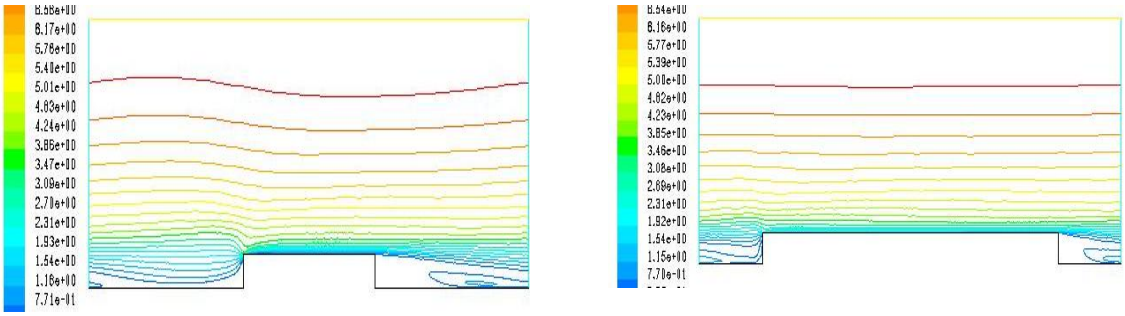

Case III Case IV

Figure 56: Velocity contours for rectangular channel II with rib spacing P/e = 20 for Reynolds number 10,000 with rib widths Case I: w/e = 1/8, Case II: w/e = 2, Case III: w/e = 6, Case IV: w/e = 10 and Case V: w/e = 14

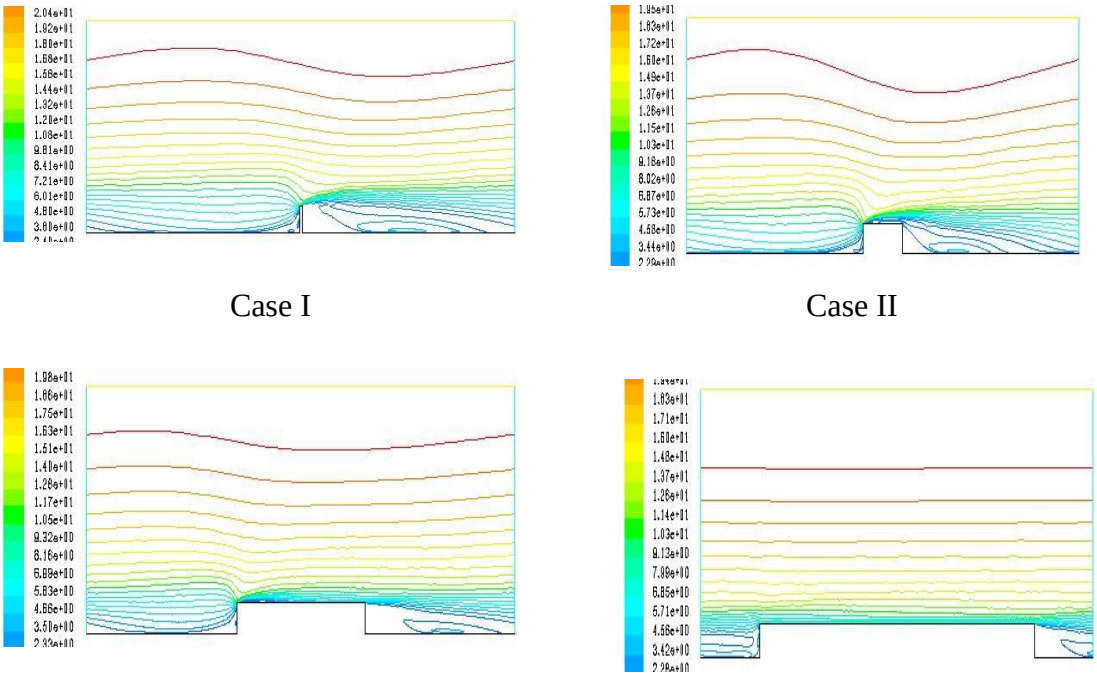

Case I Case II

Case III Case IV

Figure 57: Velocity contours for rectangular channel II with rib spacing, P/e = 20 for Reynolds number 30,000 with rib widths Case I: w/e = 1/8, Case II: w/e = 2, Case III: w/e = 6 and Case IV: w/e = 14

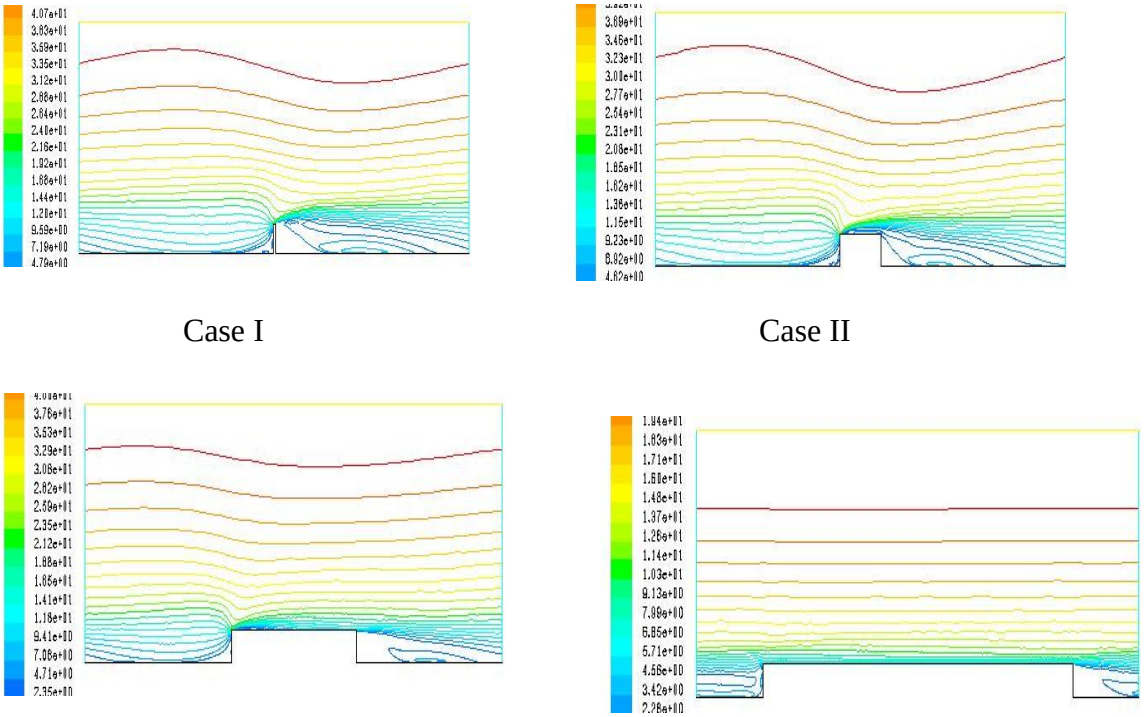

Case I Case II

Case III Case IV

Figure 58: Velocity contours for rectangular channel II with rib spacing P/e = 20 for Reynolds number 60,000 with rib widths Case I: w/e = 1/8, Case II: w/e = 2, Case III: w/e = 6 and Case IV: w/e = 14

The velocity contours for case P/e = 20 rectangular channel II does not vary much with case P/e = 20 for rectangular channel I. The flow pattern remains the same. Because of a wider aspect ratio than the rectangular channel I, the velocity values are low and hence the values of normalized Nusselt number decreases. Since the flow pattern is similar to the rectangular channel I, the case is not explained in detail.

The values of normalized friction factor also follow the same pattern. The value is high for cases with rib spacing P/e = 10. Also the value for normalized friction factor increase when the rib width ratio reaches w/e = 2 and then starts to decrease for further wider rib widths.

The values of normalized friction factor for all the cases are provided in Table 39 and Table 40 and the results are plotted in Figure 59. Due to a wider channel width, the rib causes a more pressure loss across the channel section. Due to a higher pressure loss, the friction loss is increased. The values of normalized friction factor is high than for other channel aspect ratios.

Table 39: Normalized friction factor for rectangular channel II with various rib width for rib spacing P/e = 10

w/e vs. Re	**0.125**	**1**	**2**	**3**	**4**	**6**
10,000	8.548	12.581	12.988	12.328	10.647	8.736
30,000	9.748	15.933	16.275	15.892	13.454	9.847
60,000	10.750	19.666	20.088	19.664	16.324	10.858

Table 40: Normalized friction factor for rectangular channel II with various rib width for rib spacing P/e = 20

w/e vs. Re	**0.125**	**1**	**2**	**4**	**6**	**14**
10,000	5.488	8.703	8.995	8.789	8.673	6.474
30,000	5.987	10.997	11.344	11.154	11.098	6.944
60,000	6.975	13.697	14.098	13.983	13.944	7.387

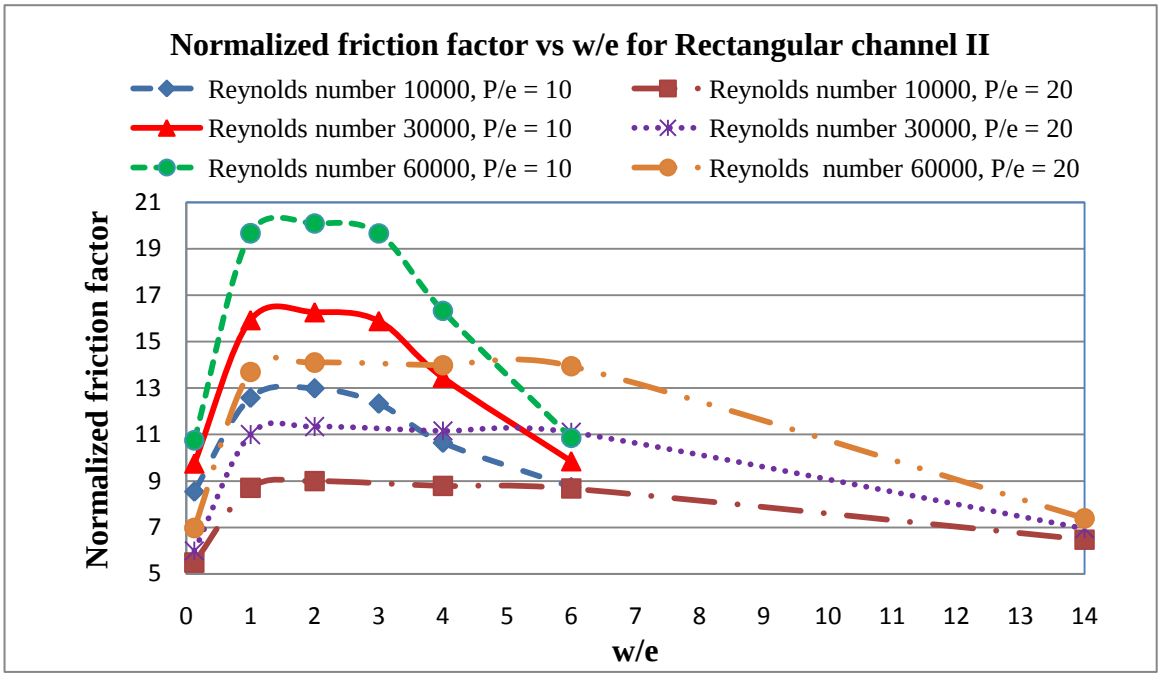

Figure 59: Normalized friction factor of rectangular channel II with various rib widths, for different Reynolds number.

7.4 Conclusion

In this study, three channels are analyzed for various rib spacing and rib width. The rib spacing, P/e = 10 produces a better result for heat transfer rate than for rib spacing, P/e = 20. The wide rib spacing causes a decrease in velocity due to presence of wider recirculation zone. The flow pattern for all the cases remains the same with flow separation occurring before the rib and reattaching behind the rib. The rib spacing P/e = 10 also produce a high normalized friction factor values for all the channel case. Though the values are high, it is compensated by a high heat transfer rates.

The effect of rib width is also analyzed in this study. The rib width ratio w/e = 1/8 is similar to that of smooth channel for all the cases. The high rib width ratio also produces a value close to that of the smooth channel. The square ribs with w/e = 1 has the

high heat transfer rate for each channel. The presence of wider ribs causes the flow to reattach several times over the ribs before reattachment. This causes a thicker boundary layer. The values are lower for rib spacing P/e = 20 with wide ribs due to the same reason. So the idea of increasing the rib width is an ineffective method to increase the heat transfer rate.

Also the normalized friction factor is high for wide ribs. The normalized friction factor increases as the rib width increases, reaches a maximum value for w/e = 2 for P/e = 10 and w/e =4 for P/e = 20 and then starts to decrease as the rib width ratio increases. So when a combined effect of rib width and rib spacing is considered, the square ribs produce a maximum heat transfer rate with minimal loss in pressure.

The study is performed for three different channels with the combined effect of rib spacing and rib width. From the study it is clear that the square ribs produces a maximum heat transfer rate with a less frictional loss.

The effect of channel aspect ratio on the heat transfer performance is analyzed and is explained in chapter VIII.

CHAPTER VIII

HEAT TRANSFER PERFORMANCE OF THE CHANNELS

The analysis was performed for various channel and rib configurations. In this chapter, the combined effect of rib spacing, rib width and Reynolds number was performed on three different channels with various aspect ratios. In previous chapters, the heat transfer rate and frictional loss was calculated for all the cases. Now, an optimum cooling configuration is to be obtained. The configuration that is selected should produce maximum heat transfer rate with a minimal pressure drop across the channel. The best way to pick an optimum cooling configuration by including the effect of all the parameters is to calculate the overall thermal performance. Before selecting the optimum cooling configuration, the effect of all the parameters on the heat transfer performance is discussed

8.1 Effect of Reynolds Number

The effect of Reynolds number on the heat transfer and pressure drop is discussed in this section. As the Reynolds number increases, the average Nusselt number for the

channels increase. This is because of the increase in velocity which causes turbulence. But the rate of increase in average Nusselt number decrease as the Reynolds number increases. This was discussed in detail for each channel in Chapter VI. Since the rate of increase in Nusselt number is low, the normalized Nusselt number values have a negative slope as the Reynolds number increases. The value of normalized Nusselt numberdecrease as the Reynolds number increases. The pattern for normalized Nusselt number vs. Reynolds number follows the same trend for all the channels and all the rib spacing.

The friction factor follows a different pattern. As the Reynolds number increases, the friction factor decreases but the rate at which the friction factor decrease is lower than the smooth channel. Thus when we normalize, the friction factor values increase as the Reynolds number increases.

The values of all the results were plotted and were discussed in detail in Chapters VI and VII.

8.2 Effect of Rib Spacing

In this study, two basic rib spacing ratios P/e = 10 and P/e = 20 were selected based on the experimental study. The values were selected based on previous experimental investigations on ribbed channels. The normalized Nusselt number and friction factor was calculated for both the rib spacing ratios. From the analysis, the normalized Nusselt number decreases as the rib spacing increases. The normalized friction factor also decreases as the rib spacing increases. The wider rib spacing has a longer recirculation zone than the closer rib spacing. In case of P/e = 10, the flow

reattaches at a shorter distance than P/e = 20. Hence a short recirculation zone ensures a minimal loss in heat transfer. The increase in heat transfer comes at the expense of a high pressure drop across the region. Since the rib spacing P/e = 10ad P/e = 20 has their own advantage and drawback, the correct rib spacing can be selected based only on the overall thermal performance which is discussed in section 8.5.

8.3 Effect of Rib Width

The effect of rib width on the heat transfer performance is discussed in this section. The strategy of selecting the rib width ratios were discussed in Chapter II. The values range from w/e = 1/8 to w/e = 14. From the analysis the change in rib width has no effect on the heat transfer rate. The values reaches a maximum peak for w/e = 1 and starts to decrease. The friction factor initially increases, reaches the maximum value at w/e =2 and then decrease as the rib width increases. So the increase in rib width has an adverse effect on the heat transfer performance. The square rib with w/e = 1 produced the best heat transfer performance. The effect of rib width on overall thermal performance is explained in section 8.5.

8.4 Effect of Channel Aspect Ratio

The analysis is performed for three channels: Square channel with AR 1, Rectangular channel with AR 2 and Rectangular channel II with AR 4. For low Reynolds number 10,000, the rectangular channel I produce the high normalized Nusselt number value followed by rectangular channel II and square channel. But as the Reynolds number increases, the rectangular channel II with wide aspect ratio of 4:1 produce the maximum heat transfer rate followed by rectangular channel - I and square channel.

Thus it is clear that irrespective of the flow parameters, the narrow channel has the low normalized Nusselt number values. The square channel with aspect ratio 1:1 produces the minimum heat transfer rates and the wider channel has a high heat transfer rate.

The friction factor should also be taken into account. The channel aspect ratio has an adverse effect on the normalized friction factor. The wider channels have a high normalized friction factor rate than the narrow channels for all the Reynolds number values.

The normalized friction factor values are as high as 19.6 for rectangular channel II at Reynolds number 60,000 and as low as 3.3 for square channel at Reynolds number 30,000. So an optimum cooling configuration is selected based on both normalized Nusselt number and normalized friction factor values.

8.5 Overall Thermal Performance

The overall thermal performance for each case is provided in Figure 60. The figure of merit which is an easy means of obtaining the required configuration is drawn between $Nu_{norm}/(f_{norm})^{1/3}$ and w/e ratios. This overall heat transfer rate correlation was obtained from literature by Wright, L. M. (2008).

From the plot it is conclusive that the rectangular channel I with rib width ratio, w/e = 1 at Reynolds number 10000 provides us with best heat transfer rate and minimal

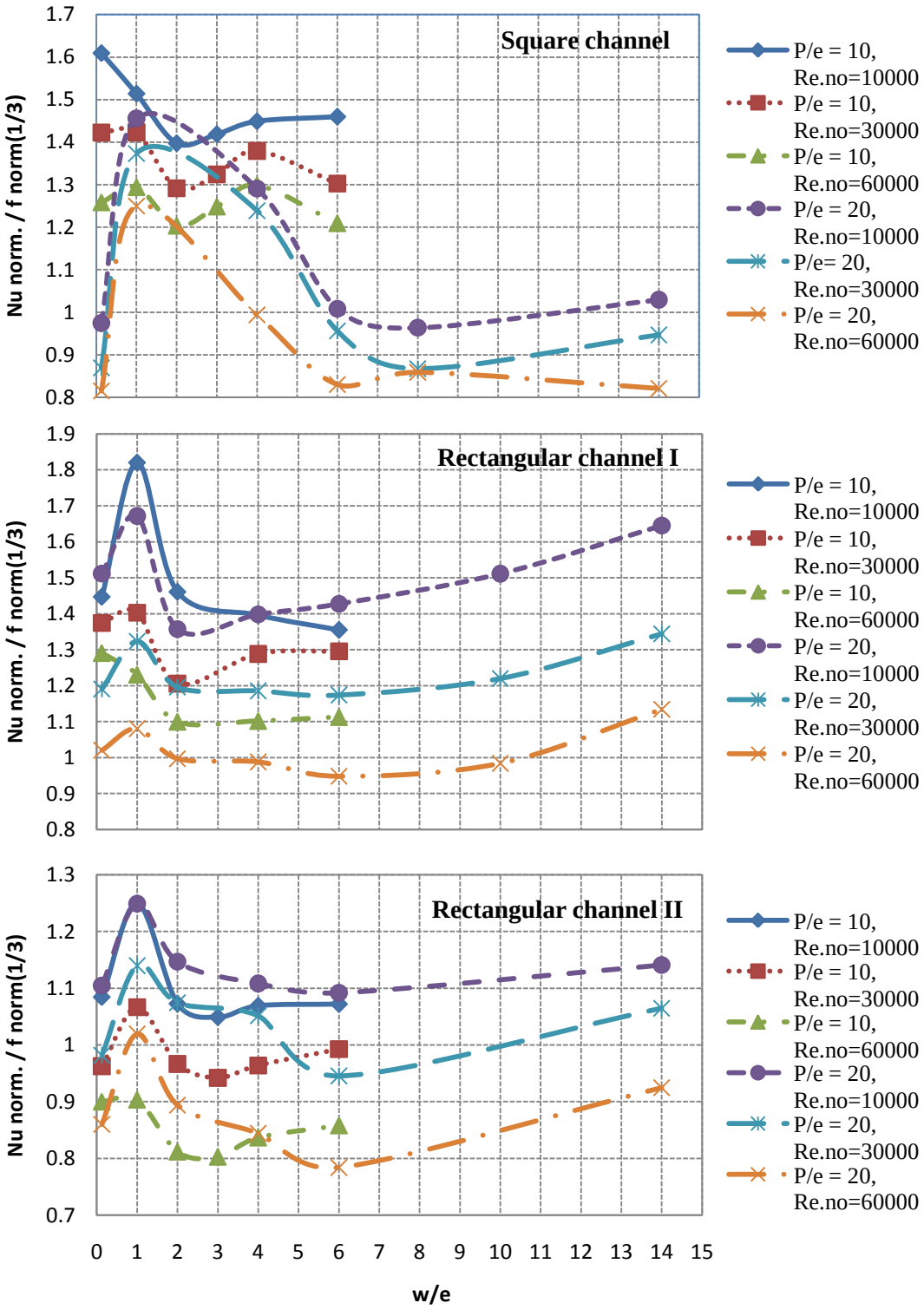

Figure 60: Heat transfer performance of the channels

frictional loss. The rectangular channel I with rib width ratio 14 and square channel with rib width ratio 0.125 have high values of 1.6 due to minimal friction rate. The heat transfer rate is minimal in these two cases.

For all the combinations, the rectangular channel II has the highest friction factor values. Thus the rectangular channel II with aspect ratio 4:1 has a less overall thermal performance.

The increase in rib width has a different pattern for each channel. The increase in rib width for square channel shows no improvement in the overall thermal performance. The values decrease as the rib spacing and rib width increases. Unlike the square channel, the rectangular channels I and II have a different pattern. The thermal performance of the channels increase for square ribs, decrease as the rib width reaches w/e = 6 and again increases. This shows that the rib width ratios w/e = 2, 4 and 6 produced values lower than smooth channel. This is because of the high frictional loss involved.

The rib spacing has the same effect on all the channels. The wider the rib spacing, lower is the thermal performance. The rib spacing P/e = 10 seems to produce optimum results.

As mentioned before, the wider channels have more heat transfer and frictional loss than the narrow channel. But the combined effect of rib spacing and rib width shows that the rectangular channel I with aspect ratio 2:1 has a good thermal performance followed by square channel and rectangular channel II.

The rectangular channel II though have a good heat transfer rates produced a very high pressure loss. This high pressure loss is not acceptable. The square channel with a

minimal heat transfer and friction factor proved to be better than the wide channel with aspect ratio 4:1.

Thus the rectangular channel I with rib spacing P/e = 10 and w/e = 1 has the optimum cooling configuration.

8.6 Future Work

The work has opened up the following potential work research

i. The heat transfer performance of other channels with aspect ratios 3:1, ½:1.
ii. The rib shape can be changed to U, V and W and the effect of rib shapes can be studied.
iii. The change in orientation of the rib can be adopted. The rib angles such as 30°, 45° and 60° can be used in the analysis. The effect of rib orientation on the heat transfer performance can be studied.
iv. The analysis can be extended to rotating channels and the rotation number can be varied for the analysis.
v. Finally, effect of turbulence model on the internal cooling passages can be studied. Turbulence models such as DNS and LES produce reliable results.

BIBLIOGRAPHY

1. Afshin, J. G., Tam, L. M., "Heat Transfer Measurements and Correlations in the Transition Region for a Circular Tube with Three Different Inlet Configurations", Journal of Thermal and Fluid Science, pp. 79 – 90, 1994.
2. Agarwal, P., "Heat/ Mass Transfer in Smooth and Ribbed Rectangular Serpentine Passages of Different Aspect Ratios and Orientation", Master's Thesis, Department of Mechanical Engineering, Louisiana State University, USA, 2001.
3. Bonhoff, B., et.al, "Experimental and Numerical Study of Developed Flow and Heat Transfer in Coolant Channels with 45 degree Ribs", Journal of Heat and Fluid Flow , Vol. 20, pp. 311 – 319, 1999.
4. Bredberg, J., "On the Wall Boundary Condition for Turbulence Models", Internal Report 00/4, Chalmers University, Sweden
5. Bredberg, J., "Turbulence Modeling for Internal Cooling of Gas Turbine Blades", Doctoral Thesis, Department of Thermo and Fluid Dynamics, Chalmers University, Sweden 2002.
6. Cengel, Y. A., "Heat and Mass Transfer: A Practical Approach", 2002, McGraw-Hill, 2nd Edition, pp. 451-482
7. Farrell, B. F., "Optimal excitation of perturbations in viscous shear flow", American Institute of Physics, pp. 2093-2102, April 1988
8. Fluent 6.1 User Guide, Fluent Inc., 2003.

9. Graham, A., Sewall, E., and Thole, K.A., "Flow Measurements in a Ribbed Channel Relevant to Internal Turbine Blade Cooling", ASME Turbo Expo, Power for Land, Sea and Air, Vienna, June 14-17, 2004.
10. Han, J. C., Dutta, S., and Ekkad, S., "Gas Turbine Heat Transfer and Cooling Technology", 2001, Rout ledge Press, 1st Edition, pp. 287-370, 2001.
11. Han, J.C., "Heat Transfer and Friction Characteristics in Rectangular Channels with Rib Turbulators", Journal of Heat Transfer, Vol. 110, pp. 321 – 328, May 1988.
12. Han, J.C., Park, J.S., and Lei, C.K., "Heat Transfer Enhancement in Channels with Turbulence Promoters", Journal of Engineering for Gas Turbines and Power, Vol. 107, pp. 628 – 635, 1985.
13. Hong, S.K., Rhee, D.H., and Cho, H.H., "Effects of Fin Shapes and Arrangements on Heat Transfer for Impingement/Effusion Cooling with Cross flow", Journal of Heat Transfer, Vol. 129, pp. 1697 – 1707, Dec. 2007.
14. Iaccarino, G., Kalitzin, G., and Elkins, C.J., "Numerical and Experimental Investigation of the Turbulent Flow in a Ribbed Serpentine Passage", Center for Turbulence Research, Annual Research Briefs, Stanford University, Stanford, CA, 2003.
15. Iacovides, H., "Computation of Flow and Heat Transfer Through Rotating Ribbed Passages", Journal of Heat and Fluid Flow, Vol. 19, pp. 393 - 400, 1998
16. Iacovides, H., and Raisee, M., "Computation of Flow and Heat Transfer in Two Dimensional Rib Roughened passages, using Low Reynolds Number Turbulence

Models", Journal of Numerical Methods for Heat and Fluid Flow, Vol. 11, pp. 138 – 155, Dec. 2000.

17. Kiml, R., Mochizuki, S., Murata, A., and Sulitka, M., "Rib Induced Secondary Flow Structures inside a High Aspect Ratio Trapezoidal Channel", International Gas Turbine Congress, Tokyo, Nov. 2003.
18. Lakshminarayana, B., "Fluid Dynamics and Heat Transfer of Turbomachinery", Wiley, NY, 1st Edition, pp. 253-276, 1996.
19. Lee, E., Wright, L.M., and Han, J.C., "Heat Transfer in Rotating Rectangular Channels with V-Shaped and Angled ribs", Journal of Thermo physics and Heat Transfer, Vol. 19, pp. 48 – 56, Jan – March 2005.
20. Lin, Y.L., Shih, T. P., Stephens, M.A., and Chyu, M.K., "A Numerical Study of Flow and Heat Transfer in a Smooth and Ribbed U-Duct with and without Rotation", Journal of Heat Transfer, Vol.123, pp. 219 – 232, April 2001.
21. Liu, Y.H., Wright, L.M., Fu, W.L. and Han, J.C., "Rib Spacing Effect on Heat Transfer in Rotating Two Pass Ribbed Channel (AR = 1:2)", Journal of Thermo physics and Heat Transfer, Vol. 21, pp. 582 – 595, July – Sept. 2007.
22. Maurer, M., Wolfersdorf, J.V. and Gritsch, M., "An Experimental and Numerical Study of Heat Transfer and Pressure Loss in a Rectangular Channel with V-shaped Ribs", Journal of Turbomachinery, Vol. 129, pp. 800 -808, Oct. 2007.
23. Park, J.S., Han, J.C., Huang, Y., and Ou, S., "Heat Transfer Performance Comparisons of Five Different Rectangular Channels with Parallel Angled Ribs", Journal of Heat Transfer, Vol. 35, pp. 2891 – 2903, Dec. 1992.

24. Qahtani, A. M., Jang, Y. J., Chen, H. C., and Han, J.C., "Prediction of Flow and Heat Transfer in Rotating Two Pass Rectangular Channels with 45 degree Rib Turbulators", Journal of Turbomachinery, Vol. 124, pp. 242 – 250, April 2002.
25. Raisee, M., Naeimi, H., Alizadeh, M., and Iacovides, H., "Prediction of Flow and Heat Transfer through Stationary and Rotating Ribbed Ducts using a non-Linear k-e model", Flow Turbulence Combust, Vol. 82, pp. 121 – 153, 2009.
26. Rhee, D.H., Nam, Y.W., and Cho, H.H., "Local Heat/Mass Transfer with Various Rib Arrangements in Impingement/Effusion Cooling System with Cross flow", Journal of Turbomachinery, Vol. 126, pp. 615 – 62, Oct. 2004.
27. Venkata, R. R., and Prabhu, V., "Pressure Drop Distribution in Smooth and Rib Roughened Square Channel with Sharp 180° Bend in the Presence of Guide Vanes", Journal of Rotating Machinery, Vol. 10, pp. 99 – 114, 2004.
28. Wee, H., et.al, "Numerical Predictions of Heat Transfer and Flow Characteristics of Heat Sinks with Ribbed and Dimpled Surfaces in Laminar Flow", Numerical Heat Transfer, Vol. 53, pp. 1156 – 1175, 2008.
29. Wright L.M., Fu W.L. and Han J.C., "Thermal Performance of Angled V-Shaped and W-Shaped Rib Turbulators in Rotating Rectangular Cooling Channels (AR = 4:1)", Journal of Turbomachinery, Vol. 126, pp. 604 – 614, Oct. 2004.
30. Wright, L.M. and Gohardani, A.S., "Effect of Cooling Ejection in Rectangular and Trapezoidal Trailing Edge Cooling Passages", ASME Turbo Expo, Berlin, Germany, June 2008.

31. Wright, L.M. and Gohardani, A.S., “Effect of Turbulator Width and Spacing on the Thermal performance of Angled Ribs in a Rectangular Channel (AR = 3:1)”, ASME Mechanical Engineering Expo., Massachusetts, USA, Oct. - Nov. 2008.
32. Wright, L.M., Fu, W.L. and Han, J.C., “Influence of Entrance Geometry on Heat Transfer in Rotating Rectangular Cooling Channels (AR = 4:1) with Angled Ribs”, Journal of Heat Transfer, Vol. 127, pp. 378 – 387, April 2005.
33. www.cfd-online.com/forum/fluent.